U.S. DEPARTMENT OF COMMERCE

PB80-175938

Emissions from Aircraft Fuel Nozzle Flames

Purdue Univ.
Lafayette, IN

Prepared for

Environmental Protection Agency
Ann Arbor, MI

July 75

U.S. Department of Commerce
National Technical Information Service
NTIS.

MOTOR VEHICLE EMISSION LAB

Library

U. S. Environmental Protection Agency
Ann Arbor, Michigan 48105

PB 80 175938

April 29, 1980

U.S. Department of Commerce
National Technical Information Service
Springfield, Virginia 22151
Attn: Input Branch

Gentlemen:

Enclosed please find the following report ready to be inputted:

DA Emissions from Aircraft Fuel Nozzle Flames, PURDU-CL-75-04

Only one copy of this report is available. We would like to have this report returned when it has been processed.

Thank you very much for your help.

Sincerely,

Darcy Enos

Darcy Enos
Assistant Librarian

PB80-175938

EMISSIONS FROM AIRCRAFT FUEL NOZZLE FLAMES

Environmental Protection Agency Grant No. R-802650-01 – Final Report

by

J.H. Tuttle, R.A. Shisler, R.W. Bilger, and A.M. Mellor

Report No. PURDU-CL-75-04

THE COMBUSTION LABORATORY
SCHOOL OF MECHANICAL ENGINEERING
PURDUE UNIVERSITY
WEST LAFAYETTE, INDIANA

JULY 1975

REPRODUCED BY
NATIONAL TECHNICAL
INFORMATION SERVICE
U.S. DEPARTMENT OF COMMERCE
SPRINGFIELD, VA. 22161

TECHNICAL REPORT DATA
(Please read Instructions on the reverse before completing)

1. REPORT NO. PURDU-CL-75-04	2.
3. RECIPIENT'S ACCESSION NO. PB 80 175938	
4. TITLE AND SUBTITLE: Emissions From Aircraft Fuel Nozzle Flames	5. REPORT DATE: July 1975
	6. PERFORMING ORGANIZATION CODE
7. AUTHOR(S): J.H.Tuttle, R.A. Shisler, R.W. Bilger, and A.M. Mellor	8. PERFORMING ORGANIZATION REPORT NO.
9. PERFORMING ORGANIZATION NAME AND ADDRESS: The Combustion Laboratory School of Mechanical Engineering Purdue University West Lafayette, Indiana	10. PROGRAM ELEMENT NO.
	11. CONTRACT/GRANT NO. R-802650-01-Final Report
12. SPONSORING AGENCY NAME AND ADDRESS: Environmental Protection Agency	13. TYPE OF REPORT AND PERIOD COVERED: Final Report
	14. SPONSORING AGENCY CODE
15. SUPPLEMENTARY NOTES	

16. ABSTRACT

With the recently set U.S. Environmental Protection Agency standards for aircraft jet engine emissions of unburned hydrocarbons, carbon monoxide, and oxides of nitrogen, it is essential that the complex physical processes with a conventional liquid fueled gas turbine combustor be better understood. These processes, dominated by the interaction of a liquid fuel spray and a recirculating flow region, are characterized by time parameters which indicate the relative importance of the ongoing heterogeneous and homogeneous phenomena.

Experimental emissions data from both internal flame and exhaust plane gathered in a simulated gas turbine primary zone at typical combustor operating conditions are analyzed in terms of the developed time parameters. Results indicate that with a well atomized fuel spray the large scale turbulent mixing controls the flame stoichiometry and hence the emissions characteristics. However as the fuel atomization becomes poorer, the flame structure is altered and emissions characteristics can be explained only by a combination of heterogeneous and homogeneous processes. Because CO and NOx emissions originate in separate regions of the flame, it was possible to alter the turbulent mixing properties of each region such that both CO and NOx were reduced simultaneously.

17. KEY WORDS AND DOCUMENT ANALYSIS

a. DESCRIPTORS	b. IDENTIFIERS/OPEN ENDED TERMS	c. COSATI Field/Group
Emission Air Pollution Jet Engines Aircraft Engines Exhaust Gases Gas Turbine Engines Exhaust Flames	Aircraft Exhaust Gas Turbine Combustor	

18. DISTRIBUTION STATEMENT: RELEASE UNLIMITED	19. SECURITY CLASS *(This Report)*: UNCLASSIFIED	21. NO. OF PAGES
	20. SECURITY CLASS *(This page)*: UNCLASSIFIED	22. PRICE

EPA Form 2220-1 (9-73)

EMISSIONS FROM AIRCRAFT FUEL NOZZLE FLAMES

Environmental Protection Agency

Grant No. R-802650-01 - Final Report

by

J. H. Tuttle, R. A. Shisler, R. W. Bilger, and A. M. Mellor

Report No. PURDU-CL-75-04

The Combustion Laboratory

School of Mechanical Engineering

Purdue University

West Lafayette, Indiana

July 1975

ACKNOWLEDGEMENTS

The authors* gratefully acknowledge Mr. Thomas Miller for his unlimited assistance in the construction, maintenance, and operation of the experimental facility. Additional aid in both data gathering and reduction was provided by the Messrs. J. Renie, W. Dodds, A. Ecker, S. Stolberg and J. Stefucza.

Particularly helpful were discussions concerning fuel injector design and performance with Harold Simmons of Parker-Hannifin Corporation and Dr. A. H. Lefebvre of Cranfield Institute of Technology.

Valuable assistance and technical suggestions were also provided by Dr. Richard Munt of the Office of Air Programs.

This research has been financed with Federal funds from the Environmental Protection Agency under Grant Number R-802650-01. The contents do not necessarily reflect the views and policies of the Environmental Protection Agency, nor does mention of trade names or commercial products constitute endorsement or recommendation for use.

*R. W. Bilger is Visiting Professor, The Combustion Laboratory, School of Mechanical Engineering.

TABLE OF CONTENTS

Page

LIST OF TABLES v

LIST OF FIGURES vi

ABSTRACT ix

SECTION I. INTRODUCTION AND SUMMARY 1

SECTION II. ATOMIZATION OF LIQUID FUEL 7

A. Methods of Atomizing Liquid Fuels and Characterizing Sprays. 8
1. Swirl Atomizers. 9
2. Air-blast Atomizers. 11
3. Representing Size Distributions of Liquid Sprays. 13

B. Results of Atomizer Drop Sizing Studies. 16
1. Simplex Atomizers. 16
2. Air-blast Atomization. 23

SECTION III. DESIGN AND OPERATION OF THE EXPERIMENTAL COMBUSTION FACILITY. 26

A. Facility Design. 26

B. Test Burner Configuration. 29

C. Gas Analysis System. 32

D. Single Point Probe Studies 32

E. Exhaust Plane Studies. 35

SECTION IV. CHARACTERISTIC TIMES FOR COMBUSTION AND POLLUTANT FORMATION IN GAS TURBINE COMBUSTORS 37

A. Heterogeneous Processes. 39

B. Turbulent Mixing Processes 41

C. Homogeneous Reaction Times 50

D. Dependence of the Flame Structure on the Characteristic Times 51

Page

SECTION V. INTERNAL COMBUSTOR MEASUREMENTS--RESULTS AND DISCUSSION 56

A. Internal Probing Results--$\dot{m}$ = 1.0 kg/sec, P = 5 atm, ϕ_o = 0.1, and $T_{inlet\ air}$ = 500°K. 63

B. Internal Probing Results--$\dot{m}$ = 1.5 kg/sec, P = 5 atm, ϕ_o = 0.2, and $T_{inlet\ air}$ = 500°K. 70

C. Internal Probing Results--$\dot{m}$ = 3.0 kg/sec, P = 5 atm, ϕ_o = 0.2, and $T_{inlet\ air}$ = 500°K. 76

D. Summary. 80

SECTION VI. EXHAUST PLANE MEASUREMENTS--RESULTS AND DISCUSSION 86

A. Calculation of Characteristic Times. 86

B. Correlation of NO_x Emissions 93

C. Correlation of CO and HC Emissions 99

D. Summary. 105

SECTION VII. FUTURE EXPERIMENTS--VARIATION OF τ_{eb} AND $\tau_{s\ell}$. 110

LIST OF REFERENCES 115

APPENDIX I. DATA LISTING 119

APPENDIX II. DERIVATION OF THE CORRSIN TIME SCALE 137

LIST OF TABLES

Table		Page
2-1.	Summary of SMD Correlations for Simplex Atomizers.	.21
3-1.	Operating Points for Single Point Probe Studies	.33
3-2.	Operating Points for Exit Plane Data	.36
4-1.	Characteristic Times for Combustion and Pollutant Formation in Two-Phase Turbulent Flow (from Mellor, 1975)	.39
4-2.	Turbulence Scales.	.44
4-3.	Values of τ_{hc} and τ_{no} (from Vranos, 1974) (P = 15 atm; $T_{inlet\ air}$ = 700°K)	.51
4-4.	Limiting Cases of $\tau_{s\ell}/\tau_{eb}$.	.53
6-1.	Calculated Values of τ_{eb}	.89
6-2.	Values of $\tau_{s\ell,co}$ and $\tau_{s\ell,no}$ (11.43 cm disc diameter).	.91
6-3.	Values of $\tau_{s\ell,co}$ and $\tau_{s\ell,no}$ (8.89 cm disc diameter).	.92
7-1.	Fuel Droplet Lifetimes, 35 gal/hr Nozzle	.111

LIST OF FIGURES

Figure		Page
2-1.	Typical Swirl Atomizer Construction.	.10
2-2.	Possible Configuration for Air-blast Atomizer	.12
2-3.	Example of Possible Droplet Size Distribution Curve	.14
3-1.	A Schematic of the Experimental Apparatus.	.27
3-2.	Test Section Housing Schematic	.30
3-3.	Schematic of Disc Mounting Arrangement	.31
3-4.	View, Looking Upstream, of Disc, Support Struts, and Probe Trace With Sampling Points	.34
4-1.	Schematic of the Postulated Flame Zone Model	.38
4-2.	Gas Turbine Flame Schematics (from Mellor, 1973).	.55
5-1.	Schematic of the Postulated Flame Zone Model	.58
5-2.	Axial CO Concentration Profile, 6.4 cm from Centerline $\dot{m}_{air}$ = 1.0 kg/sec, ϕ_o = 0.1, P = 5 atm, T_{in} = 500°K	.60
5-3.	Axial CO Concentration Profile, 2.5 cm from Centerline $\dot{m}_{air}$ = 1.0 kg/sec, ϕ_o = 0.1, P = 5 atm, T_{in} = 500°K	.61
5-4.	Axial CO Concentration Profile Along Centerline $\dot{m}_{air}$ = 1.0 kg/sec, ϕ_o = 0.1, P = 5 atm, T_{in} = 500°K.	.62
5-5.	HC Concentration Contour Map (numbers are ppmC x 10^{-3}) $\dot{m}$ = 1.0 kg/sec, P = 5 atm, ϕ_o = 0.1, $T_{inlet\ air}$ = 500°K	.64
5-6.	CO Concentration Contour Map (numbers are ppm x 10^{-3}) $\dot{m}$ = 1.0 kg/sec, P = 5 atm, ϕ_o = 0.1, $T_{inlet\ air}$ = 500°K	.65

Figure		Page
5-7.	Temperature Contour Map (numbers are ^{o}K x 10^{-2}) $\dot{m}$ = 1.0 kg/sec, P = 5 atm, ϕ_o = 0.1, $T_{inlet\ air}$ = 500^{o}K	.66
5-8.	NO Concentration Contour Map (numbers are ppm) $\dot{m}$ = 1.0 kg/sec, P = 5 atm, ϕ_o = 0.1, $T_{inlet\ air}$ = 500^{o}K	.67
5-9.	HC Concentration Contour Map (numbers are ppmC x 10^{-3}) $\dot{m}$ = 1.5 kg/sec, P = 5 atm, ϕ_o = 0.2, $T_{inlet\ air}$ = 500^{o}K	.71
5-10.	CO Concentration Contour Map (numbers are ppm x 10^{-3}) $\dot{m}$ = 1.5 kg/sec, P = 5 atm, ϕ_o = 0.2, $T_{inlet\ air}$ = 500^{o}K	.72
5-11.	Temperature Contour Map (numbers are ^{o}K x 10^{-2}) $\dot{m}$ = 1.5 kg/sec, P = 5 atm, ϕ_o = 0.2, $T_{inlet\ air}$ = 500^{o}K	.73
5-12.	NO_x Concentration Contour Map (numbers are ppm) $\dot{m}$ = 1.5 kg/sec, P = 5 atm, ϕ_o = 0.2, $T_{inlet\ air}$ = 500^{o}K	.74
5-13.	HC Concentration Contour Map (numbers are ppmC x 10^{-3}) $\dot{m}$ = 3.0 kg/sec, P = 5 atm, ϕ_o = 0.2, $T_{inlet\ air}$ = 500^{o}K	.77
5-14.	CO Concentration Contour Map (numbers are ppm x 10^{-3}) $\dot{m}$ = 3.0 kg/sec, P = 5 atm, ϕ_o = 0.2, $T_{inlet\ air}$ = 500^{o}K	.78
5-15.	NO_x Concentration Contour Map (numbers are ppm) $\dot{m}$ = 3.0 kg/sec, P = 5 atm, ϕ_o = 0.2, $T_{inlet\ air}$ = 500^{o}K	.79
5-16.	Regions of Pollutant Generation.	.82
5-17.	Schematic of the Three Probed Flames	.84
6-1.	Predicted Droplet Size for Simplex Fuel Nozzles (from Accessories Division, Parker-Hannifin Corporation)	.88
6-2.	Overall Equivalence Ratio Variation.	.96
6-3.	Net NO_x EI versus $\tau_{s\ell\ no}$. Flagged symbols represent runs with low fuel differential injection pressure	.98

Figure		Page
6-4.	HCEI versus COEI	.100
6-5.	COEI versus $\tau_{s\ell,co}^{-1}$ (Eqn. 4-7a). Flagged symbols represent runs with low fuel differential injection pressure	.102
6-6.	COEI versus $\tau_{s\ell,co}^{-1}$ (Eqn. 4-7b). Flagged symbols represent runs with low fuel differential injection pressure	.103
6-7.	COEI versus $\tau_{s\ell,co}$ (Eqn. 4-7c). Flagged symbols represent runs with low fuel differential injection pressure	.104
6-8.	COEI versus NO_xEI. Flagged symbols represent runs with low fuel differential injection pressure . . .	.107
6-9.	Emissions of Conventional Combustors (from Verkamp et al., 1974). Flagged symbols represent runs with low fuel differential injection pressure	.108
7-1.	Toothed Disc Flame Stabilizers	.113

ABSTRACT

With the recently set U. S. Environmental Protection Agency standards for aircraft jet engine emissions of unburned hydrocarbons, carbon monoxide, and oxides of nitrogen, it is essential that the complex physical processes with a conventional liquid fueled gas turbine combustor be better understood. These processes, dominated by the interaction of a liquid fuel spray and a recirculating flow region, are characterized by time parameters which indicate the relative importance of the ongoing heterogeneous and homogeneous phenomena.

Experimental emissions data both internal flame and exhaust plane gathered in a simulated gas turbine primary zone at typical combustor operating conditions are analyzed in terms of the developed time parameters. Results indicate that with a well atomized fuel spray the large scale turbulent mixing controls the flame stoichiometry and hence the emissions characteristics. However as the fuel atomization becomes poorer, the flame structure is altered and emissions characteristics can be explained only by a combination of heterogeneous and homogeneous processes. Because CO and NO_x emissions originate in separate regions of the flame, it was possible to alter the turbulent mixing properties of each region such that both CO and NO_x emissions were reduced simultaneously.

I. INTRODUCTION AND SUMMARY

The advantages of atomizing a liquid fuel into fine droplets prior to its combustion have been known and widely applied for years in various power and heating devices. In contrast however, insight into the generation of pollutant emissions within quasi-steady, turbulent liquid fuel spray flames such as are used in conventional gas turbine aircraft engines, utility boilers, and many other types of practical combustion systems has been slow to evolve. This is indeed unfortunate, as many analytical and experimental investigations in the open literature suggest the importance of the liquid fuel spray upon gas turbine emissions. For example, Hammond and Mellor (1973) noted that a primary source of discrepancies between the predicted pollutant emissions of their analytical combustor model and measured emissions was the inability of the model to simulate the heterogeneous effects within the combustion process.

From earlier gas turbine emissions studies in this laboratory (Tuttle et al., 1973), Mellor (1973) developed a simplified physical model of spray combustion in a gas turbine type burner. This physical model contains two time parameters, one to characterize the homogeneous processes and a second to characterize the heterogeneous processes. The homogeneous time was taken to be proportional to the inverse of the reference velocity through the combustor. The heterogeneous combustion process was characterized by the fuel droplet lifetime, which was related to the differential injection pressure across the fuel nozzle. This model (Mellor, 1973) was successful in qualitatively predicting the trends in the NO_x exhaust emissions of the Allison J-33 combustor over the engine operating cycle and demonstrated the importance of the fuel injector in determining the emissions levels.

Several experimental studies of spray combustion in the wake of a stabilizer disc have been published by Chigier and co-workers

(1973a, 1973b). These authors concentrated on the drop size distribution, drop trajectories, drop velocities, and temperatures within the flame structure. From their quite detailed measurements, the authors were able to formulate a flow model of their spray flame, showing clearly the interaction between the liquid drops and the aerodynamic environment. Unfortunately however, the measurement of pollutant emissions was not included in the study.

In the present study, probing for gas samples and temperature was accomplished for a flame stabilized in the wake of a disc with fuel injected into the wake from the center of the disc, similar to the arrangement used by Chigier (1973a, 1973b). However, two important differences between the two studies should be noted. First, the flame of Chigier (1973a, 1973b) was unconfined, whereas here the flame was stabilized in a duct. This difference results in some modification of the fluid mechanical properties of the flame zone. Second, the measurements reported here are for inlet air temperatures and pressures more characteristic of a gas turbine combustor. Although the present research did not allow the determination of the in situ droplet size distribution within the flame zone, selected studies of initial drop size distribution are reviewed in Section II. In particular, the atomization properties of commonly employed types of fuel injectors for a range of fuels are summarized.

The experimental combustion facility consisted of two burners in series. The upstream or heating combustor (Allison T-56) was used only to supply high temperature vitiated inlet air to the downstream test section. Both burners were fueled with liquid propane, with the inlet temperature to the test section determined by the overall equivalence ratio of the heating combustor. Operating cycle parameters of the test combustor which were varied were pressure, overall equivalence ratio, air flow rate, and inlet air temperature. Rakes were used to monitor the temperature and pollutant emissions of the vitiated inlet air to the test section. A water cooled stainless steel probe was utilized to extract gas samples from locations within the flame. Exit plane samples were gathered via a water cooled rake. All gas samples

were analyzed by a continuous flow system to determine CO, HC, NO, NO_x, and NO_2 concentrations. Temperature estimates were also obtained by a probe mounted Pt/PtRh thermocouple. Further details of the facility and measurements are given in Section III.

Prior to summarizing the experimental results, some comments are in order about the selection and use of the disc flame stabilizer. As noted, the general model of spray combustion of Mellor (1973) has as one of its key elements the liquid fuel droplet lifetime, which is determined largely by the characteristics of the fuel injector in use. It would be of value to perform an experimental investigation to isolate the influence of injector performance on gas turbine type spray flame combustion and emissions. Such an investigation would ideally retain the general character of a combustor flame while eliminating aerodynamic influences peculiar to a specific liner.

A conventional gas turbine burner can be conceptually divided into three zones, primary combustion, secondary combustion, and dilution. Although each of these zones is important for producing an exhaust gas with acceptable properties at the turbine inlet, the primary zone is of paramount importance in determining the pollutant emissions of the combustor, especially NO. In particular, the interaction of the liquid fuel and the mixing processes in the volume adjacent to the individual fuel injector is critical for pollutant characterization. In this respect, the experimental burner was selected to reproduce the physical processes occurring within the primary combustion zone of a gas turbine liner.

Past studies (Tuttle et al., 1973; Shisler et al., 1974) have found the combustor flame to resemble a turbulent diffusion flame surrounding a centerline recirculation zone. The recirculation zone established behind a disc resembles that found in combustors with some modification. Typically, the recirculation zone of a gas turbine is swirl generated and may be fed by penetration air jets. Hence the zone may be displaced from the liner dome. (See Shisler et al., 1974, for the location of the reverse flow region of the Allison T-56 combustor). With the disc geometry, the recirculation zone results from flow

separation due to the blockage of the flow by a bluff body. Thus the region of reverse flow is immediately adjacent to the disc. Note that the aerodynamics are however much simplified due to the elimination of air swirl and discrete air addition through film cooling slots or penetration holes. Here the flow is axisymmetric, as opposed to the three dimensional flow characteristic of a combustor.

The absence of a liner also allows visual and photographic observance of the fuel spray and the flame. It is possible then to vary the operating characteristics of the injector and determine the effect of these changes upon both the length and color of the flame.

The complex physical processes occurring both within the disc stabilized burner and within a conventional gas turbine combustor are analyzed in Section IV in order to examine the effect of each physical process upon pollutant emissions. In the analysis, time scale parameters are developed which characterize the five phenomena deemed of greatest importance in a combustion system with an inherent strong interaction between a liquid fuel spray and a recirculating gas flow region.

The first time parameter discussed is the fuel droplet lifetime and is important in determining the heterogeneous properties of the combustion process. The second and third time parameters are both associated with the turbulent mixing properties of the reacting flow field, one to characterize the mixing process near the fuel injector and a second to characterize the mixing process in the shear layer between the recirculation zone and the free stream. The fourth and fifth time parameters are scales which represent the times for homogeneous combustion of the fuel and NO formation.

Calculated results of the time parameters for typical gas turbine operating conditions suggest that with the exception of near blow out combustor operation the homogeneous combustion of the fuel is significantly faster than the other processes. The flame structure is then determined by the magnitudes of the turbulent mixing times and droplet lifetimes which may be of similar order. The time for NO formation does not influence the basic flame structure but rather is dependent upon it.

Internal combustor measurements of HC, CO, NO_x, and gas temperature for three widely varied operating conditions are presented and discussed in Section V. In agreement with the trend given by the calculated characteristic times for the three run conditions in going from low to high air flow rate, the importance of the heterogeneous processes increased since the mixing times decreased at a greater rate than the droplet lifetimes. The basic flame structure consists of a hollow reaction region (shear layer) along the boundary between the recirculation zone and the free stream. However as the heterogeneous processes increase in importance, a free stream flame zone following the fuel spray penetrating through the shear layer is also detectable. As the ratio of the shear layer mixing time to the droplet lifetime decreases, this free stream flame zone becomes of increasing importance to the combustor emissions levels. The internal combustor measurements also suggest that HC and CO emissions are generated in a region of the flame different from that where NO formation is occurring.

Combustor exhaust plane HC, CO, and NO_x concentrations for independent variations in the cycle operating parameters are analyzed in Section VI utilizing the time scales introduced in Section IV. Results suggest that burning occurs over a narrow range of local equivalence ratios centered about unity. For various fuel injectors and two disc sizes, HC emissions were found to correlate well with CO emissions, indicating that similar physical processes are responsible for both of these pollutant species. NO_x and CO emissions generally correlated well with a mixing time for each species, and thus are primarily mixing controlled. For run conditions with poor fuel atomization, heterogeneous effects had to also be considered in order to correlate the measurements. Two shear layer mixing times are employed to correlate NO_x and CO exhaust emissions since these two species are generated in different regions of the flame. Because these two emissions producing regions are separate, both CO and NO_x emissions were reduced simultaneously while still maintaining the same diffusion flame structure.

Both the development and the use of time parameters to characterize the complex physical processes occurring in a gas turbine combustor

are emphasized throughout each Section. It is hoped that this demonstration of the utility of these time parameters will prove useful to others both in the analysis of emissions data and in the design of new generation, low emissions combustors.

II. ATOMIZATION OF LIQUID FUEL

In most gas turbine engines fuel is introduced to the combustion chamber in the form of a finely divided spray of liquid drops. This division of fuel into droplets is accomplished by using an atomizer or injector which also has the responsibility of delivering these droplets to the desired location in the combustion zone. Conventional atomizers produce a wide range of fuel droplet diameters, which may vary from less than 10 microns to greater than 200 microns. The corresponding variation in mass content by a factor of 8000 shows that the large drops, although perhaps few in number, could be important since they contain an appreciable fraction of the fuel mass flow.

The occurance of large droplets has long been thought to contribute to combustion inefficiency (Watson and Clark, 1947) because their large inertia to drag ratio would tend to carry them through the flame zone before sufficient time had elapsed for evaporation or combustion. Mellor (1973) has also suggested that the presence of large drops, burning in wake or diffusion flames, can also be used to explain the production of nitric oxide (NO) for engine operating modes where atomization tends to be poor, such as idle. It is clear that the need for understanding atomizer operation exists and indeed much research has been done in the past on understanding and improving atomizers, primarily from the viewpoint of improving combustor stability and operating efficiency. With the concern for reducing pollutant emissions, interest in injector improvement studies has continued due to reports (see for example Norster and Lefebvre, 1972) that atomizer changes could result in reduction of engine idle pollutant emissions from gas turbines. The possibility of reducing emissions in existing engines by replacing the fuel injectors would prove highly attractive if it could be done without major changes to the remainder of the engine.

Injector studies in the past have, for the most part, examined performance with the standard aviation and diesel type fuels, which vary little in important physical properties that influence atomization. The inevitable future shortage of these high grade fuels has led to our reviewing the existing atomizer knowledge to determine if it may be applied to the possible replacement fuels. After a description of the operation of injectors this Section will summarize the results of past studies on the parameters that influence fuel atomization.

A. Methods of Atomizing Liquid Fuels and Characterizing Sprays

Numerous techniques have been employed for converting liquid fuel to drops for combustion. These include anvil or impact type atomizers where a liquid stream is shattered by directing it at a flat surface. The surface may be forced to vibrate either by an air stream or piezo-electrically (acoustic or ultrasonic injectors respectively). Spinning disc or cup atomizers allow fuel to flow onto a rotating surface where centrifugal force causes droplets to shed from the edge. MacFarlane (1971), Hunter et al. (1974), and Fraser (1957) all present descriptions of these atomizers and their operation. However, impact and spinning atomizers are generally avoided in gas turbine applications since both are susceptible to deterioration in the hostile environment of combustor primary zone.

Pressure atomizing nozzles use a high-pressure pump to force fuel through a small orifice. The exiting stream quickly disintegrates into droplets due to the turbulence and instabilities in the flow. If the pressure atomizer is constructed so the fluid in the final orifice has a tangential velocity (i.e. swirl), the liquid will exit as a thin sheet in the form of a hollow cone which breaks up into droplets. A pressure-atomizing swirl or centrifugal injector may have a single orifice (simplex) or it may contain an additional concentric annular fuel flow passage which comes into use at a given injection pressure. This duel orifice or duplex atomizer allows high flow rates at moderate pressure while maintaining higher atomizing pressure at lower flows than would be possible using a single orifice.

Since atomizers of the swirl type have been predominant in gas turbines in the past, they will be discussed more fully in the following Sections. They can suffer, however, from rapidly deteriorating atomization at low fuel flows and thus recent injector studies have examined the performance of air-assist and air-blast atomizers, which shatter the fuel stream by causing it to interact with a high velocity air stream. Air-assist implies that this air is supplied by a separate pump while air-blast atomizer air flow is a result of the pressure drop across the combustor dome. Following the discussions of atomizer operation a short section will be devoted to the methods of describing size distributions of liquid sprays.

1. Swirl Atomizers

A swirl or centrifugal atomizer must contain a system of tangentially directed inlet ports for feeding the fuel to a cylindrical or conical swirl chamber which connects with the concentric outlet orifice. Figure 2-1 shows the construction of a typical swirl atomizer which used helical slots cut in a tapered plug as the swirling mechanism. The tangential velocity of the incoming fluid generates a vortex motion in the swirl chamber and conservation of angular momentum requires that the tangential velocity vary inversely with radius as the fluid approaches the injector axis. The maximum velocity is limited however by the value of the original fluid pressure according to the conservation of energy equation. When the liquid has reached the radius corresponding to this maximum possible tangential velocity, the core of the swirl chamber is filled with gas entrained from the ambient outside the nozzle.

It can be seen then that within the swirl chamber fluid pressure is greatest next to the chamber wall and tangential velocity greatest along the gas liquid interface. As the swirling column of fluid leaves the final orifice, pressure gradients across the liquid layer are no longer possible and the pressure is transformed to an increase in axial velocity with the fluid next to the chamber wall receiving the greatest increase. At the exit of the orifice then the situation exists such that a finite annular element of fluid, if left undisturbed, would leave

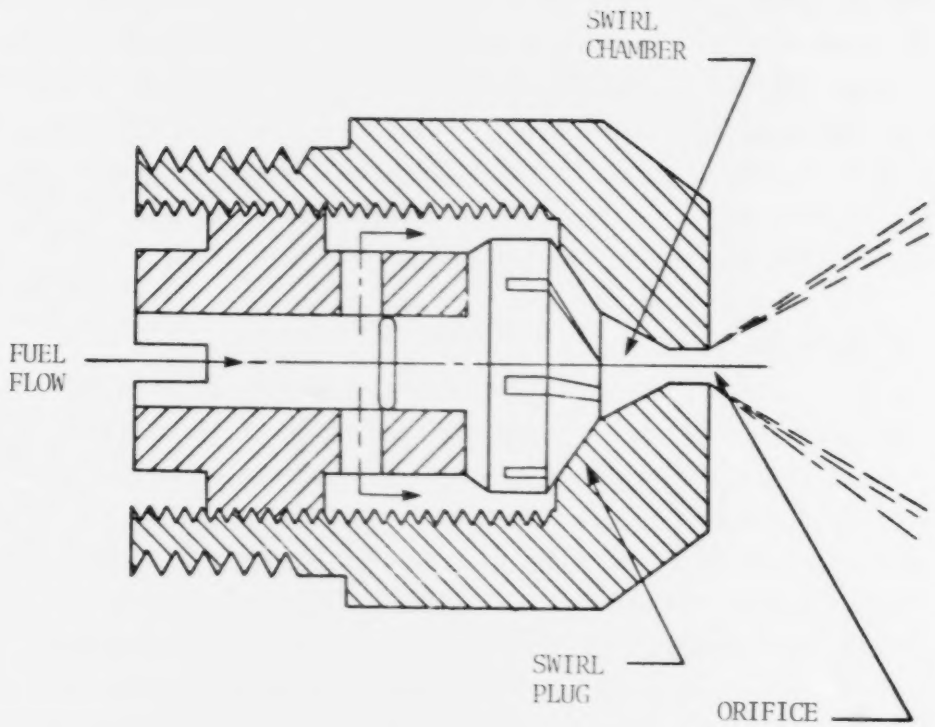

Figure 2-1. Typical Swirl Atomizer Construction

the orifice in the form of a conical sheet, the angle of which is determined by the ratio of the tangential to axial velocity. Since, as described above, this ratio is greater for the inner annular fluid elements, they would tend to move outward through the liquid sheets formed from the outer fluid elements. The turbulent mixing caused by this movement along with interaction with the ambient gas causes ripples or waves to form in the issuing film, which are observed (Watson and Clark, 1947; Radcliffe, 1960) to break up into ligaments, then droplets.

The preceding discussion, although it ignores real fluid frictional losses, is qualitatively correct as verified by experimental observance of the gas core and hollow cone spray (Mellor et al., 1971; Longwell, 1943).

2. Air-blast Atomizers

Pressure atomizing nozzles, by the very nature of their operation, must suffer from deteriorating atomization quality at low fuel flow rates. Norster and Lefebvre (1972) also note that pressure atomizing duplex nozzles are marked by an increase in the spray mean drop size at the range of flow rates where fuel begins to flow in the main orifice. The trend towards greater operating pressures in modern combustors creates another problem for pressure atomizers in that it requires development of higher pressure fuel pumps. Air-blast atomizers however avoid these problems by using the injection pressure only to supply the fuel; atomization is obtained by the effect of high velocity air flowing through the injector.

Numerous configurations of air-blast atomizers are possible. Shown in Figure 2-2 is a schematic of a typical air-blast atomizer where fuel enters the flow passage and spreads out as a thin film. The passage is designed so that at the exit the air has reached its maximum velocity. The action of the air on the inside of the fluid sheet in this region causes it to break into droplets. In studies of air-blast atomizers Byran et al. (1971) observed that atomization could be improved by the addition of another air passage so that air is applied to both sides of the fuel. Hunter et al. (1974) examined an air-assist atomizer similar to a simplex injector with the addition of the outside or shroud air

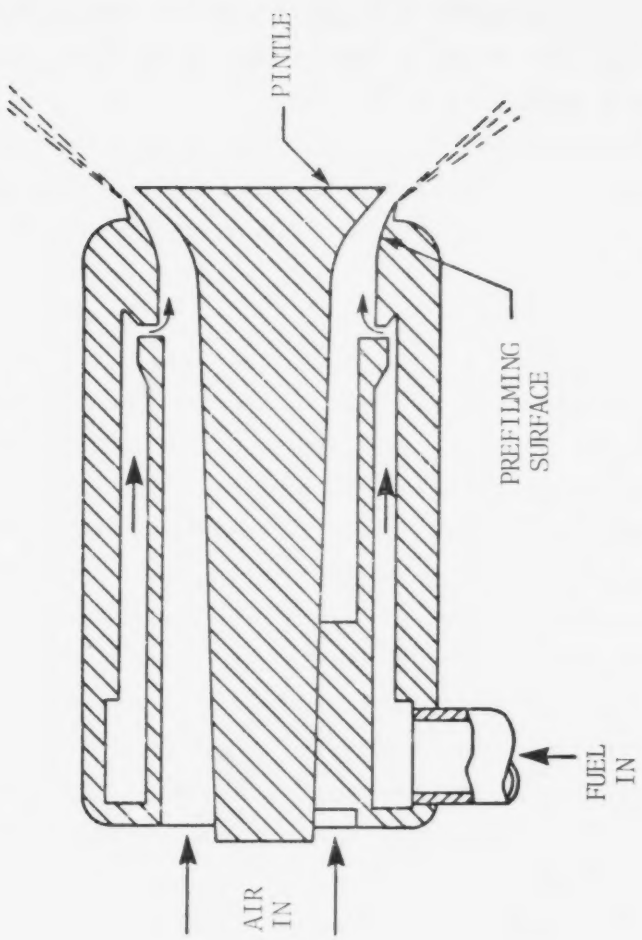

Figure 2-2. Possible Configuration for Air-blast Atomizer

passage. Again air-assist implies differential air injection pressures greater than those obtainable from pressure drop across a combustor, thus generally greater than 5 psid.

Air-blast type atomizers have the advantage that fuel flow distribution is determined primarily by air-flow pattern and is relatively unaffected by fuel-flow rates. They also require no high pressure fuel pumps to operate properly. The main disadvantages include the poor atomization at start-up, where air velocity is low, and decreased lean stability limits due to fuel mixing with air. These difficulties can be overcome by placing a small simplex injector within the pintle of the nozzle in Figure 2-2. This pilot injector is sized to give good atomization at the low fuel flows required for start-up.

Much less comparative study of air-blast atomizers has been made because of their extremely varied design. The discussion of air-blast atomizer performance to follow will contain, in addition to limited results on air-blast atomizer spray quality, measured emissions from combustors with such injectors.

3. Representating Size Distributions of Liquid Sprays

Regardless of the method of operation no atomizer will produce a spray of uniform size droplets, which makes difficult describing the degree of atomization. Several different empirical distribution functions have been developed for this purpose and are given in the literature. It is not the intention here to describe these functions: Mugele and Evans (1951) review several of these and present their own modification to the normal distribution function to account for the existence of a maximum droplet diameter.

Since the size distribution in a spray frequently does not fit any of the standard or modified statistical functions, it is usually easier to understand a graphical representation as in Figure 2-3, droplet diameter versus cumulative volume. A point on the curve represents the percentage of the total spray volume that is contained in droplets of diameter equal to or less than the value associated with that point on the ordinate. Cumulative surface and number may also be plotted on

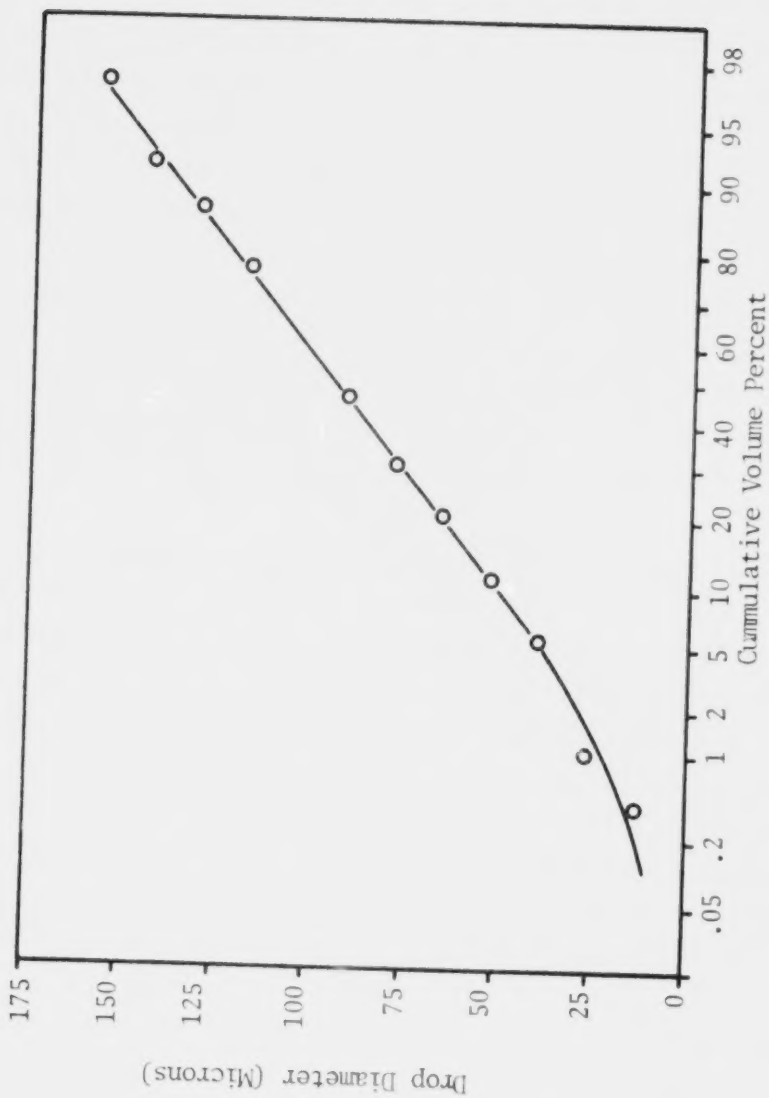

Figure 2-3. Example of Possible Droplet Size Distribution Curve

the abscissa. Plots of this type can be used to determine the value of the various median diameters, such as the mass median, which is sometimes quoted for sprays.

Depending upon the property of interest, the different mean diameters (volume, surface, etc.) are usually more descriptive of the spray than the median; for purposes of combustion a special mean, the Sauter mean diameter (SMD), is most often used. The SMD is defined as the diameter of a droplet whose volume to surface ratio is the same as the volume of surface ratio of the entire spray. The SMD can be found according to Equation 2-1 by counting and summing all of the droplets in the spray.

$$SMD = \frac{\sum nd^3}{\sum nd^2} \qquad 2\text{-}1$$

where d = diameter of droplets
n = number of droplets of diameter d.

Numerous techniques have been developed for counting the number and sizes of droplets in a spray. These range from the relatively simple methods of high-speed photographs and manual counting to highly complex techniques of electronic scanning. Early studies of sprays substituted molten wax of similar physical properties for the fuel; the wax solidified quickly after injection and the resulting drops were collected and sorted into size groups by a sieving process. Rizkalla and Lefebvre (1974) have reported success in measuring the SMD in fuel sprays by a light scattering technique. This method, although it does not produce a detailed drop count and distribution curve, is reported to give accurate values for SMD in much less time than the others.

The usefulness of the SMD for combustion applications can be seen by examining Equation 2-1 and noting that the SMD is inversely proportional to the spray surface to volume or mass ratio. This means that the Sauter mean diameter is actually an indicator of the total surface area per unit mass fuel, or a measure of the degree of atomization. It is for this reason that atomizer performance investigators often present

their results in terms of how the different variables influence the SMD.

B. Results of Atomizer Drop Sizing Studies

1. Simplex Atomizers

Three different groups of parameters influence the quality of a fuel spray: geometric aspects of the atomizer, physical properties of the fuel, and the condition of the ambient into which injection is taking place. For nozzles of the same type such as simplex, geometric considerations reduce to differences in spray angle and orifice size. Since injection angle is usually fairly constant from injector to injector, the main difference between simplex injectors is their orifice size. It is generally accepted that a simplex atomizer behaves similarly to a simple orifice in that the flow rate of fluid through it is approximately proportional to the square root of differential injection pressure. This fact is often used to characterize the size of a particular simplex atomizer by a flow number (FN).

The flow number is usually defined as the ratio of the volumetric flow rate (Q) to the square root of the differential injection pressure (ΔP) as shown in Equation 2-2, where C_d is a nozzle discharge coefficient, A is orifice area and ρ is liquid density.

$$FN = \frac{Q}{\sqrt{\Delta P}} = C_d A \left(\frac{2}{\rho}\right)^{.5} \qquad 2\text{-}2$$

If the discharge coefficient of an orifice or nozzle were constant then for a particular fluid the FN would be constant. It is well known (Radcliffe, 1960) that a simplex injector discharge coefficient changes with the flow Reynolds number. The FN then is not an injector constant. Also, even if the discharge coefficient were constant, FN is inversely proportional to the square root of fluid density. Note should also be made of the fact that FN is not a dimensionless number and care must be exercised in examining the literature to determine which units are being used; the units of U. S. gallons per hour and psid are often used. These problems create ambiguities in reporting a nozzle's size by using

a flow number unless the fluid and flow rates at which it was determined are also reported.

Fluid properties which affect atomization are viscosity, density, and surface tension. Attempts to correlate spray mean diameter as a function of these have generally disregarded the last two since they vary only slightly from fuel to fuel over the temperature range of interest. Fraser (1957) presents values of fluid properties which show that for wide ranges of hydrocarbon fuels surface tension and density vary only by a few percent while kinematic viscosity can change by a factor of 500. This does not imply that surface tension is uninvolved in droplet formation as it surely plays an important role in disintegration of the fuel sheet. The possibility of using different fuels in the future with different values of surface tension means that the importance of this property must be reexamined.

Probably the least understood of the parameters that influence injector performance is the effect of the ambient atmosphere. In a combustion chamber, air flow patterns influence the trajectory of drops, perhaps causing secondary collisions which may cause them to break into smaller drops or combine to form larger ones. These effects are usually neglected in drop formation studies and as in the analysis of droplet trajectories by Mellor et al. (1971) the processes of sheet break-up and air-droplet interaction are treated as occurring in two distinct regions. The ambient air does however influence the initial droplet formation due to the change in frictional effects between the fluid sheet and air with changes in air density. Both Decorso(1960) and Fraser (1957) observe decreases in SMD as air pressure is increased to atmospheric and attribute it to increasing air friction. Decorso (1960) however observed that further increasesin ambient pressure cause SMD to increase. This is explained as causing a reduction in spray cone angle, which permits a coalescence of the drops resulting in greater values of Sauter mean diameter. The reduction in cone angle with pressure had been observed earlier (Decorso and Kereny, 1957) and was believed to be caused by the action of entrained air flow along the sheet. Norster and Lefebvre (1972) list the decreased atomization due to spray collapse as one of the reasons

combustor smoke output increases with pressure. In general, studies of spray droplet sizes as a function of ambient pressure have been few, qualitative in nature, and no attempts at correlation are evident.

When one takes into consideration all of the above variables important for simplex atomization and performs a dimensional analysis, one obtains a set of dimensionless numbers which, when arranged in the correct functional form, should be able to predict atomization properties for a given injector, using a specified fuel and operating condition. Giffen and Murasew (1953), in performing such an analysis for simplex atomizers, suggested that the following terms should be used:

$$\frac{d}{D}, \frac{\rho_\ell V_\ell D}{\mu_\ell}, \frac{D V_\ell^2 \rho_\ell}{\sigma}, \frac{\rho_\ell}{\rho_a}, \frac{\mu_\ell}{\mu_a}$$

where d = characteristic diameter of spray, e.g. SMD
D = atomizer orifice diameter
ρ = density
V_ℓ = liquid velocity
μ = absolute viscosity
σ = surface tension of liquid
ℓ,a = subscripts for liquid and ambient gas respectively.

The second term in the set is the Reynolds number (Re) representing the ratio of fluid inertial to viscous forces, and the third is the Weber number (We), the ratio of inertial to surface tension forces. If all of the determining parameters have been accounted for, then any one of the above group may be written as a function of the remaining four. Since we are interested in the characteristic dimensions of the resulting spray this might be written as

$$\frac{SMD}{D} = \phi(Re, We, \frac{\rho_\ell}{\rho_a}, \frac{\mu_\ell}{\mu_a}). \qquad 2\text{-}3$$

It should be noted that the dimensionless groups are not unique, but they should be independent; for example We^2 might be used to replace We. Also, the omission of any important variables in the original

formulation will produce a different set of dimensionless groups than if they are considered. Some investigators (Giffen and Muraszew, 1953; Taylor, 1950) feel that the scale of turbulence in the exiting liquid is of great importance and should be accounted for in the dimensional analysis by considering the film thickness in the orifice (orifice diameter less air core diameter) as a parameter.

Ideally an experimental investigation would vary one of the dimensionless groups while keeping the others constant and determine the importance of each group, one at a time. In practice this is seldom if ever done for several reasons. First, it is often difficult to vary fluid properties and operating conditions in such a manner that only one of the groups changes; second, it is usually inconvenient if not impossible to determine some of the operating characteristics such as gas core diameter and fluid velocity. Most investigators resort to assumptions and simplifications to overcome these problems.

As already mentioned, few investigators have considered the influence of the ambient medium; this eliminates the last two dependent variables in Equation 2-3. The analysis is further simplified by measuring the differential injection pressure (ΔP) and using it to represent the fluid velocity. The nozzle size is usually replaced either by the flow number (FN) or the combination of volumetric flow rate and differential pressure. The resulting correlations are usually reported then in the form of

$$SMD = f(\nu, \sigma, \Delta P, Q) \qquad 2\text{-}4$$

where ν = kinematic liquid viscosity.

The above simplifications are significant and the limitations imposed by them should be clearly understood. The problem of using FN to characterize the basic nozzle dimension have already been discussed, and using ΔP to replace fluid velocity suffers from much the same shortcomings. That is to say one would not expect the relationship between ΔP and V_ℓ to be the same for changes in the size of the swirl atomizer or flow rate just as one would not expect it to be the same for changes

in fluid viscosity. It is for this reason that attempts to take data reported in terms of FN and ΔP and substitute it into expressions for Re and We (Giffen and Muraszew, 1953) have failed to produce the desired correlations. Despite these problems, the fact remains that swirl atomizer data have in the past almost universally been reported in terms of the approximations ΔP and mass or volume flow rate.

Keeping the above limitations in mind we can look at some of the correlations that have been determined for SMD as a function of dependent variables. They usually are presented as

$$SMD = \frac{k\ \nu^x\ \sigma^y\ W_\ell^z}{\Delta P^t} \qquad 2\text{-}5$$

with k, x, y, z and t being experimentally determined constants and W_ℓ mass flow rate. Table 2-1 lists the values of some of these constants along with the range of the variables for which they were determined or used. Not all of the constants were evaluated in every case and in some cases (Decorso, 1960) only one was determined.

The constant k has been evaluated in Table 2-1 so that the variables in each correlation have the same units. SMD is given in microns if ν is in centistokes, σ is in dynes/cm, ρ is in gm/cm^3, Q is in gal U.S./hr and ΔP is in psid. W_ℓ in Equation 2-5 has been replaced by the quantity $(\rho \cdot Q)$ in Table 2-1, where ρ has units of gm/cm^3.

The first correlation by Radcliffe (1960) was suggested after examining the results of several different investigations. The range of fluid properties is not given but most measurements were made with wax sprays simulating kerosene injection into atmospheric pressures. The results are presented in conjunction with a discussion of gas turbine combustors so it may be assumed that the fluid properties, flow rates, etc. would be comparable to those found in these devices. From the expression for SMD we can see that simplex atomization decreases as fluid viscosity, surface tension, and density increase. Fraser (1957) used a similar expression (Table 2-1) to evaluate values for SMD for liquids with properties shown. This correlation also was derived from a

Table 2-1. Summary of SMD Correlations for Simplex Atomizers

Reference	Range of Parameters Correlation Used For: ν (cs)	σ (d/cm)	ΔP (psid)	$P_{ambient}$	SMD[a]	SMD[b]
Radcliffe (1960)	----	----	----	1 atm	$= \frac{38.7\ \nu^{.2}\ \sigma^{.6}\ \rho^{.25}\ Q^{.25}}{\Delta P^{.4}}$	120
Fraser (1957)	4-15	20-24	<200	1 atm	$= \frac{120\ \nu^{.215}\ \sigma^{.33}\ \rho^{.2}\ Q^{.209}}{\Delta P^{.458}}$	104
Hunter et al. (1974)	12	----	~200	1 atm	$= \frac{308\ \nu^{.3}\ \rho^{.205}\ Q^{.205}}{\Delta P^{.354}}$	179
Decorso (1960)	----	----	25; 100	.5 psia	$\alpha \frac{1}{\Delta P^{.48}}$	----
				14.5 psia	$\alpha \frac{1}{\Delta P^{.54}}$	----
				114.5 psia	$\alpha \frac{1}{\Delta P^{.45}}$	----

[a] SMD is in microns when σ is in d/cm, ν is in cs, ρ is in gm/cm^3, Q is in U.S. gal/hr and ΔP is in psid.

[b] Calculated for ΔP = 150 psid, ν = 5 cs, σ = 25 d/cm, ρ = .85 gm/cm^3, Q = 40 gal/hr (typical of fuel).

search of the literature, although no basis is given for assuming that the values for the surface tension and density exponents, .33 and .2 respectively, are correct. Hunter et al. (1974) found that the Fraser correlation failed to predict correct values of SMD observed experimentally and presented their expression as being derived from the Parker-Hannifin Corporation, Accessories Division, for a variety of simplex injectors (see also Section VI). The expression of Hunter et al. (1974) ignores the influence of surface tension changes and shows an increase in the effect of fuel viscosity. It is claimed to predict SMD within 20% of the experimental value for their case. The effect of differential injection pressure is reduced from the other equations.

From a first examination of the correlations of Table 2-1 it might appear inconsistent with the previous discussion that SMD increases with Q. If one substitutes from Equation 2-2 the expression $Q \sim A\sqrt{\Delta P}$, the exponent on the ΔP term in the denominator (Table 2-2) is decreased and the orifice area (A) appears in the numerator. Recalling that ΔP is approximately proportional to the fluid velocity squared, it can then be seen that SMD increases with nozzle size and decreases with flow velocity.

None of the complex expressions for Sauter mean diameter consider the influence of ambient pressure. Decorso (1960) however did observe a pressure influence and gave it as a change in calculated value for the exponent of the differential pressure term. These values are presented as the last three entries in Table 2-1.

The first two expressions in Table 2-1 show general agreement as to the important variables and their degree of influence on the value of spray Sauter mean diameter. Least agreement occurs for the importance of changes in fluid surface tension. This is to be expected since surface tension for most fuels of interest changes little and in some cases (Hunter et al., 1974) is considered to be a constant. Giffen and Muraszew (1953) varied surface tension by a factor of three and found little change in SMD. Their maximum injection pressure ($\sim$ 40 psid) however is near the lower limit commonly accepted (Watson and Clark, 1947) as sufficient for proper operation of swirl atomizers. Numbers in the

correlating expression of Hunter et al. (1974) generally are slightly different from those of the others, especially for the values of surface tension and injection pressure exponents. The last column of Table 2-1 compares the calculated value of SMD for each correlation using the sample case. The last correlation should be of particular interest since it was developed most recently and one can assume is based on more accurate experimental data. It can be seen that it predicts a substantially larger value of SMD for the example case.

To summarize the discussion of SMD correlations for simplex atomizers, it can be said that older empirical correlations exist which give comparable numbers for fuels in common use. Some disagreement exists as to the exact value of the numbers in the expressions but a tradeoff occurs so that they give similar values of SMD. A relatively new correlation (Hunter et al., 1974) has been developed which differs somewhat from the others.

The effect of changes in ambient pressure and fluid surface tension have been least studied and are little understood. The correlations have been developed using fluids with properties in the range of those of conventional fuels and care should be used when applying them to fluids outside this range. The problems associated with using the approximations such as ΔP in the correlations have been described, and it was suggested that the more fundamental, but less easily determined, parameters such as fluid velocity be used instead. Finally, it should be stated that, although gaps still exist in the knowledge of centrifugal pressure atomizer operation, the need for filling these gaps becomes less important, for combustor applications, as pressure atomizers are abandoned for atomizers whose performance is not so closely linked to the fuel flow rate.

2. Air-blast Atomization

Unlike the well defined geometric construction typical of simplex atomizers air-blast atomizers are extremely varied in design. Nukiama and Tanasawa (1939) performed early experiments to determine the important variables for two fluid atomization, but present atomizers

using this idea bear little physical resemblance to their device. Although different air-blast configurations are possible it is claimed (Byran et al., 1971; Norster and Lefebvre, 1972) that optimum atomization is obtained by spreading the fluid into a thin film and exposing it to the action of air streams on both sides. A well-defined investigation of the influence of fluid properties and air-flow rates was performed by Rizkalla and Lefebvre (1974) using this type of atomizer.

An empirical correlation was developed from their results which expresses the Sauter mean diameter in microns with the equation:

$$SMD = 521\ V_a^{-1}\ \sigma^{.5}\ \rho^{.75}\ \left(1 + \frac{W_\ell}{W_a}\right) + .037\ \mu^{.85}\ (\sigma\rho)^{1.2}\ \left(1 + \frac{W_\ell}{W_a}\right)^2 \qquad 2\text{-}6$$

where V_a is in m/sec, μ is in centipoise, and W_ℓ and W_a are mass flow rates. The correlation was developed for the following ranges of fluid properties and air flow velocities from 60 to 125 m/sec.

Viscosity:	1.3 - 124 centipoise
Surface tension:	26 - 73 dynes/cm
Density:	.8 - 1.8 gm/cm^3

This range of air velocities is possible with conventional combustor dome pressure drops.

The correlation shows that atomization is, as might be expected, most dependent on air-flow rate and the ratio of liquid to air flows. Viscosity and surface tension increases oppose the atomization process. When one compares the correlation with the parent experimental data some discrepancies are noticed with regard to the effect of liquid density. The experimental results show plots of SMD versus ρ (all other parameters constant) go through a maximum at a value of $\rho \sim 1.5$ gm/cm^3. No indication of a extremum exists in Equation 2-6. Observance of the maximum is noted in the discussion and it is stated that further work is necessary to explain this effect.

An air-assist atomizer was examined by Hunter et al. (1974) and an empirical expression for SMD was developed. The atomizer in this study

applied air to the outside of a fluid sheet produced by a simplex atomizer. Results of adding atomizing air in the configuration are inconclusive since results are not presented for the same values of fuel flow with and without air. The correlation will not be presented here but in general it exhibits the same dominance of the air velocity and ratio of flow-rate terms.

Although the details of improving atomization with air-blast or air-assist nozzles are not completely understood the ability of these devices to improve combustor emissions has been reported. Norster and Lefebvre (1972) report reductions in all pollutant species of common interest when a dual-orifice pressure atomizer was replaced with an air-blast atomizer. For a laboratory flame at low equivalence ratios, Appleton and Heywood (1973) also report reductions in nitric oxide production as air-assist atomizer air-flow is increased. A controversy exists (see Mellor, 1974; 1975) as to whether increased atomization is the predominant contributor to these results. Appleton and Heywood (1973) attribute their results to an increase in mixing rate of the reacting species.

Whether increased atomization or increased mixing of fuel and air is more important in reducing emissions is important in understanding basic combustor operation. In order to answer this question much experimental information is needed from flames where both effects can be controlled. Section III contains a description of an experimental facility for simulating the liquid fuel spray combustion of gas turbines. Detailed study of these flames is possible by analyzing the species concentration of various internal regions. Section V presents the results of such a study for three particular flames.

III. DESIGN AND OPERATION OF THE EXPERIMENTAL COMBUSTION FACILITY

The experimental combustion facility utilized in this research was conceived and has evolved as a system capable of simulation of the combustion process within full-scale gas turbine can combustors. The basic hardware has been used in the past for examination of real combustors and details of the system can be found in descriptions by Mellor et al. (1972), Tuttle et al. (1973), and Shisler et al. (1974).

A. Facility Design

Compressed air, for burner operation, is supplied from a blow-down type storage system with a volume of approximately 85 m^3. Maximum system pressure of 150 atm permits an air flow rate of about 3 kg/sec for 40 min; smaller air flow rates can be maintained for correspondingly greater times. For short periods of time air flow rates of approximately 4.5 kg/sec are possible. Air flow rate is monitored with a differential pressure, orifice type flowmeter and is controlled by a pneumatically operated air throttle valve.

Shown schematically in Figure 3-1, the combustion facility utilizes a slave burner (a standard Allison T-56 combustor with a duplex pressure atomizer) to supply heated, vitiated inlet air to the test section. Fuel flow rates of commerical grade liquid propane to both burners are controlled via hand operated valves and are monitored with turbine flowmeters. Test section pressure is controlled by a remotely operated back pressure valve. Consisting of a moveable, conical center body, the valve determines the available flow exit area. Before being released to the atmosphere, the exhaust flow is quieted by a commercial gas turbine exhaust silencer.

At the entrance to the test section, the temperature of the incoming gas is estimated by means of a temperature rake mounted across

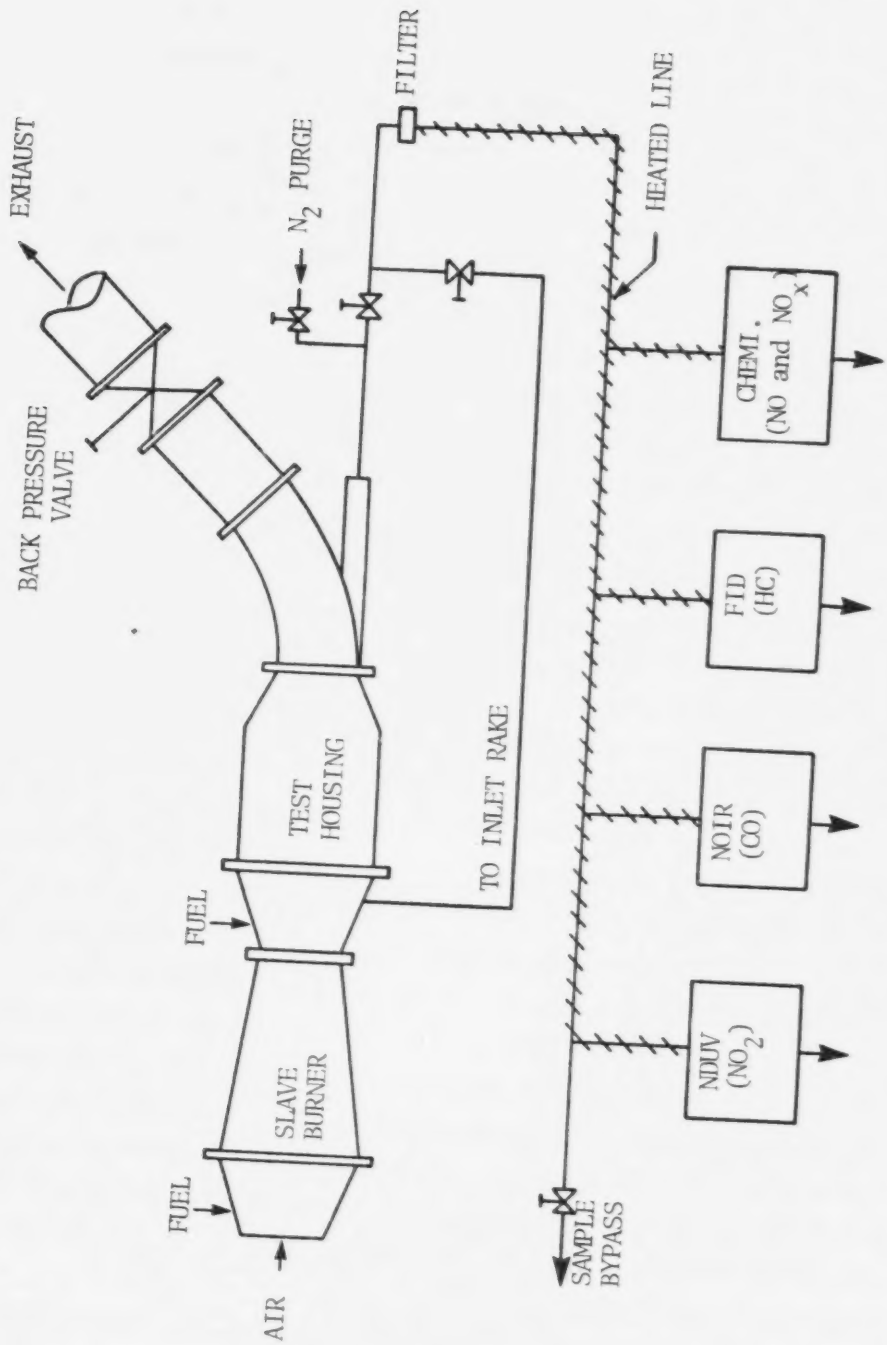

Figure 3-1. A Schematic of the Experimental Apparatus

the duct. Eight chromel-alumel thermocouple beads are positioned along a stainless steel "V" shaped bar such that they will provide an area averaged temperature. Protruding through the point of the "V", the thermocouple wires are insulated from the bar by ceramic Al_2O_3. Inlet temperature is adjusted by controlling the fuel flow to the heating combustor.

Just downstream of the thermocouple rake, samples of the vitiated inlet air to the test section can be extracted and sent to the gas analysis system via an uncooled gas sampling rake. Constructed of stainless steel tubing in the shape of a "cross", the rake has a total of sixteen collection holes, spaced so as to give an area averaged sample.

As can be seen in Figure 3-1, the gas flow is turned 45^o after leaving the test section. This allows either a water-cooled area averaging rake (described by Shisler et al., 1974) or a single point gas sampling probe to be inserted through the elbow into the flow. The single point probe is constructed of three concentric stainless steel tubes. Cooling H_2O flows in and out of the outer two passages; gas sample flows in the inner-most passage to the analyzing instruments and is quenched by both a converging nozzle inlet and the H_2O. The probe tip is offset from the main body so that, as it is rotated, the probe tip sweeps out an arc. Additional freedom of movement in the direction parallel to the combustor axis allows samples to be taken from any point along the arc in any axial plane of the test section. A platinum/10% platinum rhodium thermocouple mounted to the side of the probe allows estimates of local gas temperature.

This basic equipment is capable, with the exception of vitiated inlet air, of effectively producing in the test section conditions representative of gas turbine can type combustor operation. Inlet temperatures have been varied from 273 to 950^oK, the upper value being typical of regenerative combustor operation. Test chamber operating pressures from slightly greater than one atm to approximately 10 atm are routinely attainable. It should be emphasized at this point that, over the range of the system, it is possible to vary any one of the basic combustor operating parameters (inlet temperature, pressure, air flow rate or overall equivalence ratio) independently of the others.

B. Test Burner Configuration

The test section housing for these experiments is made of stainless steel pipe of inner diameter 14.63 cm and wall thickness of about 1.1 cm. Depicted schematically in Figure 3-2, the test section has five quartz windows 6.35 mm thick mounted 6.35 cm apart to allow visual access to the test section interior. The available viewing area for each window is a circle of diameter 3.45 cm. Figure 3-2 also shows the downstream reducing section of the housing which is kept at an acceptable temperature by circulating water through the cooling jacket. At the location of minimum area, high pressure water is injected into the gas flow via 20, 3.2 mm diameter holes, equispaced around the housing circumference. This cooling is done to protect the downstream equipment from the high temperature of the combustor exhaust gases.

For these experiments, a circular disc mounted flush with the edge of the first window is used as a flame holder. Shown in Figure 3-3, the disc is mounted to the housing by thin support struts made of 3 mm thick stainless steel, with the thin edge oriented perpendicular to the air stream in order to minimize flow disturbances. The disc has a liquid fuel pressure atomizer mounted at its center. All mounting arrangements are such that both the disc and atomizer can be easily changed. It was found that both the disc stabilized flame and the heating combustor could be ignited conveniently using CH_4/O_2 torch type igniters.

All experimental measurements obtained with the single point probe were made using an 11.43 cm diameter disc flame-holder. Exit plane data were gathered for both an 11.43 cm and an 8.89 cm disc. These flame-holders represent duct area blockage ratios of 61% and 37% respectively.

The test flame injectors were off the shelf simplex pressure atomizers similar to the one illustrated in Figure 2-1. Purchased from the Delevan Manufacturing Company, they are constructed entirely of stainless steel and were rated by the supplier at 16, 24, 35, and 50 gal/hr (water) for an injection pressure of 125 psid. The swirl atomizers have a nominal spray angle of 90° and orifice diameters of 1.2, 1.5, 1.8,

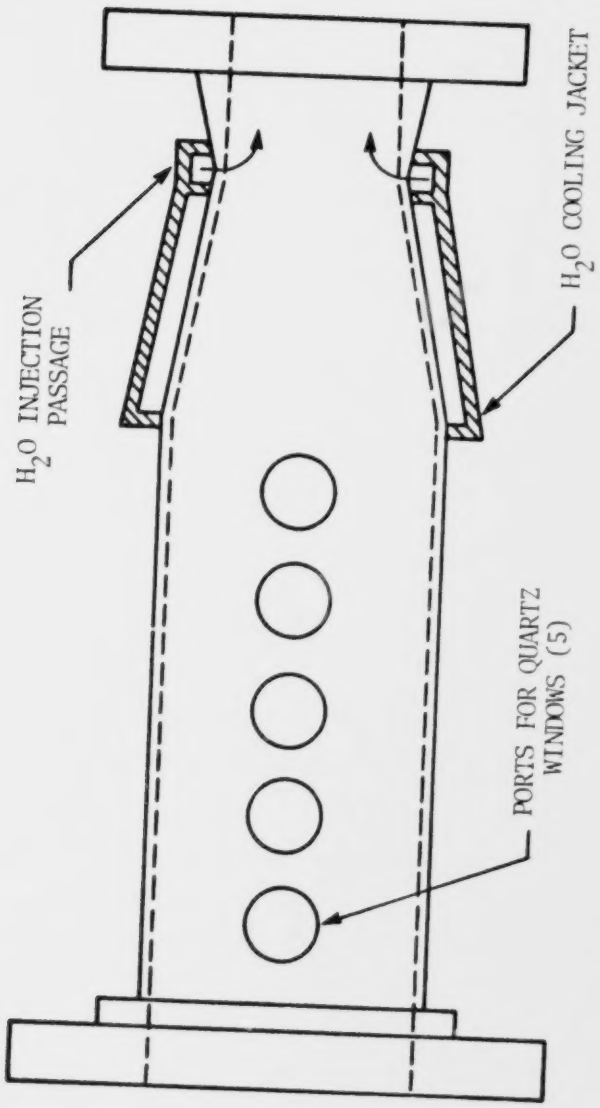

Figure 3-2. Test Section Housing Schematic

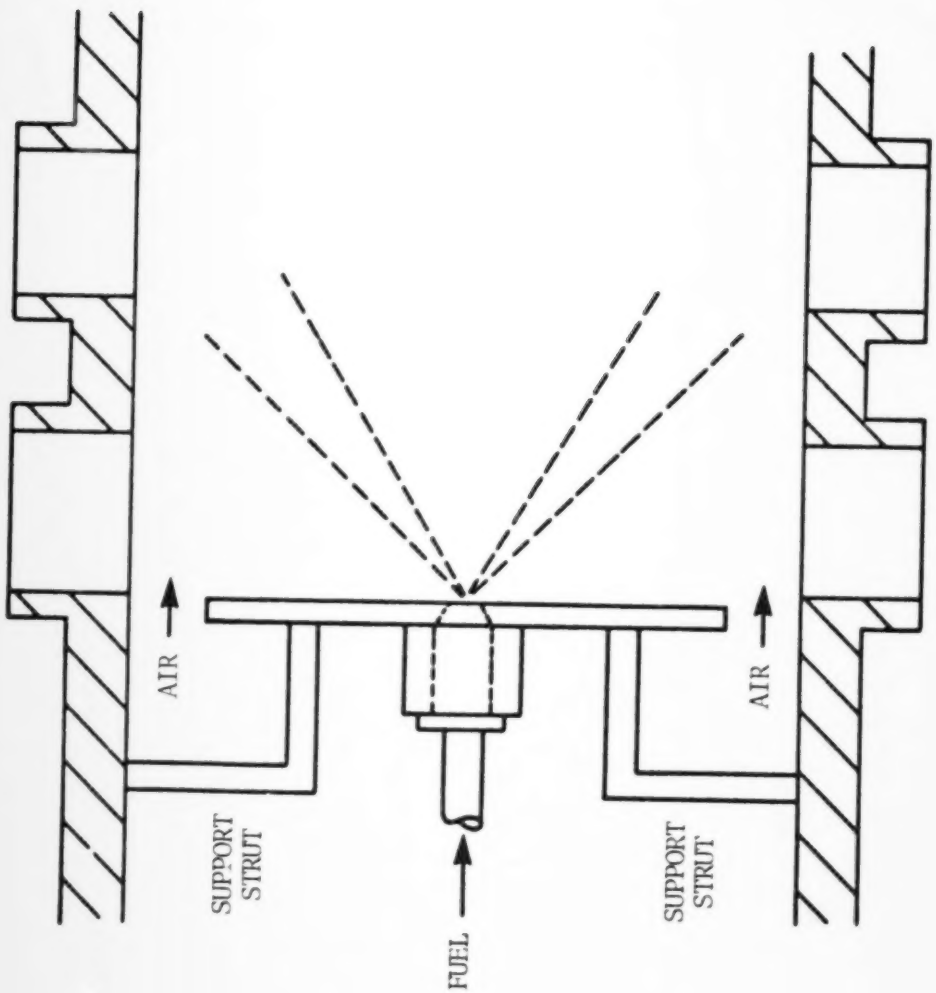

Figure 3-3. Schematic of Disc Mounting Arrangement

and 2.1 mm respectively. The nozzles were used to inject liquid propane to the disc stabilized flame in all cases.

C. Gas Analysis System

Gas samples extracted from either the test section or the inlet gas rake (see Figure 3-1) are channeled, by the use of appropriate valves, to the gas analysis system. From the valves to the instruments, the 8 m of stainless steel sample line are maintained at approximately 425^{o}K by thermostatically controlled resistive heat tapes after Vaught et al. (1971). The sample flow passes through a glass fiber filter to remove carbon particulate (98% collection efficiency for 0.05 micron particles). The sample stream was analyzed on a continuous basis for concentrations of carbon monoxide, unburned hydrocarbons, nitric oxide and nitrogen dioxide. Concentrations of carbon monoxide and unburned hydrocarbons were measured by a nondispersive infrared analyzer (Beckman model 315A) and a flame ionization detector (Beckman model 402) respectively. A chemiluminescent NO analyzer equipped with an NO_2 stainless steel converter allowed alternate monitoring of NO and total NO_x (NO + NO_2) levels. NO_2 concentrations were also measured via a nondispersive ultraviolent analyzer (Beckman model 255B).

Each of the gas analysis instruments produced an output signal in the form of a meter deflection which was visually observed and manually recorded. In addition, a complete, permanent record of the output signal was made by strip chart recorders connected to each instrument. Similar records were obtained for the voltage readings of the temperature monitoring thermocouples.

D. Single Point Probe Studies

The single point gas sampling probe was used to withdraw samples from three flames, corresponding to the three test combustor operating points listed in Table 3-1. The first operating condition, low overall equivalence ratio and low air flow rate, corresponds to an idle condition of a turbine combustor. The second flame examined is representative of a combustor operating at a cruise condition, and the third is characteristic

of full power operation. The 35 gal/hr simplex nozzle was used for all three flames.

Table 3-1. Operating Points for Single Point Probe Studies

Overall Equivalence Ratio	Air Flow Rate (kg/sec)	Combustor Pressure (atm, abs)	Inlet Air Temperature (^{o}K)
0.1	1.0	5	500
0.2	1.5	5	500
0.2	3.0	5	500

Starting 1.27 cm downstream of the disc, concentration and temperature data were collected with the single probe at selected axial and radial positions for the three flames listed in Table 3-1. For the first flame, data were taken at 12 axial planes spaced at 2.54 cm intervals. Radial probe positions were 0.0, 1.3, 2.5, 3.8, 5.1, 5.7, and 6.4 cm from the centerline of the disc. The radial probe trace and the sampling points are shown in Figure 3-4 along with the orientation of the disc support struts. The remaining two flames listed in Table 3-1 are for increased air flow rates. Here the mixing processes in the flow are improved and the concentration gradients are expected to be less steep. Thus for these two flames a coarser grid was selected, and no data were taken at the 26.67 cm axial plane or the 5.7 cm radial position. In addition, only limited data were collected at the 21.59 cm axial plane.

A high degree of accuracy in the axial probe position is assured by the design of the motor driven carriage upon which the probe is mounted. However lesser accuracy is inherent in the radial positioning. In particular due to the length of the axial traverse ($\approx$ 30 cm), a slight misalignment of the probe (i.e., the probe and duct centerlines not being exactly parallel) results in a change in the radial position of the probe tip from the duct centerline as the axial movement occurs. A probe misalignment error of

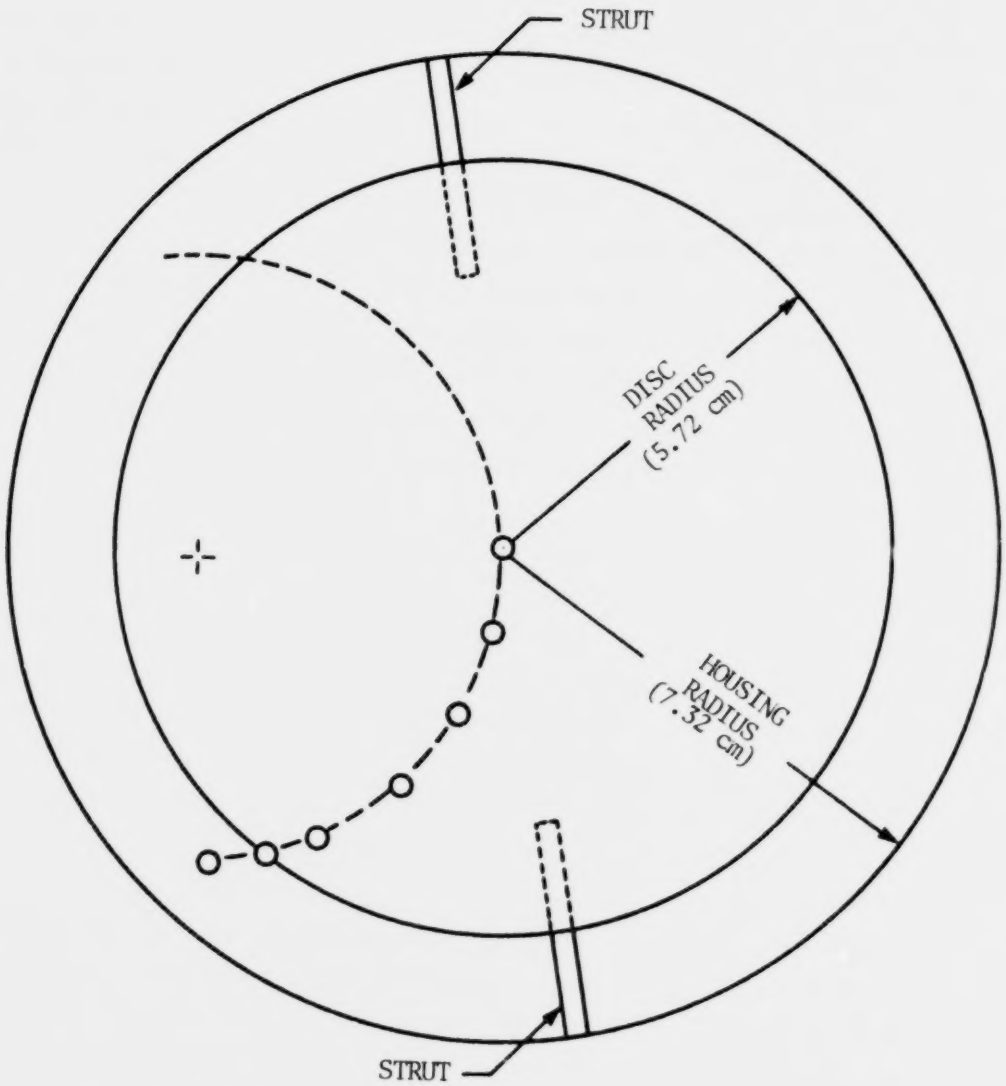

Figure 3-4. View, Looking Upstream, of Disc, Support Struts, and Probe Trace With Sampling Points

only an angle of 0.5^{o} between the probe and the duct centerlines gives rise to a 0.25 cm error in radial placement after a 30 cm traverse.

As a consequence of the large length to diameter ratio of the probe, some error in the sample tip location due to flexing of the probe during combustor operation does occur. This oscillation of the probe tip about an equilibrium position is greatest in the region behind the disc where the main flow streamlines bend toward the duct centerline. Hence in this region of the flow field, only an average sample over the amplitude of the oscillation is possible.

The above mentioned causes of radial probe placement error along with any initial positioning error will be shown in Section V to be a major source of data scatter from run to run. In particular any inability to accurately position the probe will greatly contribute to the irreproducibility of measurements taken at grid points where large gradients exist in the flow.

Normal operating procedure for single point probe data acquisition was, after proper calibration of the temperature and gas concentration monitoring instruments, to ignite both the heating and test combustors and adjust them to the desired operating conditions. When it was determined that the values of the incoming pollutant concentrations (as measured using the inlet gas sampling rake) were no longer changing, the actual sampling began. This warm-up and adjustment period took on the order of 5-10 min. Starting with the probe tip at one of the radial positions in Figure 3-4 and in the axial plane closest to the disc (1.27 cm), it would then be withdrawn, stopping at each selected axial plane. In this manner, data were collected at each of the sampling points. At least two readings (taken on different days) were obtained at each sampling point. Thus if the gathering of a complete set of data for one radial position is called a run, a minimum of fourteen runs was required to obtain and reproduce the information necessary to provide a picture of the structure of the low air flow rate flame.

E. Exhaust Plane Studies

Exit plane emissions data for independent variations in overall equivalence ratio, air flow rate, combustor pressure, and inlet air

temperature were collected using a water cooled, area averaging rake located 32.2 cm downstream of the disc. The selected operating conditions for these variations from a base point are listed in Table 3-2. The procedure for gathering the exit plane data was, after adjusting the combustion system to the desired operating parameters, to measure the values of the incoming pollutant concentrations via the inlet gas sampling rake and then to measure the emissions of the test burner. Samples at all nine operating conditions listed in Table 3-2 could be taken during a single run.

The experimental results are presented in the following sections along with a discussion about the flame characteristics and the physical processes occurring in the flame. A complete listing of data obtained with both the single point probe and the water cooled rake is contained in Appendix I.

Table 3-2. Operating Points for Exit Plane Data

Overall Equivalence Ratio	Air Flow Rate (kg/sec)	Combustor Pressure (atm, abs)	Inlet Air Temperature (^{o}K)
Base Operating Point:			
0.2	1.0	5	500
Other Operating Points:			
0.2	1.0	5	450
0.2	1.0	5	550
0.2	1.0	2	500
0.2	1.0	8	500
0.2	0.5	5	500
0.2	1.5	5	500
0.1	1.0	5	500
0.3	1.0	5	500

IV. CHARACTERISTIC TIMES FOR COMBUSTION AND POLLUTANT FORMATION IN GAS TURBINE COMBUSTORS

The combustion of liquid fuel sprays in a realistic burner is an extremely complex phenomenon, involving the simultaneous processes of heat, mass, and momentum transfer in a reacting turbulent flow. Before a mathematical simulation of liquid spray combustion is justified, an improved knowledge of the controlling physical parameters must be realized. These controlling parameters are expected to include fuel characteristics, fuel drop size, spatial distribution of the fuel droplets, and the aerodynamics of the combustion device. One of the goals of the present research is to develop these parameters (via time scales) which characterize the complex physical processes occurring within a gas turbine combustor. It is hoped that these time scales will prove useful as design aids in the development of low emission combustors.

To aid in the identification of characteristic times with a particular region of the flame structure, a schematic of the flame model for the present experiments is shown in Fig. 4-1. Notice that although the experimental burner, discussed in the previous section, is axi-symmetric, the device does retain many of the characteristics of a conventional combustor. In particular a strong interaction between the liquid fuel spray and recirculation zone is simulated.

Following Mellor (1975) (Table 4-1), five time parameters will be used to characterize gas turbine combustion and pollution formation phenomena. The first time listed, the fuel droplet lifetime, is of paramount importance in determing the heterogeneous properties of the combustion process and is of course associated with the fuel spray region of Fig. 4-1.

The second and third time parameters of Mellor (1975) are both associated with the turbulent mixing properties of the reacting flow field. τ_{fi}, which characterizes the mixing process near the fuel injector,

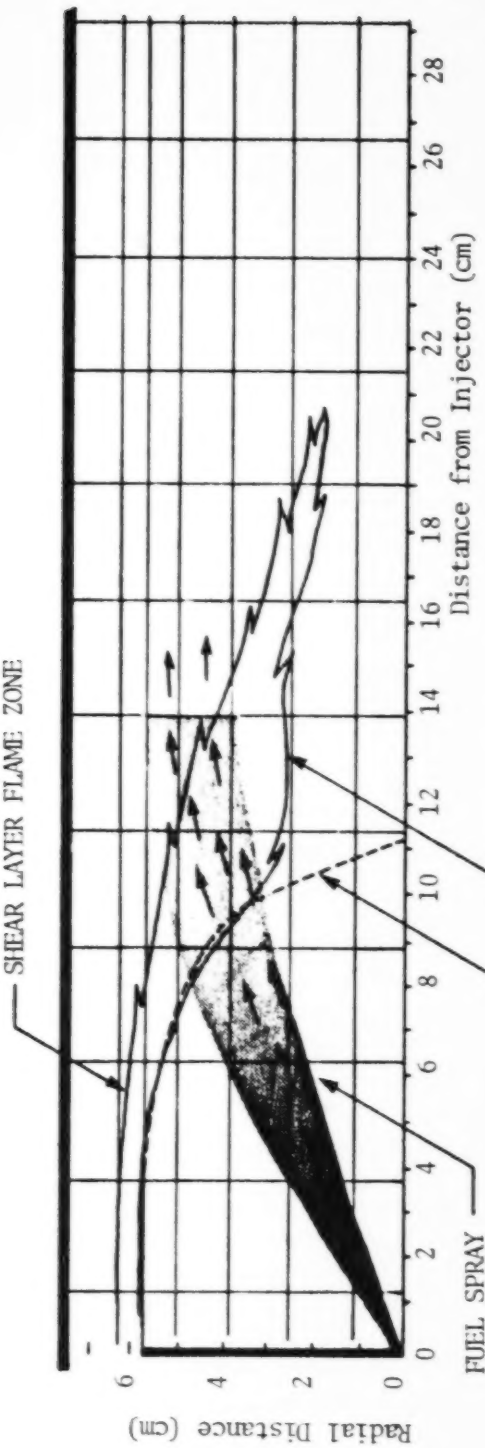

Figure 4-1. Schematic of the Postulated Flame Zone Model

is expected to be of increasing importance in combustors utilizing air blast or air assist nozzles. The turbulent mixing occurring in the shear layer region (see Fig. 4-1) is characterized by $\tau_{s\ell}$ and is associated with all combustors which have a recirculating flow region.

Table 4-1. Characteristic Times for Combustion and Pollutant Formation in Two-Phase Turbulent Flow (from Mellor, 1975)

Time	Symbol	Physical or Chemical Processes
Fuel droplet lifetime	τ_{eb}	Droplet evaporation and/or combustion
Eddy dissipation time for injected fluid	τ_{fi}	Small scale turbulent mixing near the fuel injector in the recirculation zone
Eddy dissipation time in the shear layer	$\tau_{s\ell}$	Large scale turbulent mixing between fresh air and the recirculating burned gas - fuel mixture
Fuel ignition delay and burning time	τ_{hc}	Homogeneous combustion of the fuel to CO_2
NO formation time	τ_{no}	Homogeneous kinetics for NO formation

The last two times listed in Table 4-1, τ_{hc} and τ_{no}, are scales which represent the times required for homogeneous combustion of the fuel and NO formation, respectively. As will be seen, τ_{hc} is generally very short compared to τ_{no}

Each of the five times listed in Table 4-1 is discussed in detail below. Not only will the effect of each time on the overall combustion process be included, but also methods of estimating these time parameters. Finally, the utility of these times will be demonstrated in the analysis of the experimental results (Sections V and VI).

A. Heterogeneous Processes

Mellor (1973) showed that for a gas turbine combustor operating near idle, poor atomization of the liquid fuel spray could result in

increased emission indices of CO, HC, and NO. Hence in order to correlate burner emissions over a wide range of operating parameters, the atomization properties of the fuel nozzle must be considered over the same range. The atomization efficiency at a given operating point will determine the importance of heterogenous processes in the overall combustion process.

As discussed in Section II, the degree of atomization of the liquid fuel spray can be characterized by the SMD of the spray. For a simplex pressure atomizer, Equation 2-4 shows that the SMD of the spray is dependent upon fuel properties, fuel differential injection pressure, and volumetric fuel flow rate. It now remains to define a characteristic heterogeneous time as a function of the SMD.

For droplet evaporation or combustion which obeys the "d^2 law" of Godsave (1953),

$$d^2 = d_o^2 - \beta t \qquad 4\text{-}1$$

where d = instantaneous drop diameter
d_o = initial drop diameter
β = evaporation or combustion coefficient
t = time.

A characteristic time for droplet evaporation or combustion can now be taken to be the droplet lifetime. From Equation 4-1, the droplet lifetime, τ_{eb}, is seen to be

$$\tau_{eb} = d_o^2/\beta \qquad 4\text{-}2$$

β (defined by Equations 4-3, 4-4, and 4-5 below) is a function of fuel and ambient gas properties. For convective atmospheres, β is also a function of the Reynolds number based on the mean drop size and drop relative velocity. Mellor (1972) summarizes the empirically determined dependence of β upon the Reynolds number.

$$\beta = \beta_o \, (1.0 + f(Re, Sc)) \qquad 4\text{-}3$$

$$\beta_o = \frac{8k}{\rho_\ell \, c_p} \ln (1 + B) \qquad 4\text{-}4$$

$$B = \frac{c_p \, (T - T_\ell)}{L} \qquad 4\text{-}5$$

where β_o = evaporation coefficient in a stagnant atmosphere

k = gaseous thermal conductivity

ρ_ℓ = density of liquid fuel at T_ℓ

c_p = gaseous specific heat at constant pressure

B = transfer number for droplet evaporation

T = temperature of ambient gas

T_ℓ = boiling point of liquid fuel at the local pressure

L = sensible enthaply of the liquid fuel from the initial temperature to T_ℓ plus the latent heat of evaporation.

Any parameter capable of correlating combustor emissions is expected to include a functional dependence on τ_{eb}, with the strongest dependence being at idle. As can be seen from Equation 4-2, the magnitude of τ_{eb} is determined by the initial drop diameter and the evaporation coefficient. Hence to vary τ_{eb} at a constant operating condition (i.e. no change in ϕ_o, $\dot{m}_{air}$, $T_{inlet\ air}$, or P) will require either a change in fuel injector or a change in fuel type.

B. Turbulent Mixing Processes

Before the fuel and air can react they must be mixed together. This mixing must occur at the molecular level and at this level it can only be carried out by molecular diffusion. Turbulent mixing greatly enhances this molecular diffusion process by:

a. large scale transport of fuel-rich mixture into air-rich mixture zones and vice versa;

b. rapid and very extensive straining of the fluid elements

> so produced so that concentration gradients become very large and are continually steepened and the areas of isopleths (the highly convoluted surfaces of constant concentration) also become very large and are continually increased*. These processes give molecular diffusion the two things needed (large area and steep gradients) to achieve very high molecular mixing rates.

The isopleths of course fluctuate in position rapidly with time so that the concentration at a point varies. Mean concentrations of fuel and oxidant may indicate that fuel and oxygen are both present at a point, but due to these fluctuations they may be present at the point at different times. This is the phenomenon of "unmixedness" (Hawthorne et al., 1949) that limits chemical reaction rates below those indicated by mean concentrations.

Gas turbine primary zones and the model combustor studied here have a combustion mechanism which is characteristic of diffusion flames (Mellor et al. (1972), Tuttle et al. (1973), and Shisler et al. (1974)). The rates of chemical reaction are limited by the rate of mixing of fuel and air. Thus it can be expected that a characteristic time (or times) associated with turbulent mixing processes will be most important in the correlation of combustion and pollutant formation phenomena.

Another feature of diffusion flames is that chemical reaction occurs at or near the stoichiometric isopleth (Hawthorne et al., 1949). In turbulent flow this isopleth fluctuates and thus there is an appearance of the chemical reaction being spread out over a zone, whereas instantaneously reaction is being carried out over quite a small volume. It is in this small volume around the stoichiometric isopleth that temperatures are high and nitric oxide is formed. Thus it will be characteristic times associated with this stoichiometric isopleth that will be important for nitric oxide formation.

---

*Molecular diffusion decreases the gradient and reduces isopleth area (by nibbling away proturberances) so that a dynamic balance is reached.

Soot formation on the other hand occurs under very fuel rich conditions and so will be characterized by time scales associated with the fuel rich regions of the mixing pattern particularly near the fuel nozzle.

Carbon monoxide is a combustion intermediary which is stable in quite large concentrations at flame temperatures and burns out in the relatively fuel lean regions on the air side of the flame and so will be characterized by times appropriate for this region.

Mixing processes in diffusion flames are analogous (Hawthorne et al., 1949) to those in mixing without chemical reaction. Although the analogy is not completely quantitative due to the effects of heat release turbulent processes can be expected to occur by essentially the same mechanisms and to be characterized by similar parameters. Table 4-2 shows some characteristic turbulence scales important in turbulent mixing. The relationships between these scales, originally developed for isotropic turbulence, have been found to be good approximations in inhomogeneous shear flow turbulence where mixing occurs without chemical reaction. These relationships have been assumed to hold for combustion conditions and turbulence scales have been computed for a typical combustor. The wide range of values shown emphasize the complex structure of the flow in a gas turbine combustion chamber. The same range will apply to the model combustor of the present study as this shows the same features of a thin shear layer associated with the air entry. This substructure has its own "largest eddy" size or integral length scale; it is a turbulent flow structure within the general turbulent flow which can be important for such things as stability. For air blast atomizers another such substructure exists. At the other end of the scale we can consider the flow which is turbulent on the scale of the whole combustor diameter. This turbulence is of much larger scale and is not really fully developed in the primary zone of a gas turbine combustor. It represents the limit to which the gross mixing scales (responsible for a. above), that grow with distance in the shear layer and jets, can reach. (It is the large scale processes which are controlling and set the rates for process b. above).

This large range of turbulence scales can be very important in determining combustion phenomena. It has already been pointed out

Table 4-2. Turbulence Scales

Type	Symbol	Name	Formal Definition	Relationship	Value in Combustor Shear Layer/Main Flow	Description
Length	L	Integral Length Scale	$L \equiv \int_0^\infty R_{vv} dy$	$\epsilon \approx u'^3/L$	5 to 150 mm	Largest eddy size
	λ	Taylor Microscale	$\epsilon \equiv 15\,\nu \frac{u'^2}{\lambda^2}$	$\lambda \approx 4L\, Re_L^{-1/2}$	0.2 to 4 mm	Smallest eddy size; characteristic of the dissipation of energy
	η	Kolmogoroff Length Scale	$\eta \equiv \left(\frac{\nu^3}{\epsilon}\right)^{1/4}$	$\eta \approx L\, Re_L^{-3/4}$	5 to 100 μm	Smallest fluctuation size (wave) at viscous cutoff
Velocity	u'	RMS Velocity Fluctuation	$u' \equiv \left(\overline{u^2}\right)^{1/2}$	----	50 to 10 m/sec	Velocity fluctuation of large eddies
	υ	Kolmogoroff Velocity Scale	$\upsilon \equiv (\nu\epsilon)^{1/4}$	$\upsilon \approx u'\, Re_L^{-1/4}$	5 to 1 m/sec	Velocity fluctuation in smallest waves
Time	T_L	Internal Time Scale	$T_L \equiv L/u'$	----	0.1 to 15 msec	Lagrangian time scale of largest eddies
	T_K	Kolmogoroff Time Scale	$T_K \equiv \left(\frac{\nu}{\epsilon}\right)^{1/2}$	$T_K \approx \frac{L}{u'} Re_L^{-1/2}$	1 to 100 μsec	Langrangian time scale of smallest wave

Table 4-2. Cont'd

Type	Symbol	Name	Formal Definition	Relationship	Value in Combustor Shear Layer/Main Flow	Description
	T_c	Corrsin Time Scale	$T_c \equiv \lambda^2/6\nu$	$T_c \tilde{\propto} 2\frac{L}{u'}$	0.2 to 20 msec	Time scale for dissipation of concentration fluctuations
	χ^{-1}	Molecular Diffusion Time Scale	$\chi \equiv 2D\ \overline{(\nabla\xi)^2}$	$\chi \tilde{\propto} \frac{2u'}{L}\ \overline{\xi'^2}$	0.1 to 20 sec	See Bilger (1975).
Scalar	ξ'	RMS Fuel Fraction Fluctuation	$\xi' \equiv \left(\overline{\xi'^2}\right)^{1/2}$	----	0.02 (0.3 equivalence ratio)	Fuel fraction fluctuation in largest eddies
	Σ	Scalar Scale	$\Sigma \equiv \left[\overline{\chi\left(\frac{\nu}{\epsilon}\right)^{1/2}}\right]^{1/2}$	$\Sigma \tilde{\propto} \sqrt{2}\ \xi'\ Re_L^{-1/4}$	0.04 equivalence ratio	Fuel fraction fluctuation in smallest waves

ϵ = dissipation rate of turbulent kinetic energy per unit mass

ν = kinematic visocity and taken as approximately equal to the diffusivity, D

R_{vv} = y spatial correlation of turbulent velocity

Combustor Conditions: 5 atm, Re_L (shear layer) = 10^4, Re_L (main flow) = 2×10^4, can diameter = 15 cm, air penetration jet hole diameter = 5 mm

that many of these combustion phenomena are strongly coupled to stoichiometry. Denoting the equivalence ratio by ϕ we have that soot formation is important for $\phi \sim 2\text{-}5$, NO formation for $\phi \sim 1$ and CO burn out for $\phi \sim 0.7$. Depending on the design of the combustor and the mixing patterns generated these isopleths will lie in regions having different factors controlling the turbulence scales.

Thus in a gas turbine combustor with a stoichiometric primary zone the $\phi = 1$ isopleth fills the whole primary zone while the $\phi = 0.7$ isopleth will lie close to the air jets and shear layers and the $\phi = 2\text{-}5$ isopleth will be close to the fuel nozzle and spray cone. The turbulence scales will be associated correspondingly: for nitric oxide ($\phi \sim 1$) turbulence scales associated with the flame tube diameter, and for soot and carbon monoxide the much smaller turbulence scales associated with the mixing around the injector and the air inlets respectively. Leaning-out or richening-up the primary zone does not change the stoichiometry under which these reactions occur (we still have a diffusion flame) but it does change the positions of the $\phi = 2\text{-}5$, 1, and 0.7 isopleths and the time scales that will be associated with them. Thus a lean primary zone will have $\phi = 2\text{-}5$ and 1 closer to the fuel spray where time scales are shorter thus reducing soot and NO formation and the $\phi = 0.7$ contour almost filling the whole primary zone with longer time scales to give CO burn out. A rich primary zone will have the opposite effects on $\phi = 2\text{-}5$ and 0.7 and hence on soot and CO but will have the same effect on $\phi = 1$ and hence NO by moving this contour closer to the air inlets.

In the model combustor studied here there is no purposely formed primary zone but the same concepts apply. The mixing patterns are more like those in a turbulent jet diffusion flame with the added complication of a strong recirculation zone behind the baffle. Near the baffle the $\phi = 2\text{-}5$, 1 and 0.7 isopleths all lie in the shear layer extending downstream from the disc rim. These isopleths will come to the centerline of the combustor some distance downstream of the baffle, the distance depending on the fueling rate compared to the air entrainment rate. Provided the $\phi = 0.7$ isopleth never reaches the combustor exit plane CO emissions should scale with a time scale appropriate to the

shear layer near the rim of the disc since quenching will occur here whereas near the centerline there will be sufficient time for burn-out. For NO on the other hand very little will be formed in the shear layer near the rim, most of it being formed in the downstream half of the shear layer and in the region near the centerline downstream of the recirculation zone; the appropriate time scale will thus be one associated with large scale turbulence which fills the duct at that point.

Returning to Table 4-2 it can be seen that four different time scales can be associated with the turbulence. Only one of these, the Kolmogoroff time scale, has an inherently different behaviour, incorporating as it does a Reynolds number dependence. This time is associated with molecular processes at the finest scales of turbulence but since these processes go in both directions, e.g. first richening the mixture and then leaning it, this time has little to do with the total time available for chemical reaction. An appropriate time scale for this is the Corrsin time scale T_c (derived in Appendix II) and this is of the order of the integral time scale, T_L; it describes the time required for dissipation of concentration fluctuations which of course is allied to the time for the loss of coherence of an eddy. It is also closely related to the molecular diffusion time scale X^{-1} which incorporates the actual level of concentration fluctuations (note $T_c = X^{-1} \overline{\xi'^2}$) which is often important where chemical reactions are involved (see Bilger 1975). Another time scale which can be important is a convective or mean dilution time which is associated with the mean flow velocity and not the turbulence. In most systems however turbulence and mean flow are closely interrelated and the two will be proportional. In summary then we can take the various time scales of importance as being essentially determined by L/u', but we have to make sure that we choose L and u' correctly for the region of interest.

For the case of a fixed combustor geometry, the time scales discussed above are inversely proportional to the turbulent (rms) velocity. However if the rms velocity is but some fraction of the mean convective velocity, then the turbulent time scales are just inversely proportional to the convective velocity. Hence for this case, pollutant emissions

should correlate with a representative convective velocity (inverse of time). This is the basis for the correlation of NO, CO, and HC emissions with the reference velocity (defined as the total combustor air flow divided by the product of the combustor inlet density and the maximum cross-sectional area), a parameter used successfully by NASA workers for many years. (See, for example, Grobman (1972) and Jones and Grobman (1973)).

For geometrically similar combustors operating at the same overall equivalence ratio all the relevant L's and u's will scale with V_{ref} and D, the overall combustor scales. Thus all the turbulent mixing times will under these conditions be proportional to D/V_{ref} which itself is proportional to the combustor residence time. This explains the correlations obtained with unmodified combustors for emissions vs. residence time; the design philosophy led to similar geometrical relationships and mixing patterns. However once geometry and equivalence ratio are modified the different pollutants will not correlate in the same way with residence time since now the relationships of the relevant L/u's to the residence time are being changed.

In the present work the geometry of the model combustor has been varied and the results do show that CO and NO have different time scale behaviour. In the light of the above it would appear that the time scale chosen for CO burnout should reflect that in the outer (and colder) portion of the shear layer while that for NO should be for the inner (and hotter) portion of the shear layer and for the centerline region immediately downstream of the recirculation zone. Hence a unique shear layer mixing time scale, $\tau_{s\ell}$, is not appropriate for the correlation of both CO and NO_x emissions.

For the outer periphery of the shear layer the appropriate turbulence velocity scale, u', will be a function of the velocity through the annulus. Hence it is convenient to define the following reference velocity for the experimental combustion system:

$$V_{ref} = \frac{\dot{m}_{air}}{\rho A} = \frac{\dot{m}_{air} R T_{inlet\ air}}{P A} \qquad 4\text{-}6$$

Here $\dot{m}_{air}$ is the mass flow rate of air through the burner, ρ is the combustor density, A is taken to be the flow area at the disc location (area of duct minus area of disc), R is the gas constant, $T_{inlet\ air}$ is the temperature of the incoming air stream, and P is the combustor pressure. Note that V_{ref} is based only on the incoming fluid mechanics properties, and that the assumption of an ideal gas has been applied.

The length scale, L, is more difficult to choose as in the shear layer it grows linearly with distance from the disc rim. An appropriate length scale might be the one where the shear layer meets the fuel spray which will be proportional to the disc diameter, d, yielding

$$\tau_{s\ell,co} = \frac{d}{V_{ref}} \qquad 4\text{-}7a$$

Alternatively the actual gas velocity in the outer periphery of the shear layer is expected to fall between V_{ref} and the burned gas velocity through the full duct area. Hence an average of these two velocities could be taken for the CO time parameter. In addition, an appropriate length scale for the turbulence in the outer shear layer could also be taken as the gap dimension between the disc and the duct wall. Thus a second possible time scale for CO quenching in the shear layer is

$$\tau_{s\ell,co} = \frac{D - d}{V_{ref}\left[1 + \frac{T_b}{T_{inlet\ air}}\left(1 - \left(\frac{d}{D}\right)^2\right)\right]} \qquad 4\text{-}7b$$

where D is the duct diameter and T_b is the temperature of the burnt gas.

The whole shear layer can also be considered as a turbulent reactor and the Corrsin time scale (see Table 4-2) calculated for the average dissipation of concentration fluctuations in this volume (which is related to the quenching rate) could be taken as $\tau_{s\ell,co}$. From the derivation of Appendix II, this yields

$$\tau_{s\ell,co} = C\left(\frac{ML^2}{\dot{W}}\right)^{1/3} \qquad 4\text{-}7c$$

Each of the above three time scales for use in the correlation of CO emissions resulting from turbulent mixing phenomena in the shear layer appears equally valid. Hence all three methods of calculating $\tau_{s\ell,co}$ will be employed in Section VI for the correlation of the experimental burner CO emissions.

For NO formation the appropriate length scale will be the disc diameter d and a velocity somewhere between that for unburnt and fully burnt flow through the full duct area. This yields

$$\tau_{s\ell,no} = d/\left[\frac{V_o}{2}\left(1 + \frac{T_b}{T_{inlet}}\right)\right] \qquad 4\text{-}8$$

where V_o is the duct velocity of the unburnt gas and T_b is the temperature of the burnt gas.

It should be pointed out that the two geometries (two different disc sizes) will give mixing patterns which are only quasisimilar. The above time scales do not reflect the changes in the $\phi = 1$ and $\phi = 0.7$ isopleths which will occur because of the geometry change and the altered spray characteristics. Accordingly perfect correlation should not be expected.

C. Homogeneous Reaction Times

Two additional times also inherent to gas turbine combustion have yet to be discussed. Both of these times are associated with the homogeneous chemistry of the fuel/air combustion. The first is the fuel ignition delay and burning time, τ_{hc}, and is the time required for the molecular reactions to proceed once the fuel vapor and air are mixed. This time is most easily varied through variation of the local gas temperature and is pertinent to performance and low power emissions. Values of τ_{hc} versus overall equivalence ratio were estimated by Vranos (1974) by dividing laminar combustion wave thickness by the laminar burning velocity. For convenience the results of the τ_{hc} calculations of Vranos (1974) are listed in Table 4-3.

The last characteristic time of significant importance in a gas turbine combustor is the time for the formation of NO emissions. A characteristic time for NO formation, τ_{no}, was also defined by Vranos (1974) as

$$\tau_{no}^{-1} = \frac{1}{[NO]_{equil}} \quad \frac{d[NO]}{dt} \qquad 4\text{-}9$$

Values of τ_{no} were estimated by Vranos (1974) utilizing the kinetics model of Heywood et al. (1970). Again, the results of the calculations are listed in Table 4-3 for convenience.

Table 4-3. Values of τ_{hc} and τ_{no} (from Vranos, 1974) (P = 15 atm; $T_{inlet\ air}$ = 700°K)

ϕ	τ_{hc} msec	τ_{no} msec
0.7	0.20	330
0.8	0.17	53
0.9	0.15	15
1.0	0.13	7
1.1	0.16	23
1.2	0.20	109
1.4	0.40	>1000

D. Dependence of the Flame Structure on the Characteristic Times

In a conventional gas turbine combustor, the flame structure is strongly dependent upon the rate of gaseous fuel addition from droplet evaporation (characterized by τ_{eb}) and the subsequent mixing of the fuel vapor with fresh oxidizer (characterized by $\tau_{s\ell}$). Typically, τ_{hc} is significantly lower than either τ_{eb} or $\tau_{s\ell}$ and hence this time does not appreciably affect the flame structure. The magnitude of τ_{hc} is however important to stability considerations. Also, the time for NO formation, τ_{no}, does not influence the basic flame structure but rather is dependent upon it.

The physical structure and appearance of a liquid fueled flame will change significantly as the magnitudes of τ_{eb}, $\tau_{s\ell}$, and τ_{fi} are altered. With pressure atomizing nozzles, τ_{fi} is long which leads to extremely fuel rich regions in the vicinity of the injector. As these rich regions are at an elevated temperature, an excessive amount of soot is generated. Hence a high value of τ_{fi} yields a very luminous flame accompanied by excessive radiative heat transfer. Variation of the fuel flow rate through a pressure atomizer has little affect upon τ_{fi} and thus soot will be formed at nearly all combustor operating points.

One means of dramatically reducing τ_{fi} is through the use of an air atomizing nozzle. Both the injected air and the increased shearing action produced by it help to decrease τ_{fi}. Several investigators have indeed noted a large reduction in smoke emissions through use of an air assist nozzle. (See, for example, Norster and Lefebvre (1972)).

Perhaps the easiest way to analyze the importance of τ_{eb} and $\tau_{s\ell}$ in determining the flame properties is to examine the ratio of $\tau_{s\ell}$ to τ_{eb}. Three cases of this ratio are listed in Table 4-4.

In case (a), the time required for mixing is much greater than that for droplet evaporation. Here eddies of vaporous fuel will form prior to any mixing. This could lead to burning on the surface of these fuel eddies which would result in sustained high temperatures and thus high NO_x formation even though the fuel injector efficiency is good. The relative slowness of the mixing process results in fuel rich regions within the flame zone which gives rise to soot formation and hence a yellow flame. These values of $\tau_{s\ell}$ and τ_{eb} will result in a combustor operating near idle (low air flow rate) but with a fuel injector selected for good atomization at the idle fuel flow.

τ_{eb} and $\tau_{s\ell}$ are of comparable magnitudes in case (b) of Table 4-4, and both have to be included in any parameter used to correlate combustor emissions. The atomization of the liquid fuel is somewhat poorer and the mixing is improved over case (a). This flame structure is typical of a gas turbine combustor operating at a cruise condition if the fuel nozzle is selected to give a well atomized spray at the full power design point.

Table 4-4. Limiting Cases of $\tau_{s\ell}/\tau_{eb}$

Case	Characteristic Time Ratio	Flame Characteristics	Atomization	Mixing
(a)	$\tau_{s\ell}/\tau_{eb} >> 1$	Small drops, poor mixing	Good	Poor
(b)	$\tau_{s\ell}/\tau_{eb} \sim 1$	Larger drops, improved mixing	Fair	Fair
(c)	$\tau_{s\ell}/\tau_{eb} << 1$	Large drops, good mixing	Poor	Good

The last entry of Table 4-4 is the case of good fluid mixing but poor fuel atomization, so that τ_{eb} controls. For this spray flame, the possibility of droplet burning exists, either as an envelop or wake flame, depending on the relative velocity between the droplet and the air stream. These values of $\tau_{s\ell}$ and τ_{eb} are not typical of a gas turbine combustor, since the values would exist only for the case of poor fuel atomization at a high power setting.

By considering the gas turbine flame schematics of Mellor (1973) (shown in Figure 4-2), further insight into the importance of the ratio of $\tau_{s\ell}$ to τ_{eb} can be gained. In Figure 4-2a, fuel droplets are large and the resulting flame structure corresponds to case (c) of Table 4-4. This flame length is long as a result of the fuel droplets penetrating far downstream before they completely evaporate.

Shown in Figure 4-2b is a flame schematic for case (b) of Table 4-4. Here the droplets evaporate earlier in the combustion process and the overall flame structure resembles more closely that of a turbulent diffusion flame.

The flame schematic shown in Figure 4-2c is for a gas turbine combustor operating near the design point. The high air flow rate produces good mixing (small $\tau_{s\ell}$) and the fuel flow is that for which the fuel injector was designed. Here the improved mixing leans out the fuel rich regions which in turn limits soot formation. The resulting flame may appear blue in color.

All of the characteristic times discussed should be thought of as order of magnitude estimates since each takes on a range of values in an actual combustor. However, these times do identify the key physical processes affecting both emissions and performance and can be used as aids in both combustor design and emissions data analysis.

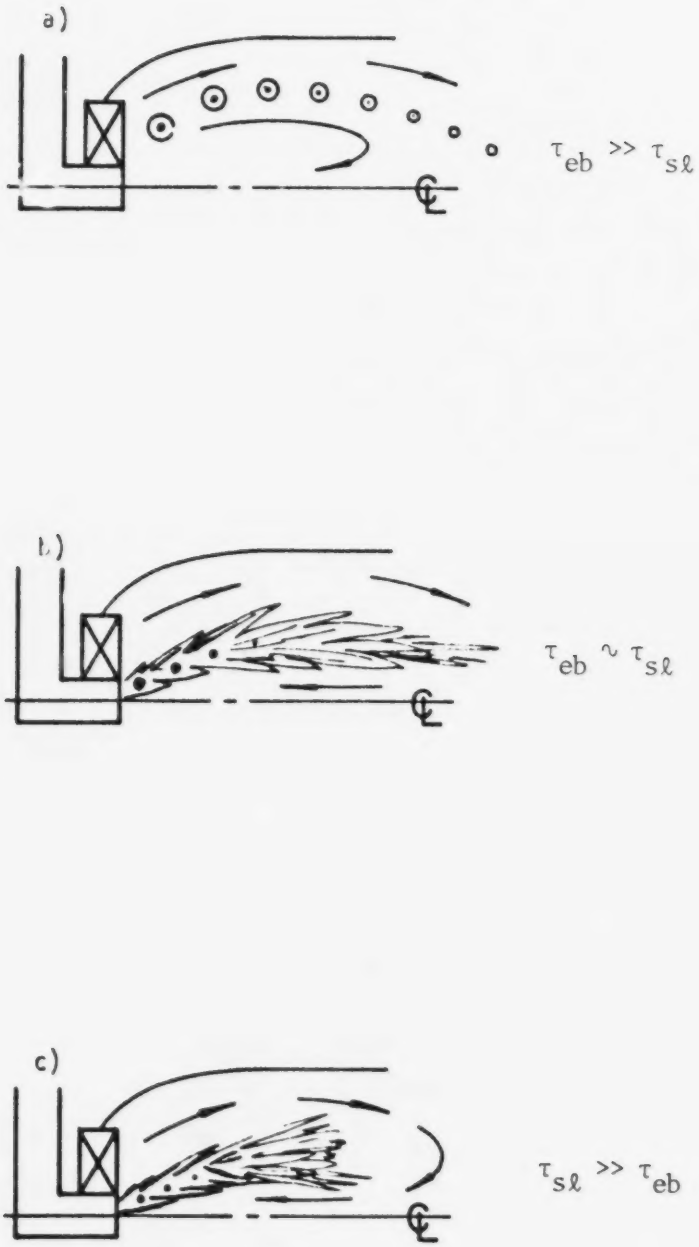

Figure 4-2. Gas Turbine Flame Schematics (from Mellor, 1973)

V. INTERNAL COMBUSTOR MEASUREMENTS-- RESULTS AND DISCUSSION

As noted previously, both internal flame and exit plane data were obtained during the experimental investigation. After a brief discussion of the effects of vitiated inlet air on the results, the single point probe data will be presented and analyzed. Exit plane emissions measurements are the subject of Section VI.

The use of vitiated inlet air for emissions studies is always subject to some criticism for the influence it has on pollutant formation and destruction rates. Such comments are of course quite valid and must be kept in mind if data obtained with vitiated air are to be compared with results for clean air. To heat the air flow through the slave burner from 273°K to 500°K, the approximate overall reaction is the following assuming complete combustion:

$$C_3H_8 + 64\ O_2 + 241\ N_2 \rightarrow 3\ CO_2 + 4\ H_2O + 59\ O_2 + 241\ N_2$$

The products also, of course, include trace amounts of NO_x, CO, and HC. However, the mole fractions of these species were measured and found to be at least three orders of magnitude lower than the major constituents given in the above reaction. The percent deviations of the O_2 and N_2 concentrations of the products from that of standard air were then 8.5% and 0.38% lower respectively. In addition, the mole fractions of CO_2 and H_2O in the products can be seen to be much less than the levels of O_2 and N_2. It is felt then that since the goal of the project is not concerned with determining absolute emissions levels and since the deviation from standard air is small, the examination of spray flame emission characteristics with vitiated inlet air will provide valuable insight into processes of importance in non-vitiated flames.

The internal probing studies allowed the formulation of physical models for three disc stabilized flames. It is most instructive to first

present the basic flame structure (common to each of the three flames) and then the experimental concentration and temperature profiles used to develop it. Shown in Figure 5-1, with the sampling grid in the background, the model consists of three regions, central recirculation zone, shear layer, and free stream. Within the recirculation zone, the hollow cone fuel spray penetrates nearly to the edge of the shear layer separating the free stream and the recirculation zone. The experimental data will show that a portion of the fuel spray (large droplets) actually reaches and extends through the shear layer. Evidence will also be seen that suggests that some fuel (vapor and small droplets) flows toward the disc in the backflow region and moves radially outward along the disc towards the point of the flow separation. The shear layer is a region of intense turbulent mixing between the free stream and the recirculation zone. The shear layer is then the region of the flame, which is hollow and surrounds the recirculation zone. Hence the flame structure is not unlike the flame structures suggested by Mellor et al. (1972) and Tuttle et al. (1973) for a gas turbine liner.

Also included in Figure 5-1 is a sketch of the probe tip drawn to the same scale as the sampling grid. Although the probe represents a decrease in duct flow area of less than 0.5% and hence should not appreciably affect the combustion flow field, it is physically somewhat large in comparison to the grid spacing and thus a finer grid spacing was unwarranted. As can be seen from Figure 5-1, the grid spacing is sufficiently fine to allow the identification of the three regions of the flame discussed previously. However care must be taken not to extrapolate too much flame detail from the internal measurements. In particular, identification of physical processes or subregions of the flame which occur over a dimension which is less than the radial grid spacing would be unwise.

The location of the liquid spray and flame region was determined from analysis of the concentration and temperature profiles as well as high speed movies of the flames. As is commonly found in experimental measurements of this type, some problems were encountered in reproducing the values of measured pollutant concentrations from run to run. Inlet concentration and test flame exhaust data reproducibility was excellent from run to run.

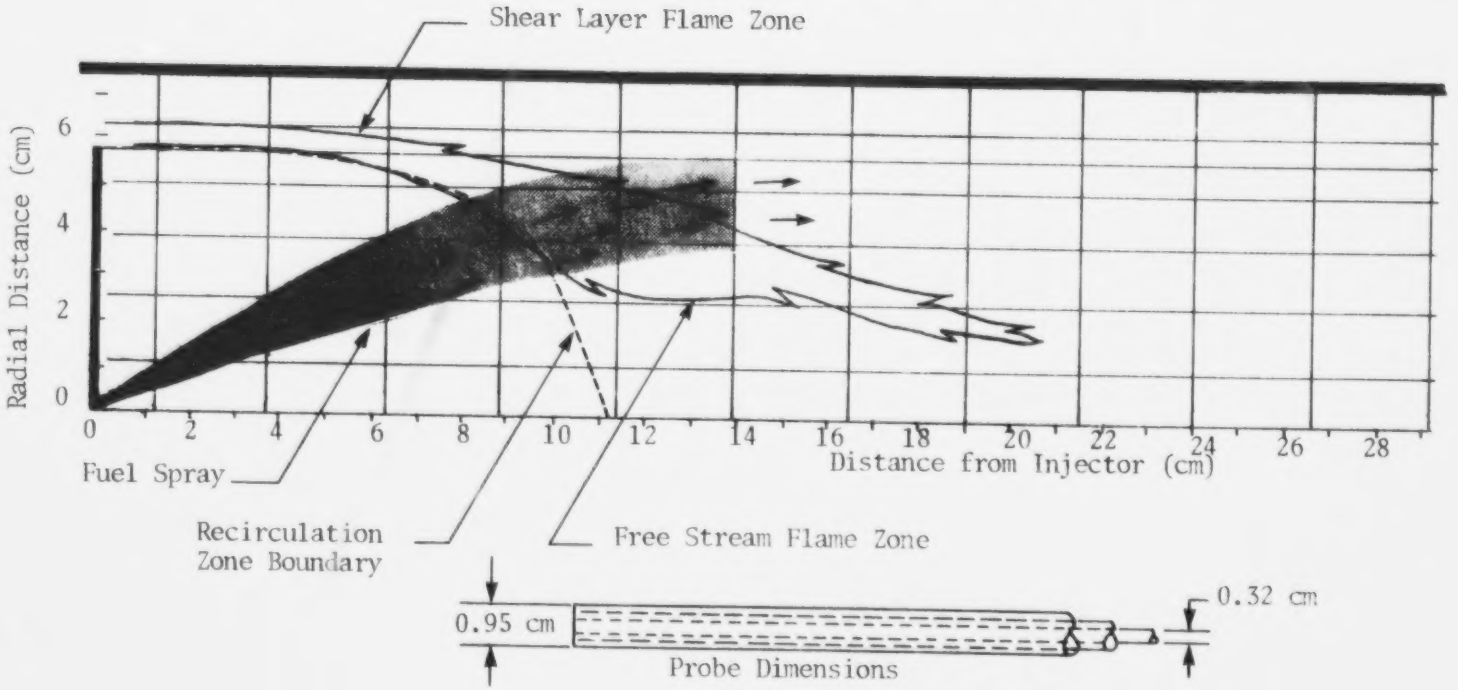

Figure 5-1. Schematic of the Postulated Flame Zone Model

In order to demonstrate the concentration measurement reproducibility, axial profiles of CO data for the 6.4 cm, 2.5 cm, and centerline radial probe positions are given in Figure 5-2, 5-3, and 5-4 respectively for the low air flow rate flame. The worst concentration data scatter occurred near the disc at the outermost radial sampling point (Figure 5-2). Scatter in this region (near the disc edge) results from probe placement errors which are critical in zones of steep concentration gradients. The reproducibility of the CO data displayed in Figures 5-3 and 5-4 is typical and is much improved over that of Figure 5-2. The data scatter in the 2.5 cm and the centerline radial position axial profiles is seen to be greatest in the region of the shear layer. Here steep concentration gradients also exist which tend to magnify any probe placement error. Note the decreased scatter in all three axial profiles as the exit plane is approached.

Errors in probe positioning also explain the increased scatter in the thermocouple output in the vicinity of the fuel spray. Near the spray sheath, probe placement is again critical in reproducing the temperature data due to the cooling action of the liquid fuel impinging on the exposed thermocouple junction. It is not suggested that the thermocouple reading in the region of the fuel spray represents the actual gas temperature as liquid fuel impingement, radiation, and catalytic effects are not considered. Following the procedure of Hunter et al. (1974) however, the output from this region can be used to locate the fuel spray.

Generally, data scatter decreased as the air flow rate was increased. Thus a higher mass flow increases the turbulent mixing intensity, which decreased the steepness of the gradients in the flow. As a result, probe placement error has a less pronounced effect upon reproducibility.

The detailed data of the experimental measurements will not be presented in this section; they may however be found in Appendix I. Instead the results will be presented in the compressed form of computer generated contour maps. In order to construct the contours, an average value of the measurements at each grid point was obtained. The average values were then input to a plotting routine which curve fits the data

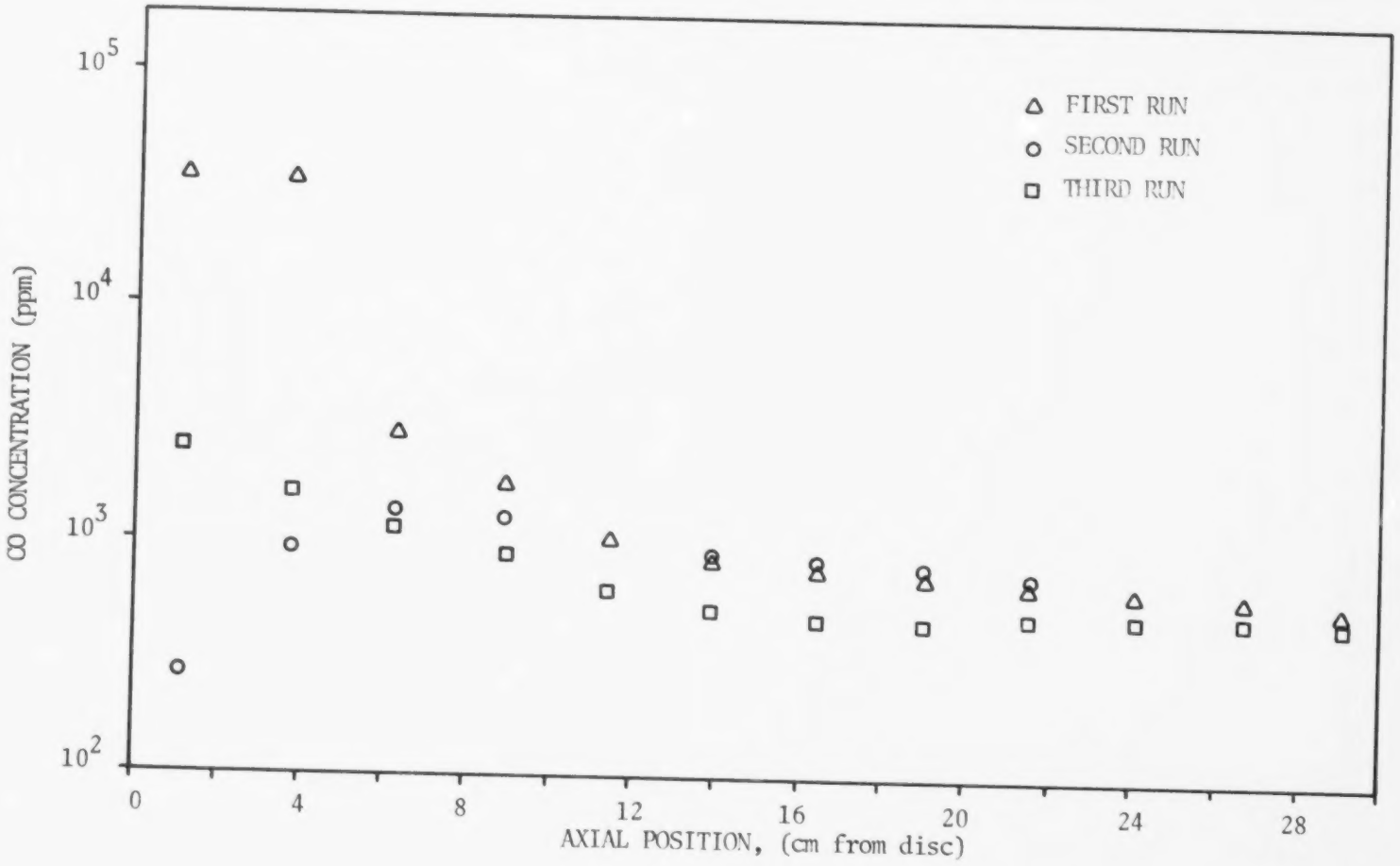

Figure 5-2. Axial CO Concentration Profile, 6.4 cm from Centerline
$\dot{m}_{air}$ = 1.0 kg/sec, ϕ_o = 0.1, P = 5 atm, T_{in} = 500°K

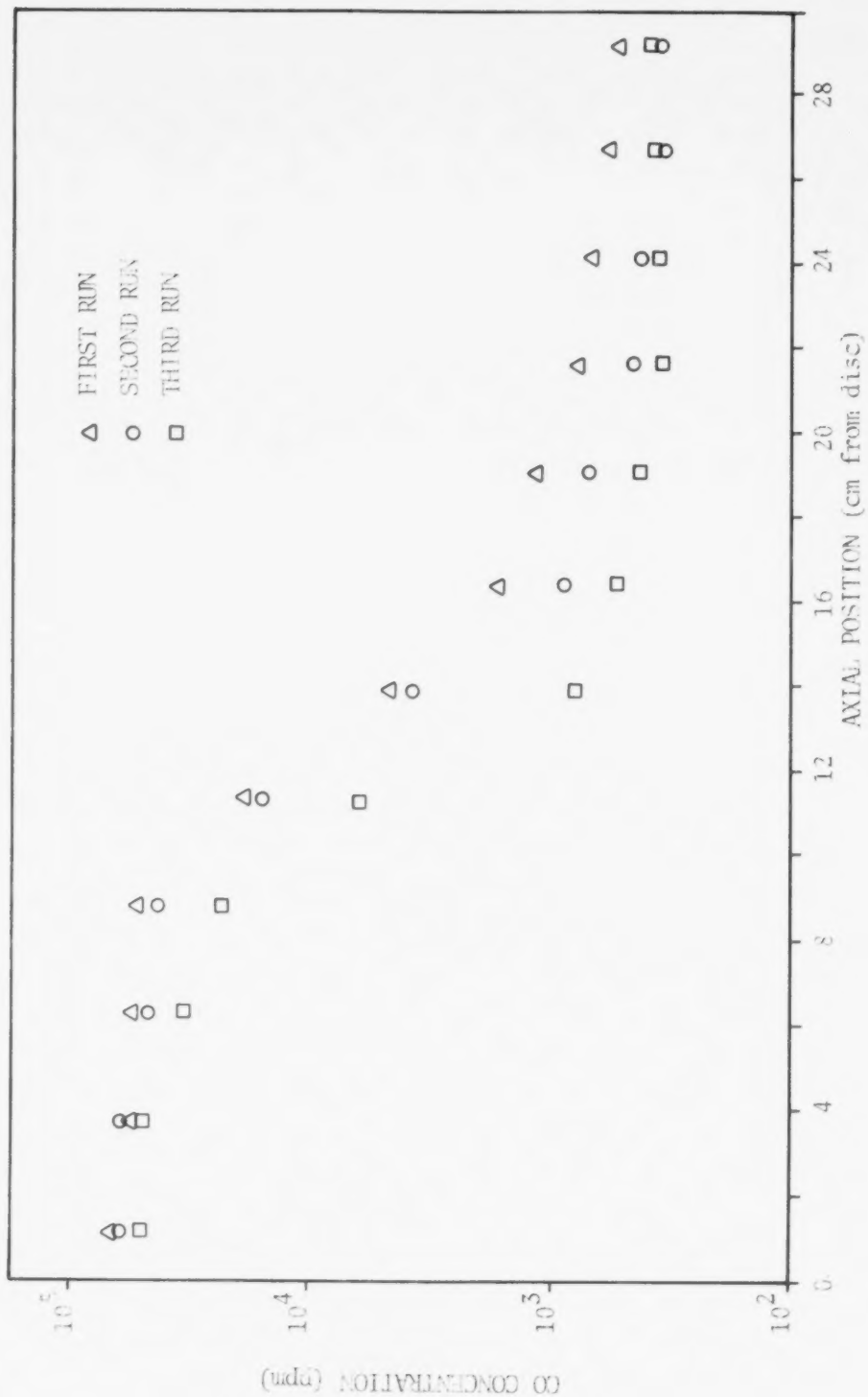

Figure 5-3. Axial CO Concentration Profile, 2.5 cm from Centerline
$\dot{m}_{air}$ = 1.0 kg/sec, ϕ_o = 0.1, P = 5 atm, T_{in} = 500°K

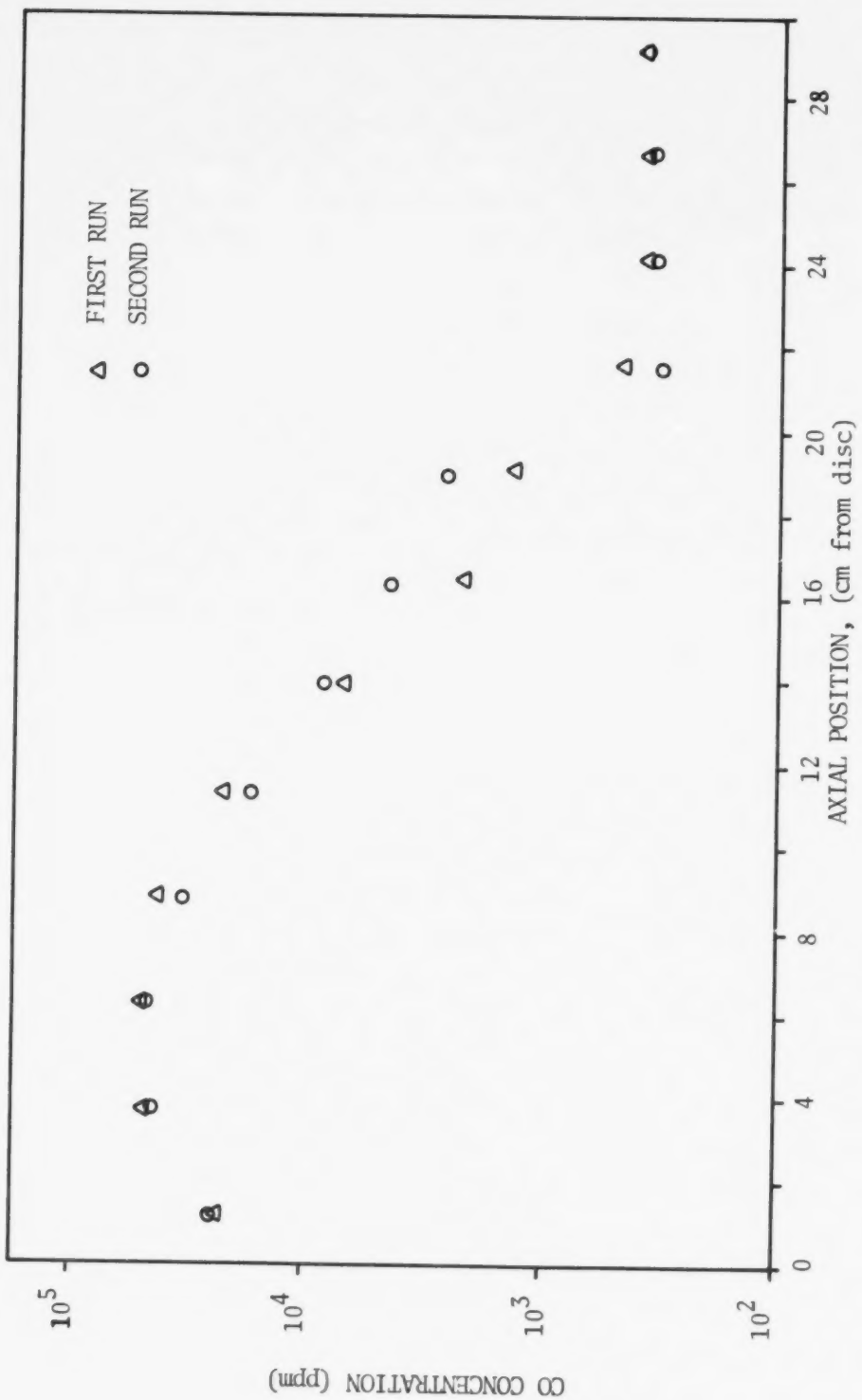

Figure 5-4. Axial CO Concentration Profile Along Centerline
$\dot{m}_{air}$ = 1.0 kg/sec, ϕ_o = 0.1, P = 5 atm, T_{in} = 500°K

in both the radial and axial directions. Isopleths were then calculated and computer drawn for selected levels of the species concentration. On the resulting contour maps, the radial distance is normalized by the duct diameter and is designated as R/DUCT. Thus the disc edge is located at R/DUCT of 0.39. In a similar manner, the axial dimension from the disc is normalized by the disc diameter and is designated as X/DISC.

In analyzing the single point probe data, no attempt was made to subtract the emissions of the vitiated inlet air flow from the levels measured in the test combustor because these incoming emissions are significantly lower than the recorded levels in the test housing. For convenience, the concentrations of the pollutants of the vitiated inlet air for the three flames are listed as the first entry in each of the probe data tables of Appendix I (Tables A-1 through A-19).

The characteristic times for fuel droplet evaporation and turbulent mixing discussed in Section IV do vary for the three flames discussed below. Calculations of τ_{eb}, $\tau_{s\ell,no}$, and $\tau_{s\ell,co}$ for the three internally probed flames (Table 3-1) are included in Tables 6-1 and 6-2. Although the turbulent mixing time decreases by a factor of at least three in going from the 1.0 kg/sec to the 3.0 kg/sec air flow rate flames, τ_{eb} decreases only from 0.7 to 0.5 msec. Hence the heterogeneous processes should be increasing in relative importance in going from the low to the high air flow rate flames.

A. Internal Probing Results--$\dot{m}$ = 1.0 kg/sec, P = 5 atm, ϕ_o = 0.1, and $T_{inlet\ air}$ = 500°K

Contour maps for HC, CO, indicated gas temperature, and NO are shown in Figures 5-5, 5-6, 5-7, and 5-8, respectively, for this low air flow rate flame which is dominated by slow mixing processes and hence extremely fuel rich regions. The relatively large amount of soot generated within these fuel rich regions was evidenced in the bright yellow color of the flame and the high accumulation rate of carbon particles on the sample gas filter.

For gas samples extracted from within the fuel rich regions, NO_2 measurement was not possible, in agreement with the earlier findings

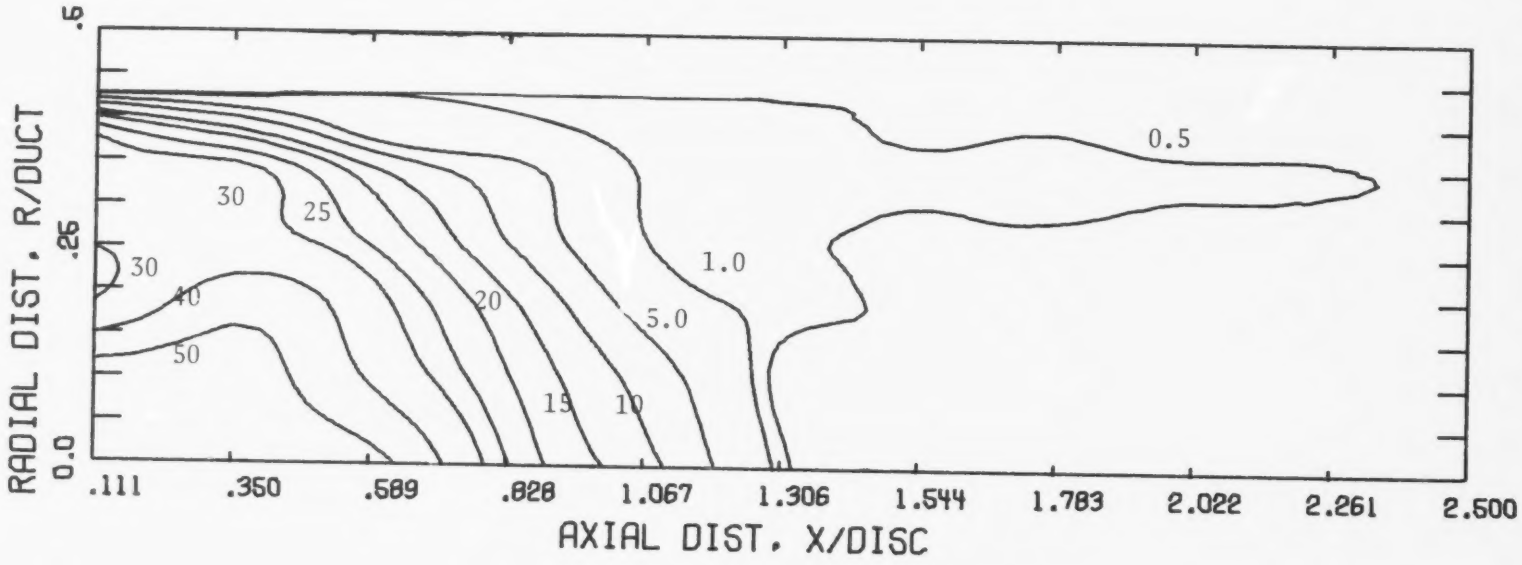

Figure 5-5. HC Concentration Contour Map (numbers are ppmC x 10^{-3})
$\dot{m}$ = 1.0 kg/sec, P = 5 atm, ϕ_o = 0.1, $T_{\text{inlet air}}$ = 500°K

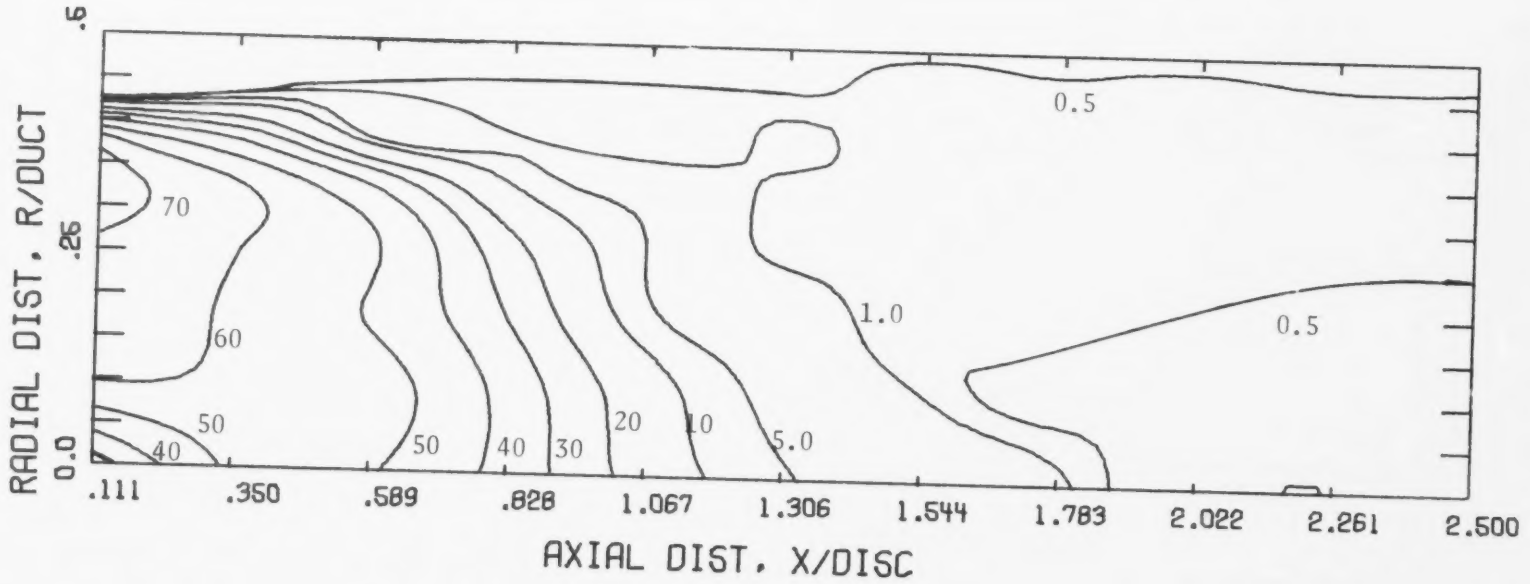

Figure 5-6. CO Concentration Contour Map (numbers are ppm x 10^{-3})
$\dot{m}$ = 1.0 kg/sec, P = 5 atm, ϕ_o = 0.1, $T_{inlet\ air}$ = 500°K

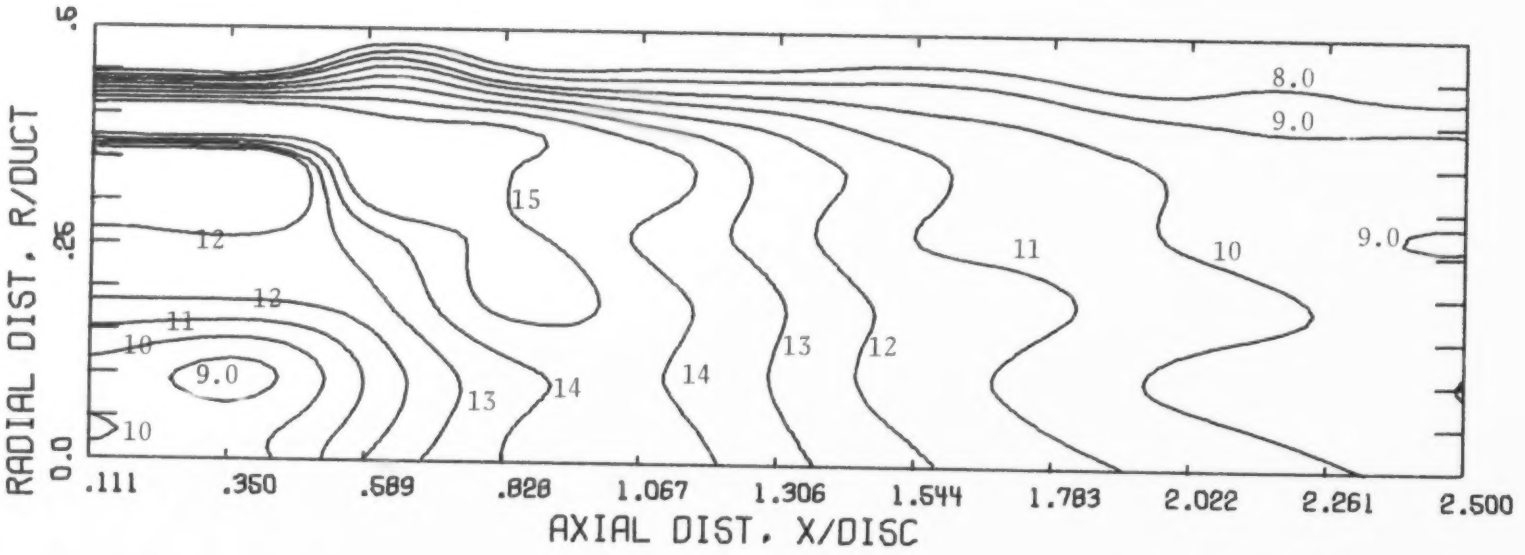

Figure 5-7. Temperature Contour Map (numbers are $^{o}K \times 10^{-2}$)
$\dot{m}$ = 1.0 kg/sec, P = 5 atm, ϕ_o = 0.1, $T_{inlet\ air}$ = $500^{o}K$

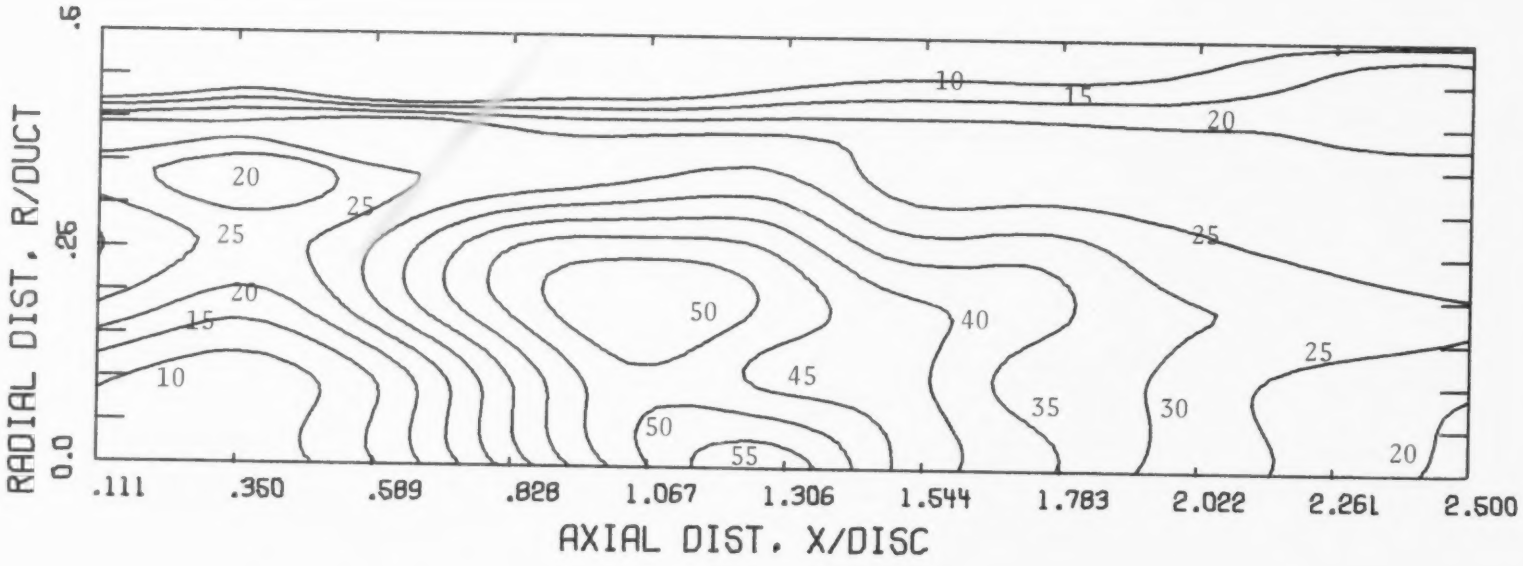

Figure 5-8. NO Concentration Contour Map (numbers are ppm)
$\dot{m}$ = 1.0 kg/sec, P = 5 atm, ϕ_o = 0.1, $T_{inlet\ air}$ = 500°K

of Tuttle et al. (1974). Thus an NO contour map is displayed in Figure 5-8 rather than one for NO_x. Outside of the recirculation zone where NO_x measurements were possible the recorded NO_x concentrations were approximately 5 ppm greater than the NO levels.

The recirculation zone behind the disc flame stabilizer is characterized by extremely high HC and CO concentrations. In particular the area adjacent to the fuel injector in Figure 5-5 shows unburned hydrocarbons in excess of the 50,000 ppmC upper limit of the measuring instrument. The initial fuel spray cone angle (as indicated by high speed movies) can be seen intersecting the 50,000 ppmC and 40,000 ppmC contours at X/DISC of 0.4 and 0.5 respectively. Note that high HC levels were measured on each side of the hollow spray cone and that fuel (either small droplets or vapor) is swept by the recirculating gas flow outward toward the disc edge. The CO contour map (Figure 5-6) reveals that a significant amount of the fuel vapor is partially oxidized to CO in the vicinity of the fuel spray and throughout the recirculation zone. Between the fuel spray and the disc a large zone of nearly constant and particularly high CO concentration is seen. The high values of CO and HC within the recirculation zone decrease steadily due to oxidation and dilution rates exceeding the formation and vaporization rates as the shear layer is approached.

The recorded gas temperatures (Figure 5-7) show that the recirculation region is relatively cold. The low temperatures are attributable in part to liquid fuel impingement upon the thermocouple and the required transfer of energy from the recirculating gas flow into the vaporization of the liquid fuel.

Examination of the NO contour map in Figure 5-8 shows low concentrations near the fuel injector and throughout the recirculation region. This is expected both as a result of dilution from the fuel addition and from the fact that the temperatures are too cold and oxygen is not available in this region for NO formation.

As stated earlier, the shear layer is the region surrounding the recirculation zone and is characterized by intensely reacting turbulent flow as a result of the turbulent mixing between the oxidizer

of the mainstream and the fuel vapor in the recirculated flow. Both HC and CO concentrations decrease by at least an order of magnitude across the shear layer. In addition both the HC and CO contours (Figures 5-5 and 5-6) show the shear layer to be very narrow in the high fluid shearing region near the disc edge. The shear layer becomes much thicker downstream and nearer the centerline as the relative velocity between the recirculating gas and the free stream is decreased.

The high destruction rates of CO and HC in the shear layer are accompanied by the high gas temperatures and the high NO levels seen in Figures 5-7 and 5-8 respectively. In particular, the upstream peaks in the NO profiles at an X/DISC of 0.6 and an R/DUCT of 0.25 appear to outline the shear layer as it moves downstream and toward the burner centerline. The shear layer closes to the centerline at an X/DISC of 1.2 where the highest NO levels were recorded.

The relative maxima in the HC and CO contours at an X/DISC of 1.1 and an R/DUCT of 0.3 might suggest that a small number of initially large droplets move in nearly a straight line from the fuel injector to the shear layer and pass through the shear layer to reach the free stream. However the location of these relative maxima is more likely due to quenching of the CO and HC oxidation reactions along the outer periphery of the shear layer. The relative maximum in both the CO and HC contours becomes more pronounced as the exit plane is neared because of the continued oxidation of these species close to the centerline of the burner where gas temperatures are higher and velocities lower.

Any fuel spray penetrating to the shear layer or into the free stream is convected toward the burner centerline. It is this fuel that gives rise to the relative maxima in HC and CO concentration at X/DISC of 1.4 and R/DUCT of 0.2 just downstream of the shear layer. In addition, the fuel that is swept downstream from the shear layer is surrounded by a hollow flame which is ignited and stabilized by the shear layer reactions. This free stream flame does not close to the centerline as evidenced by both the gas temperature and NO peaks off the centerline through this region. The flame structure is like that of Figure 5-1 which shows a free stream flame extending downstream from the shear layer but not closing to the centerline for this low equivalence ratio case.

B. Internal Probing Results--$\dot{m}$ = 1.5 kg/sec, P = 5 atm, ϕ_o = 0.2, and $T_{inlet\ air}$ = 500°K

Contour maps for HC, CO, gas temperature, and NO_x concentrations at this intermediate run condition are given in Figures 5-9, 5-10, 5-11, and 5-12, respectively. Although the resulting flame appearance at these operating points was somewhat yellow, the amount of soot collected by the sample filter was not excessive. NO_x measurements via the converter-chemiluminescent detector were possible at most grid points. At grid points where the high equivalence ratio of the sample gas prohibited this instrument from working properly, the NO_x concentration was taken to be the sum of the NO measurement by the chemiluminescent NO detector and the NO_2 measurement via the NDUV instrument.

The recirculating flow region of this flame is dominated by the fuel spray which penetrates through it. The smaller fuel droplets evaporate within this region either near the fuel spray or after being swept along with fuel vapor outward toward the disc edge. As a result of the fuel richness of this region which Figure 5-9 shows to exceed 50,000 ppmC for the most part, the only significant reaction is the formation of CO. The high CO concentration of Figure 5-10 indicates that CO formation occurs throughout this region directly behind the disc stabilizer. However further oxidation to CO_2 is not probable because of the lack of oxygen and the low gas temperatures in this region shown in Figure 5-11. In addition the relatively constant NO_x levels outside of the fuel spray but within the recirculation zone suggest that no NO formation occurs here. Lower NO_x levels are expected near the fuel spray as a result of dilution effects.

The general outline of the shear layer mixing region is detectable from the shape of the contour lines for HC and CO given in Figures 5-9 and 5-10. The large decreases in the concentrations of both of these species across the shear layer are evidence of the high oxidation rates occurring here. A sharp rise in gas temperature (Figure 5-11) also indicates the high intensity of the reactions in the shear layer. The hollow structure of the shear layer is also easily detectable from the upstream peaks in both the gas temperatures and NO_x

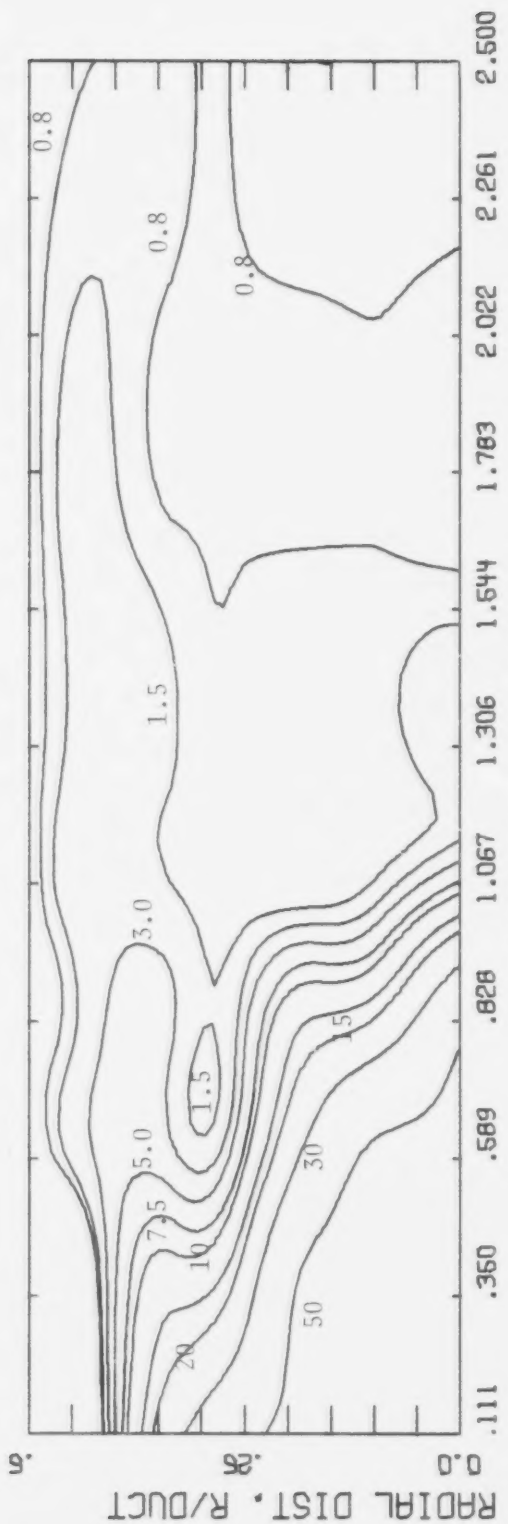

Figure 5-9. HC Concentration Contour Map (numbers are ppmC x 10^{-3})
$\dot{m}$ = 1.5 kg/sec, P = 5 atm, ϕ_o = 0.2, $T_{inlet\ air}$ = 500°K

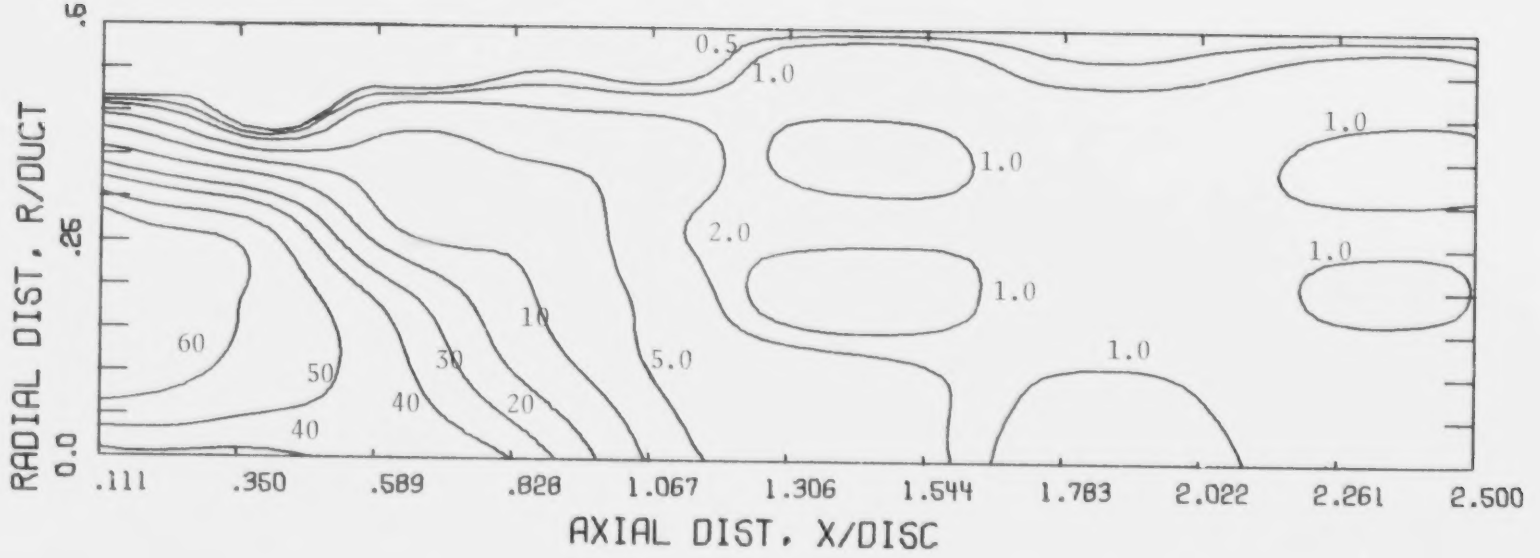

Figure 5-10. CO Concentration Contour Map (numbers are ppm x 10^{-3})
$\dot{m}$ = 1.5 kg/sec, P = 5 atm, ϕ_o = 0.2, $T_{inlet\ air}$ = 500°K

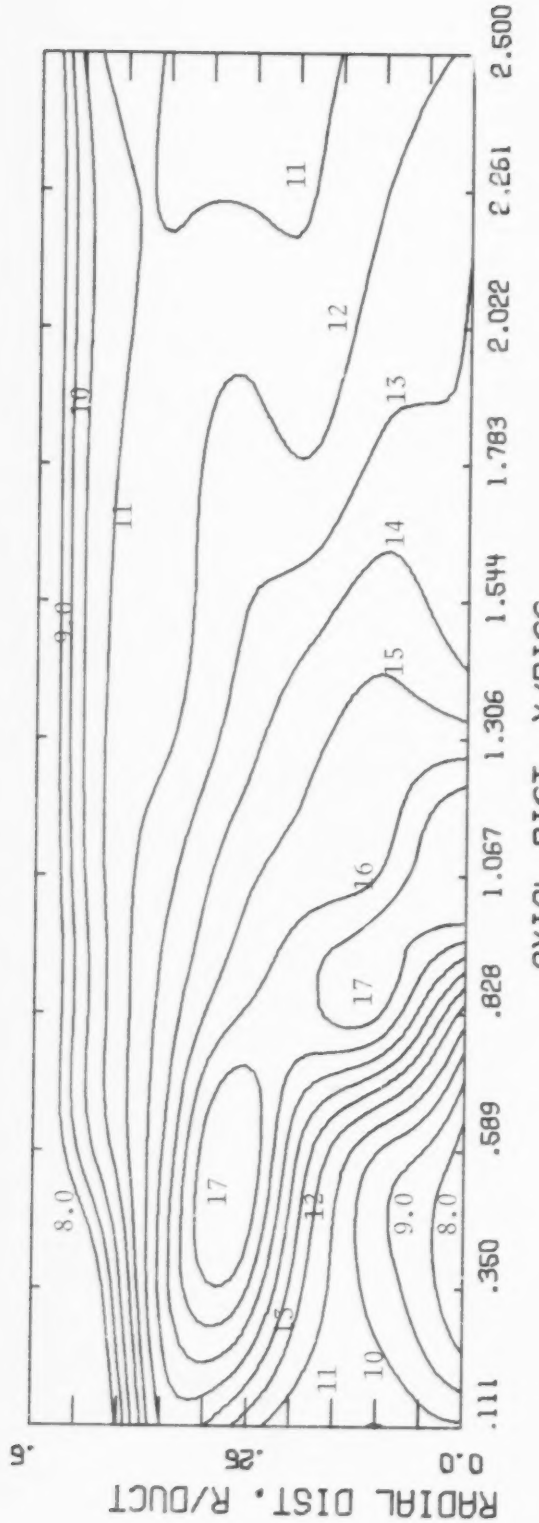

Figure 5-11. Temperature Contour Map (numbers are $^{o}K \times 10^{-2}$)
$\dot{m}$ = 1.5 kg/sec, P = 5 atm, ϕ_o = 0.2, $T_{inlet\ air}$ = 500^{o}K

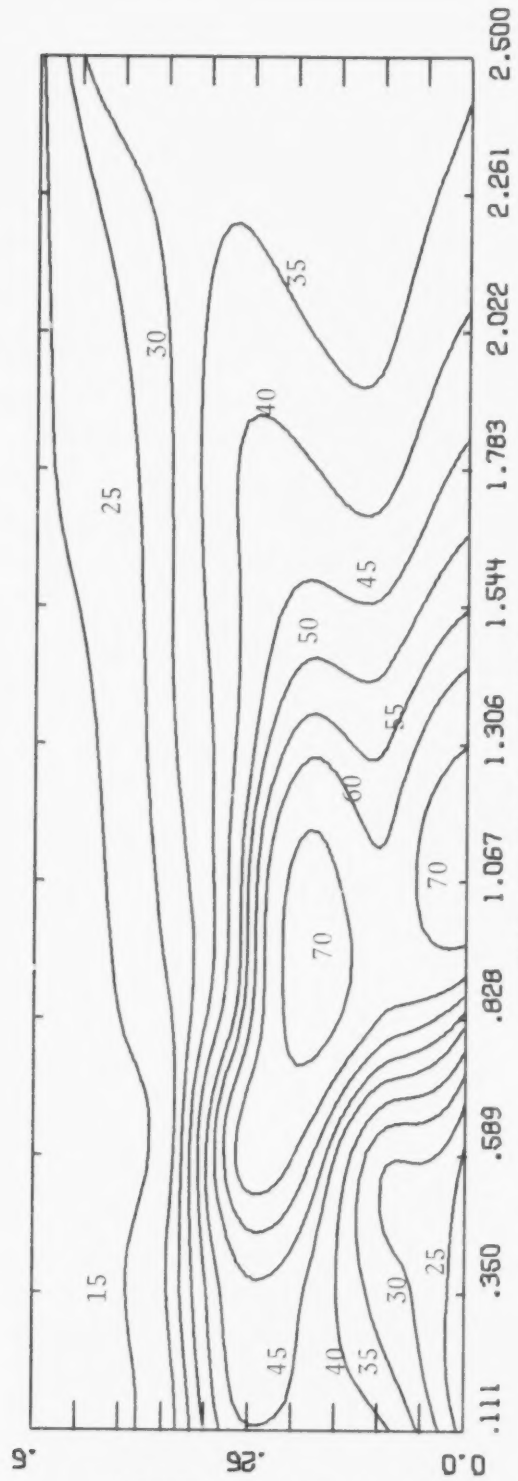

Figure 5-12. NO_x Concentration Contour Map (numbers are ppm)
$\dot{m}$ = 1.5 kg/sec, P = 5 atm, ϕ_o = 0.2, $T_{inlet\ air}$ = 500°K

levels between X/DISC values of 0.15 and 1.0. However it should be noted that the upstream NO_x peaks are slightly radially inward from the temperature peaks, as expected due to the lower quench rate for NO_x at the inner boundary of the shear layer. The shear layer appears to have completely closed to the centerline at X/DISC of 1.25.

At the boundary between the shear layer and the free stream, the HC contour map (Figure 5-9) exhibits two relative maxima. The outer one at R/DUCT of 0.4 results from the quenching of HC oxidation reactions along the outer boundary of the shear layer. As expected, a similar relative maximum is also seen in the CO contour map in the same region. These CO and HC molecules which were mixed by turbulent processes into the colder high velocity free stream are convected toward the exhaust as evidenced by the downstream relative maximum in the HC contour map at the same radial position.

The second HC relative maximum along the boundary layer between the shear layer and the free stream at R/DUCT of 0.25 corresponds to the location of the projected initial fuel spray cone angle which was measured from high speed movies of the flame. Thus for this flame, the fuel spray does penetrate through the shear layer into the free stream. A free stream flame zone, anchored by the shear layer, begins where the fuel spray penetrates into the free stream. This secondary reaction zone follows the trajectory of the fuel droplets and is sufficiently intense that relative maxima in both the gas temperature and the NO_x contours are seen at this radial position near the exhaust plane of the burner. The NO formation rate should be high in this secondary reaction zone because of the increased abundance of oxygen in the free stream. The NO_x peaks in this region are seen to be somewhat radially inward from those of the gas temperature.

A portion of the fuel which penetrates the shear layer is swept toward the combustor centerline where it continues to burn in the lower velocity gas flow. This is evidenced by the gas temperature peak off the burner centerline at X/DISC of 1.7 but moving to the centerline as the exhaust plane is neared. The NO_x contours in Figure 5-12 also demonstrate similar maxima along the centerline but inside of the temperature maxima.

The free stream flame structure at this burner run point is then quite different from that of Figure 5-1. Here the momentum of the gas flow causes the free stream flame zone shown in Figure 5-1 to be pushed to the centerline. In addition, the penetration of fuel droplets into the free stream gives rise to a second free stream flame zone which is stabilized by the fuel droplets.

C. Internal Probing Results--$\dot{m}$ = 3.0 kg/sec
P = 5 atm, ϕ_o = 0.2, and $T_{\text{inlet air}}$ = 500°K

The contour maps for HC, CO, and NO_x concentrations at this high air loading condition are given in Figures 5-13, 5-14, and 5-15, respectively. At this run condition, the flame appearance was blue and little soot was collected by the sample gas filter during a data run. No gas temperature measurements were possible at this run point due to the rapid erosion and subsequent breaking of the stainless steel thermocouple sheath.

The recirculating flow region of this flame is also dominated by the presence of the liquid fuel spray. The vaporization of the smaller droplets occurs within this region which yields the high HC levels seen in Figure 5-13. Again, the high CO concentrations within this zone suggest that partial oxidation of the HC closely follows the vaporization of the fuel. Since NO formation is unlikely within this fuel rich region, the gradients in the NO_x contour map (Figure 5-15) result from dilution effects from the liquid fuel injection rather than NO formation.

The general outline of the shear layer is detectable in all three species contour maps. The high air flow rate increases the axial length and decreases the radial width of the shear layer from the previous flames. In addition because of the greater mixing rate of this run condition, the shear layer is not as well defined as in previous cases. Large decreases in the concentrations of CO and HC are still seen, but the gradients are much less steep than in the former two cases. In particular using only the HC and CO contour maps, it is difficult of define the axial length at which the shear layer closes to the burner centerline. The NO_x concentrations indicate that the shear layer closes to the centerline near an X/DISC of 1.5.

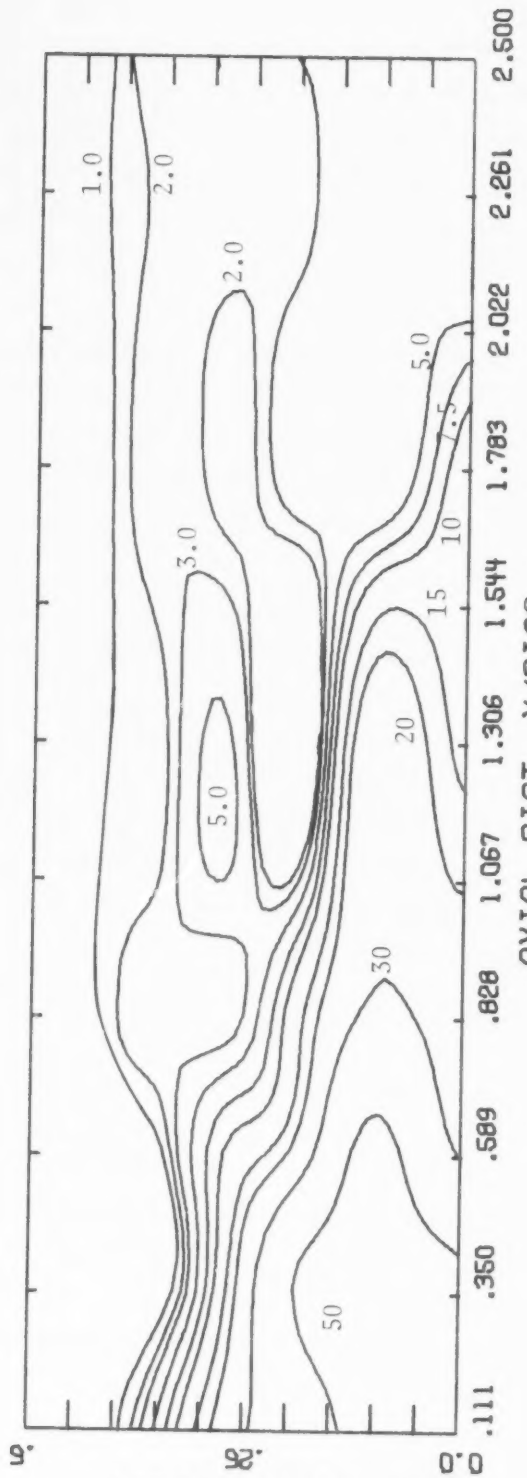

Figure 5-13. HC Concentration Contour Map (numbers are ppmC x 10^{-3})
$\dot{m}$ = 3.0 kg/sec, P = 5 atm, ϕ_o = 0.2, $T_{inlet\ air}$ = 500^oK

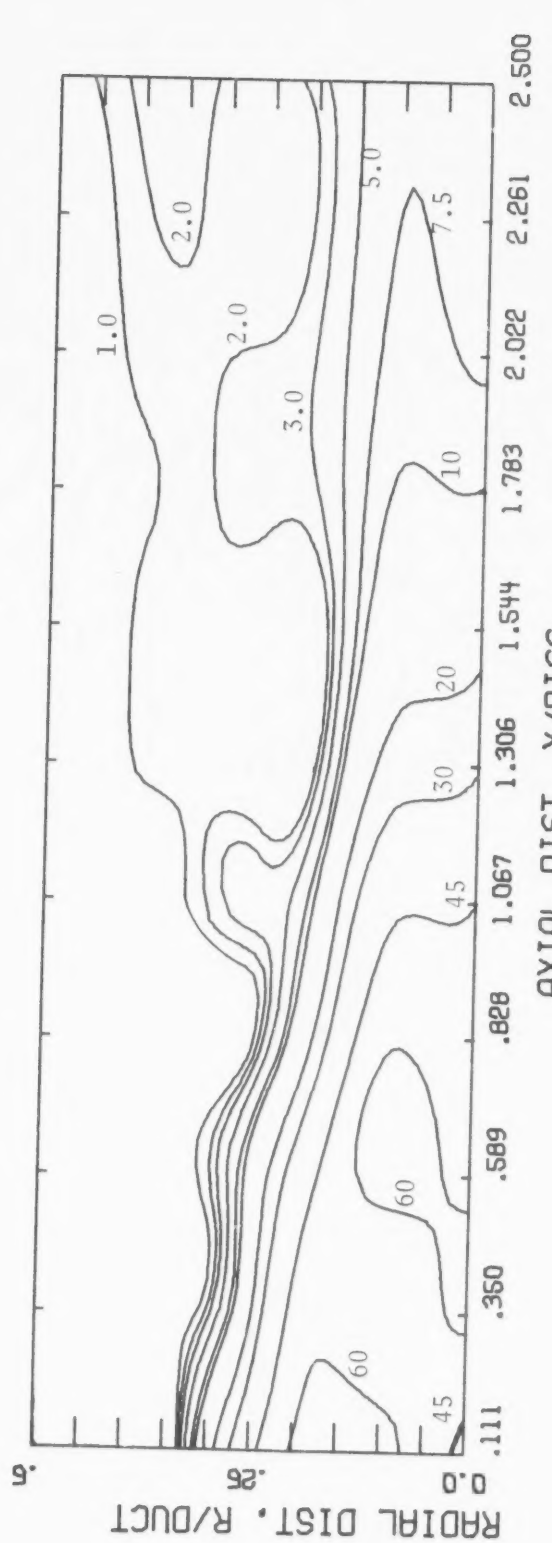

Figure 5-14. CO Concentration Contour Map (numbers are ppm x 10^{-3})
$\dot{m}$ = 3.0 kg/sec, P = 5 atm, ϕ_o = 0.2, $T_{inlet\ air}$ = 500°K

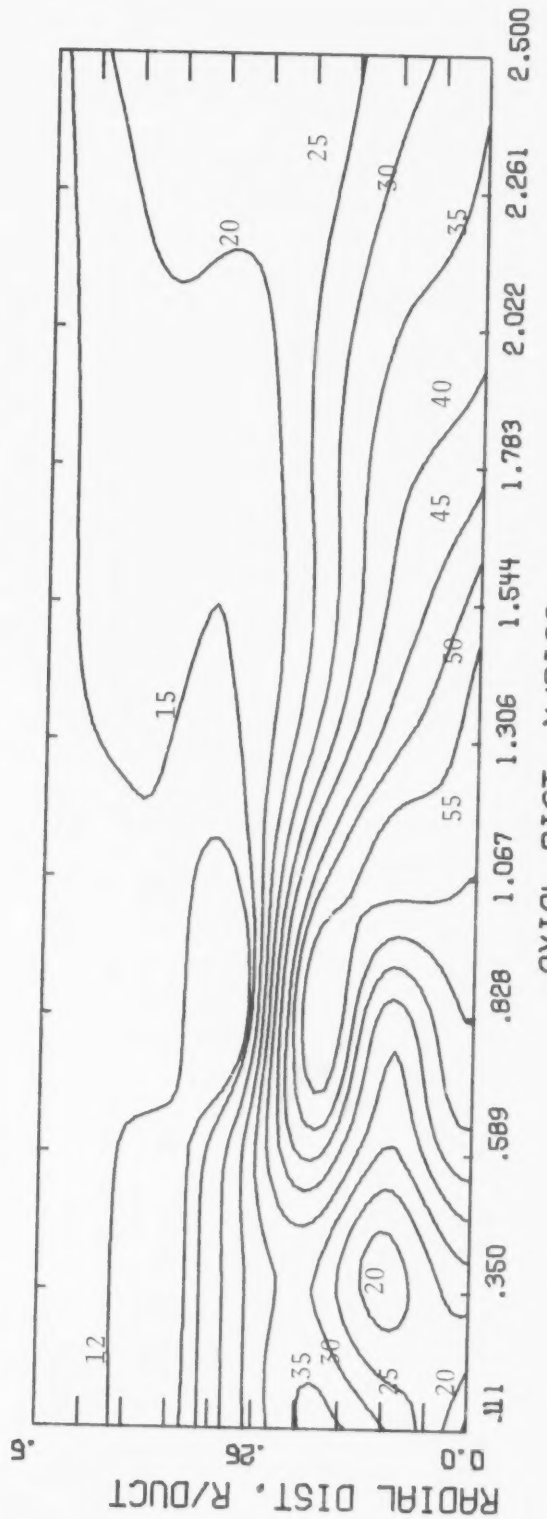

Figure 5-15. NO_x Concentration Contour Map (numbers are ppm)
$\dot{m}$ = 3.0 kg/sec, P = 5 atm, ϕ_o = 0.2, $T_{inlet\ air}$ = 500°K

Along the boundary between the shear layer and the free stream, the HC and CO contour maps again display two relative maxima. The outer maximum at R/DUCT of 0.33 and X/DISC of 0.7 results from the high quenching rate along the outer shear layer. The bending of the 1000 ppm CO contour toward the duct wall as the exit plane is approached gives evidence of the turbulent mixing occurring throughout the length of the burner.

The second relative maximum in the HC and CO contours along the boundary between the shear layer and the free stream at R/DUCT of 0.3 and X/DISC of 1.15 results from the penetration of the liquid fuel spray. A free stream flame zone, ignited by the shear layer flame zone, begins where the fuel spray enters the free stream and is stabilized on the liquid fuel droplets. Although the quenching rate is high in the free stream, this droplet held flame is sufficiently intense that a relative maximum is seen in the NO_x contours downstream of this zone.

Oxidation of both HC and CO molecules continues downstream of the shear layer in the lower velocity gas near the burner centerline. However either the gas temperature in this region is too cold or the NO quenching rate is high since no significant NO formation is detectable here in Figure 5-15.

The free stream flame structure at this burner run point is then somewhat similar to that at the previous run point. The high gas flow through the test section again pushes the free stream flame structure of Figure 5-1 to the centerline. In addition, a second free stream flame zone is stabilized on the fuel spray which penetrates through the shear layer. However the wider spray cone angle for this run point moves the fuel spray stabilized flame nearer to the duct wall.

D. Summary

The interaction of the recirculation zone, the liquid fuel spray, and the reaction process can now be more completely described. Immediately after the fuel injection, CO formation from vaporous fuel begins to occur. Fuel that is not rapidly converted to CO may follow one of two paths. Small droplets and vapor which are more susceptible

to aerodynamic influence are swept backward toward the disc then outward toward its edge: CO formation continues along this path resulting in the zone of maximum concentration observed near the disc, behind the fuel spray. Large droplets with their greater momentum tend to move more in a straight line and reach the shear layer directly.

Near the edge of the disc is the region where the CO and HC in the recirculation zone start to mix and react with the incoming air. Moving along in the shear layer, HC and CO oxidation continues as more oxidizer is provided via the turbulent mixing. Temperatures and NO concentrations increase sharply in this region and continue to do so until the flow intersects the path of the larger fuel droplets. Passing through this fuel rich region, the shear layer flame closes to the centerline. Where the shear layer closes to the centerline, the highest temperatures and the highest NO_x concentrations are found. A second reaction zone begins where the fuel spray penetrates the shear layer. This flame follows the free stream flow and exhibits CO formation and NO formation.

The regions of the flame structure critical to pollutant emissions of CO, HC, and NO_x are summarized below and correspond to the numbered regions of Figure 5-16.

1. Region 1 is the recirculation zone which is extremely fuel rich as a result of the fuel spray passing through it. High CO formation occurs throughout this region but gas temperatures are too low for NO formation.
2. Mixing of the vaporous fuel swept outward along the disc and the incoming gas flow occurs here. If this mixing process is too rapid, high CO and HC emissions result due to reaction quenching in the colder free stream.
3. The shear layer flame zone closes to the burner centerline in region 3. Temperatures are high and significant NO formation occurs here.
4. Region 4 is where the fuel spray penetrates through the shear layer. A flame follows the fuel spray trajectory and exhibits CO formation. Both CO and HC emissions are

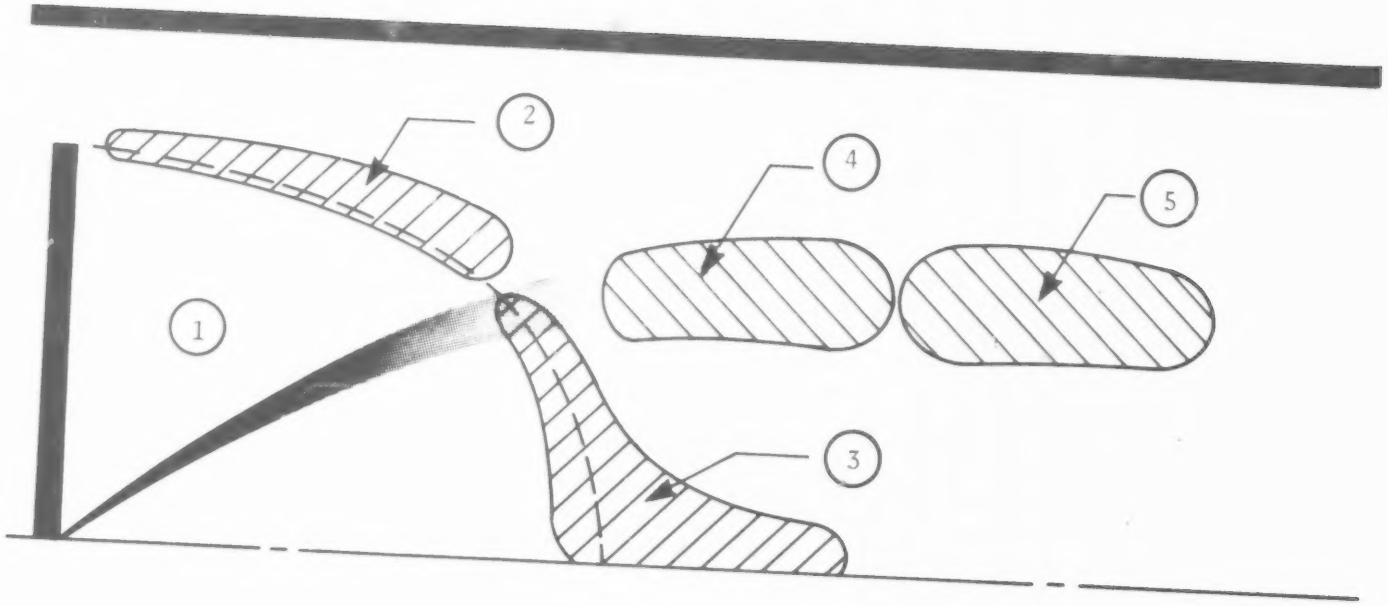

Figure 5-16. Regions of Pollutant Generation

high from this region due to the rapid mixing with the higher velocity free stream along the flame boundaries.

5. This region is directly downstream of the flame stabilized on the fuel spray and does exhibit NO formation.

In agreement with the calculated values of τ_{eb} and $\tau_{s\ell}$ given in Tables 6-1 and 6-2, the heterogeneous processes were found to be of increasing importance in going from the low to the high air flow rate flame. This can be seen in the basic flame structures for the three flames which are shown schematically in Figure 5-17. For the low air flow rate case (Figure 5-17a), no significant effect of the liquid fuel spray penetrating through the shear layer and into the free stream is noticable. A single free stream flame zone exists and is fueled by HC and CO molecules that were not consumed in the shear layer because of the slow mixing of this low air flow rate. If any fuel spray does penetrate through the shear layer at this run condition, it must occur at the location of the free stream flame zone and thus is undetectable.

At the second run point (Figure 5-17b), penetration of the liquid fuel spray into the free stream greatly alters the free stream flame structure. A free stream flame similar to that of Figure 5-17a extends from the shear layer and burns CO and HC that were not oxidized in the shear layer. However a second free stream flame zone also exists at this run condition and is fueled by the liquid spray which penetrates through the shear layer. This second free stream flame zone is detectable in both the NO_x and gas temperature contours.

The flame structure of the high air flow rate case (Figure 5-17c) is not too different from the intermediate air flow rate flame structure. Again two free stream reaction regions extend downstream from the shear layer. However as a result of the high convective velocity, here the reaction zones are more spread out.

A comparison of the disc stabilized flame structure with flame models developed for turbine liners (see Tuttle et al., 1973 and Shisler et al., 1974) reveals strong similarities. The basic picture of the liquid fuel spray feeding a diffusion type flame surrounding a region of reverse flow appears in all cases. Some differences occur however

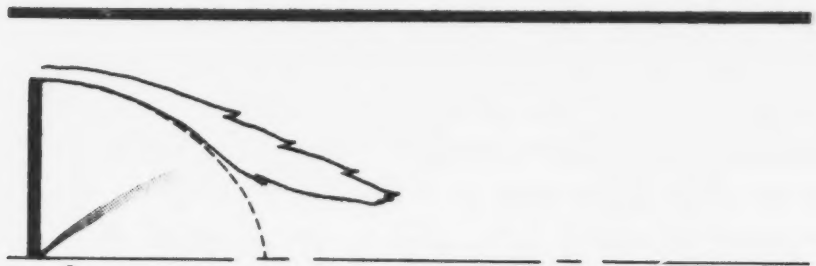

a) $\dot{m}$ = 1.0 kg/sec; P = 5 atm, ϕ_o = 0.1, $T_{inlet\ air}$ = 500°K

b) $\dot{m}$ = 1.5 kg/sec, P = 5 atm, ϕ_o = 0.2, $T_{inlet\ air}$ = 500°K

c) $\dot{m}$ = 3.0 kg/sec, P = 5 atm, ϕ_o = 0.2, $T_{inlet\ air}$ = 500°K

Figure 5-17. Schematic of the Three Probed Flames

in just where the fuel is injected relative to the recirculation zone. Behind the disc, fuel is injected directly into the recirculation zone from within while the swirl or jet established combustor recirculation zone may lie downstream of the spray. The evidence of NO formation outside the shear layer found with the disc corresponds with the concept developed by Mellor (1973) that at conditions of poor fuel atomization, the combustor NO emissions may be determined by the combustion of large liquid drops.

The disc anchored flame model has two distinct regions of combustion and NO formation. The shear layer and downstream formation zones result from the combustion of small and large fuel droplets respectively. On the other hand, with the recirculation zone positioned downstream of the fuel spray in a turbine liner, most of the fuel, including the larger drops, enters the shear layer. Thus with the combustion of all fuel particles taking place in the same region it is difficult to determine whether or not droplets play a role in combustor NO formation. Thus the disc stabilized flame, with its tendency to separate large and small droplet effects, is ideally suited for studies pertaining to the influence of fuel spray atomization upon liquid spray combustion and pollutant formation.

VI. EXHAUST PLANE MEASUREMENTS-- RESULTS AND DISCUSSION

The interaction between the aerodynamics of the disc stabilizer and the fuel spray to form the flame structure has been discussed in the previous section. While exhaust plane emissions measurements are not as helpful in determining the flame structure, studies of this type can exhibit the dependence of emissions upon the parameters controlling the combustion process.

As discussed in Section III, exit plane gas samples were gathered via a water-cooled, area averaging rake for the cycle operating conditions listed in Table 3-2. Instead of analyzing these data in terms of variations in the cycle parameters, the data will be discussed in terms of the characteristic times introduced in Section IV.

A. Calculation of Characteristic Times

Values of the homogeneous reaction times, τ_{hc} and τ_{no}, (taken from Vranos (1974)) were listed previously in Section IV (Table 4-3). Since only order of magnitude values are possible, additional calculations are unwarranted.

No means of estimating τ_{fi} was given in Section IV. However, it was noted that this time is highly dependent upon the type of fuel injector employed. Suffice it to say that for a pressure atomizing nozzle, τ_{fi} is long and additional studies are necessary to clarify the calculation of τ_{fi} for an air assist nozzle.

In order to calculate values of τ_{eb} with Equation 4-2, the magnitudes of d_o and β must first be estimated. Assuming an ambient gas temperature of 1000^oK and taking the necessary physical data for propane from Maxwell (1957), β_o was calculated via Equations 4-4 and 4-5. The empirical correlation for forced convection effects of Frössling (see Ranz and Marshall, 1952), Equation 6-1, was used in Equation 4-3 to

determine β, with the relative velocity between the droplet and gas flow assumed to be 50 m/sec.

$$\beta = \beta_o \ (1.0 + 0.276 \ Re^{1/2} \ Sc^{1/3}) \qquad 6\text{-}1$$

To complete the calculation of the droplet lifetime, the SMD of the fuel droplet size distribution must be estimated. Unfortunately due to the high volatility of liquid propane at low pressures, experimentally determined values of the SMD were not possible. However an estimation of the SMD of the propane spray was possible via the graph shown in Figure 6-1. This graph of the SMD of a simplex nozzle versus the ΔP across the nozzle and the fuel flow rate was provided by the Accessories Division of the Parker-Hannifin Corporation. Figure 6-1 is in agreement with the SMD correlation of Hunter et al. (1974) which was presented in Section II (see Table 2-1) and based upon data from the Parker-Hannifin Corporation. It should be noted that Figure 6-1 is valid only for liquids with properties similar to JP-5. The SMD of the liquid propane spray was estimated by first determining the SMD of the JP-5 spray at the same fuel flow rate and ΔP. The obtained value of the SMD was then corrected for the change in fuel properties between JP-5 and propane, utilizing the correlation of Radcliffe (1960) (see Table 2-1).

The calculated values of τ_{eb} are listed in Table 6-1 along with the measured pressure drops across the fuel nozzle. As can be seen, the values of τ_{eb} are low and not too unalike. These low values are expected as a consequence of the high volatility of liquid propane. Also as a result of the high volatility of this fuel, some vaporization of the liquid propane was occurring in the swirl chamber of the simplex nozzle at the lowest fuel flow rates since the experimental measurements of the fuel flow rate versus ΔP did not exhibit a square-root relationship as suggested by Equation 2-2. Although the vaporization of some fuel within the nozzle might suggest that the values of τ_{eb} in Table 6-1 could be considered as an upper bound, more likely the flow of fuel vapor out of the swirl nozzle would tend to destroy the central core of the swirl chamber which is normally filled with gas entrained from the ambient outside of the nozzle. If this central gas core is not allowed to develop, the atomization properties of a swirl nozzle are extremely poor (Simmons, 1975).

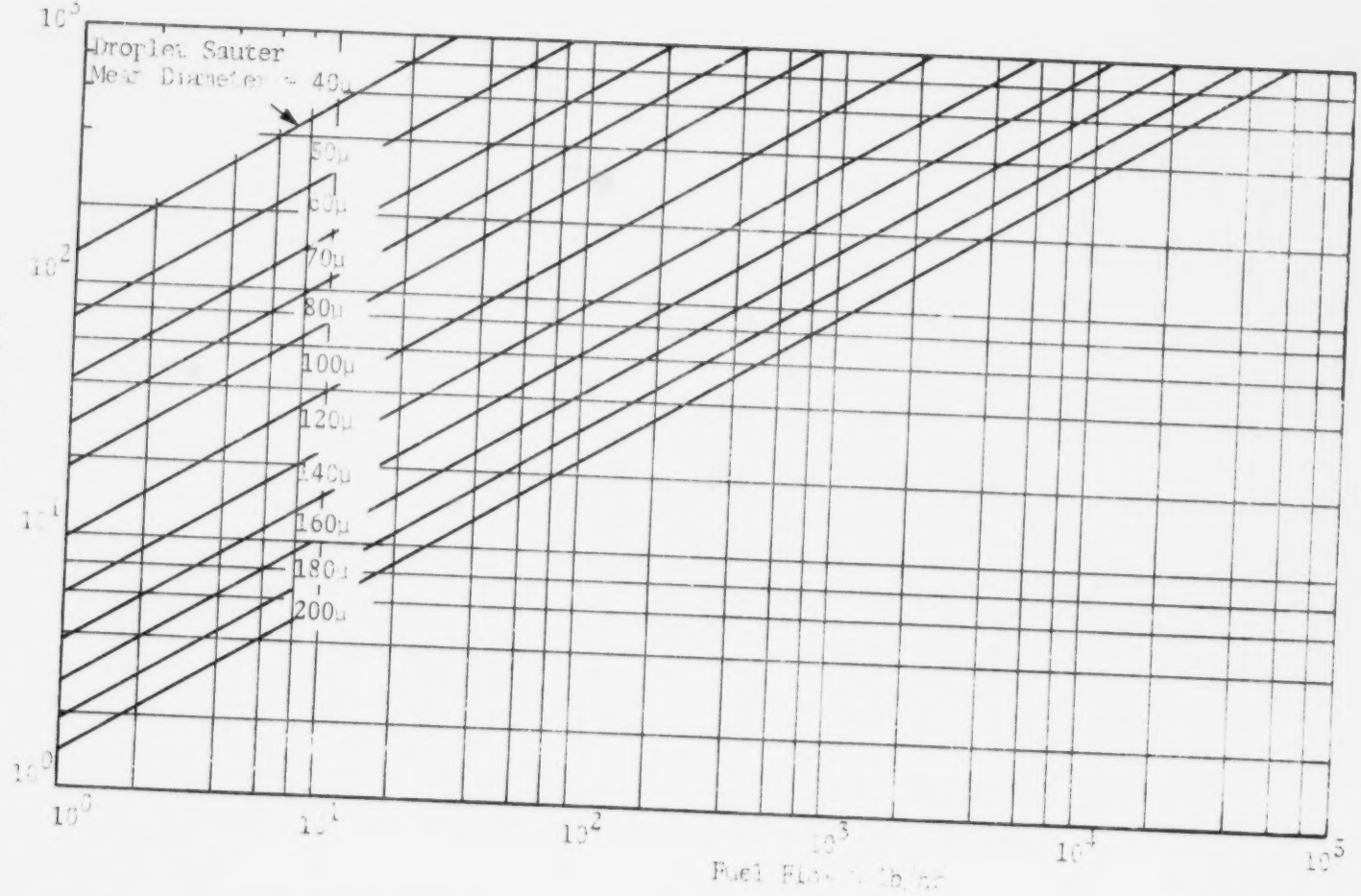

Figure 6-1. Predicted Droplet Size for Simplex Fuel Nozzles (from Accessories Division, Parker-Hannifin Corporation)

Table 6-1. Calculated Values of τ_{eb}

$\dot{m}$ kg/sec	P atm	$T_{inlet\ air}$ °K	ϕ_o	ΔP_f, 35 gal/hr Nozzle, atm	τ_{eb} msec
3.0*	5	500	0.2	29.3	0.5
1.0	2	500	0.2	12.8	0.7
1.5	5	500	0.2	13.2	0.6
1.0	5	550	0.2	9.4	0.6
1.0	5	500	0.2	9.4	0.6
1.0	5	500	0.1	6.7	0.7
1.0	5	500	0.3	13.1	0.6
1.0	5	450	0.2	9.4	0.7
1.0	8	500	0.2	6.6	0.7
0.5	5	500	0.2	6.3	0.7

*Single point probe study only

Values of the reference velocity for the two disc sizes were calculated directly via Equation 4-6. This in turn allowed the calculation of $\tau_{s\ell,co}$ from both Equations 4-7a and 4-7b, with the temperature of the burned gas in Equation 4-7b taken to be that at the exhaust plane. These values of $\tau_{s\ell,co}$ are listed in Tables 6-2 and 6-3 for the two disc sizes along with the values of V_{ref}.

Before $\tau_{s\ell,co}$ can be calculated via Equation 4-7c, an expression for the power input to the turbulent mixer is needed. This power input to the turbulent mixing process in the shear layer is extracted from the main flow by the shearing action which gives rise to a kinetic energy loss of the main flow. The resulting change in the kinetic energy of the main flow can be detected as a pressure drop, ΔP_a, across the turbulent region. Thus the power input to the shear layer mixing zone can be taken as

$$\dot{W} \sim \frac{\Delta P_a}{\rho} \dot{m}_{air} \qquad 6\text{-}2$$

Upon substituting Equation 6-2 into Equation 4-7c, utilizing Equation 4-6, expressing the mass of the mixer as the volume times the density of the mixer, and applying the ideal gas law, a result suitable for computational purposes is obtained.

$$\tau_{s\ell,co} = C \left[\frac{Vo\ell \; L^2}{R \; T \; A \; V_{ref}} \frac{P}{\Delta P_a} \right]^{1/3} \qquad 6\text{-}3$$

where C is a proportionality constant and T is the temperature in the mixer.

Corrsin (1957) estimated the proportionality constant to have a value of approximately 2, based on turbulence measurements behind grids in wind tunnel experiments. From the correlation of Van De Vusse's (1955) data for stirred reactors, Evangelista et al. (1969a) deduced the proportionality constant to be 10. However Evangelista et al. (1969b) do note that the estimated proportionality constant cannot be taken as anything more than a rough indication of the order of magnitude. The value will depend strongly upon the geometrical design and should be obtained experimentally for a given mixing configuration. Following Vranos (1974), a value of 10 will be used in the calculations.

Although the shear layer is the region of mixing of greatest interest, mixing does occur within the recirculation zone as well. Hence

Table 6-2. Values of $\tau_{s\ell,co}$ and $\tau_{s\ell,no}$ (11.43 cm disc diameter)

$\dot{m}$ kg/sec	P atm	$T_{inlet\ air}$ °K	ϕ_o	V_{ref} m/sec	$\Delta P_a/P$ %	$\tau_{s\ell,co}$ Eqn. 4-7a msec	$\tau_{s\ell,co}$ Eqn. 4-7b msec	$\tau_{s\ell,co}$ Eqn. 4-7c msec	$\tau_{s\ell,no}$ Eqn. 4-8 msec
3.0*	5	500	0.2	125	8.0	0.91	0.14	2.5	1.5
1.0	2	500	0.2	104	11.7	1.1	0.17	2.4	1.8
1.5	5	500	0.2	63	2.0	1.8	0.29	5.1	3.0
1.0	5	550	0.2	46	1.4	2.5	0.40	6.3	4.2
1.0	5	500	0.2	42	1.3	2.7	0.43	6.7	4.5
1.0	5	500	0.1	42	1.2	2.7	0.49	6.9	5.3
1.0	5	500	0.3	42	1.4	2.7	0.39	6.5	3.8
1.0	5	450	0.2	38	1.2	3.0	0.47	7.1	4.8
1.0	8	500	0.2	26	0.6	4.4	0.69	10.2	7.2
0.5	5	500	0.2	21	0.7	5.5	0.87	10.4	8.9

*Single point probe study only

Table 6-3. Values of $\tau_{s\ell,co}$ and $\tau_{s\ell,no}$ (8.89 cm disc diameter)

$\dot{m}$ kg/sec	P atm	$T_{inlet\ air}$ °K	ϕ_o	V_{ref} m/sec	$\frac{\Delta P_a}{P}$ %	$\tau_{s\ell,co}$ Eqn. 4-7a msec	$\tau_{s\ell,co}$ Eqn. 4-7b msec	$\tau_{s\ell,co}$ Eqn. 4-7c msec	$\tau_{s\ell,no}$ Eqn. 4-8 msec
1.0	2	500	.2	65	4.6	1.4	0.4	3.7	1.4
1.5	5	500	.2	39	0.8	2.3	0.7	7.9	2.3
1.0	5	550	.2	29	0.6	3.1	0.9	9.6	3.3
1.0	5	500	.2	26	0.5	3.4	1.0	10.6	3.5
1.0	5	500	.1	26	0.5	3.4	1.1	10.6	4.2
1.0	5	500	.3	26	0.6	3.4	0.9	9.9	3.0
1.0	5	450	.2	24	0.5	3.7	1.0	10.8	3.7
1.0	8	500	.2	16	0.2	5.6	1.6	16.8	5.7
0.5	5	500	.2	13	0.3	6.8	2.0	15.8	7.0

the volume of the mixing zone is taken to be a cylinder of diameter equal to the disc diameter and following Winterfeld (1965) a length which is proportional to the disc diameter. From the results of the internal probing studies, the cylinder length was taken as 1.5 times the disc diameter. Since the size of the largest eddies in the turbulent field is limited by the flow geometry, the integral scale of the turbulence was taken to be the spacing between the disc and the duct wall. For a mixing zone temperature of 1500°K, values of $\tau_{s\ell,co}$ via Equation 4-7c are listed in Tables 6-2 and 6-3 along with the values of the combustion zone pressure drop, ΔP_a.

The characteristic eddy decay time relevant to NO formation in the shear layer, $\tau_{s\ell,no}$, was calculated directly from Equation 4-8. T_b was again taken as the temperature of the burned gas at the exhaust plane and V_o differs from V_{ref} only by a geometric factor. The computed values of $\tau_{s\ell,no}$ are also listed in Tables 6-2 and 6-3.

Again it should be emphasized that the values of $\tau_{s\ell,co}$ and $\tau_{s\ell,no}$ given in Tables 6-2 and 6-3 are only order of magnitude calculations. Uncertainties exist in the turbulent velocity (taken as proportional to a convective velocity) and also upon the proportionality constant of Equation 4-7c. However the relative magnitudes of τ_{eb}, $\tau_{s\ell,co}$ and $\tau_{s\ell,no}$ should be deducible from the success of each of these time parameters in correlating the exhaust plane emissions.

B. Correlation of NO_x Emissions

On comparison of the values of the fuel ignition delay and burning time, τ_{hc} (Table 4-3), and the values of the shear layer mixing times listed in Tables 6-2 and 6-3, it is seen that the mixing time is generally much greater in all cases. Thus the combustion precess is mixing controlled and in agreement with the internal probing results, the resultant flame structure will resemble a turbulent diffusion flame. As a result of the diffusion flame structure, combustion will occur only over a narrow range of local equivalence ratios centered about unity.

The values of the characteristic NO formation time (Table 4-3) should also be compared with the mixing times of Tables 6-2 and 6-3. Note that for local equivalence ratios near unity, τ_{no} is generally greater

than $\tau_{s\ell,no}$. Hence the rate of NO formation will be determined by the rate at which the hot combustion products are diluted with colder species. If the mixing is faster than the NO formation time, then NO formation is mixing limited and NO emissions should correlate with $\tau_{s\ell,no}$.

Consider the rate of NO formation about an eddy of fuel within the shear layer. Combustion will occur at the boundaries of the fuel eddy as the mixing process proceeds. The rate of NO formation can then be expressed as a function of the local equivalence ratio of the combustion process occurring at the boundaries of the eddy

$$\frac{d[NO]}{dt} \Big/ _{\text{fuel eddy}} = f(\phi) \qquad 6\text{-}4$$

However it was noted earlier that due to the combustion time being much less than the mixing time, combustion occurs only over a narrow range of local equivalence ratios. Stated otherwise, the NO formation is greatest over a narrow range of equivalence ratios centered about unity. This is then the regime of combustion that must be considered in order to correlate NO emissions. Thus $f(\phi)$ in Equation 6-4 can be assumed constant, and the integration is direct.

$$[NO]_{\text{fuel eddy}} \sim \tau_{s\ell,no} \qquad 6\text{-}5$$

Since the rate of NO formation is limited by the mixing of colder species into the hot combustion products, the time for NO production is taken to be the mixing time.

To determine the total NO generated by the gas turbine combustion process, a sum must be taken over all of the fuel eddies. However the number of fuel eddies in the system is just proportional to the amount of fuel supplied to the burner. Hence the total NO emissions are proportional to the mass of fuel supplied.

$$[NO]_{\text{total}} \sim (\text{fuel supplied})\ \tau_{s\ell,no} \qquad 6\text{-}6$$

On dividing both sides of Equation 6-6 by the mass of the fuel, the NO emissions index, NOEI, is formed.

$$NOEI = \text{constant} \cdot \tau_{s\ell,no} \qquad 6\text{-}7$$

If the analysis leading to Equation 6-6 is valid, then NOEI should remain constant for a fixed mixing time as the fuel flow rate is varied, assuming that τ_{eb} either remains constant or is much less than $\tau_{s\ell,no}$.

In order to examine the validity of Equation 6-6, experimental measurements of NO_x were gathered for overall equivalence ratios of 0.1, 0.2, and 0.3 at constant values of air flow rate, combustor pressure, and inlet air temperature. In presenting the results, the dependence of $\tau_{s\ell,no}$ has been included through division of the NO_xEI values by the appropriate values of $\tau_{s\ell,no}$ taken from Tables 6-2 and 6-3. Net NO_x emissions (test combustor measurement minus heating combustor measurement) data, taken from Tables A-22 and A-24, are plotted in Figure 6-2. Although NO_xEI does decrease almost linearly with increasing overall equivalence ratio over the three fold change in fuel flow rate, the reduction is small compared to the predictions of chemical kinetics for similar changes in the local equivalence ratio. This is evident upon noting the change in the characteristic NO formation times for variation of the local equivalence ratio (Table 4-3). The experimental results presented in Figure 6-2 do suggest that combustion occurs at a nearly constant local equivalence ratio with changing overall equivalence ratio. The decrease in NO_xEI with increasing fuel flow could in part result from improved mixing at the higher fuel flows due to increased flame generated turbulence. In addition, some heterogeneous effects may be coming into play as the SMD of the fuel spray does decrease with increasing fuel flow.

In going from an overall equivalence ratio of 0.2 to 0.3 in Figure 6-2, the larger decrease in NO_xEI for the smaller disc can be attributed in part to the higher fuel loading per unit volume in the shear layer zone behind this disc. Since the combustion efficiency is not too different for the two discs, the mixing rate in the shear layer region of the smaller disc must be significantly greater than that of the larger disc.

Similar results for variation of the fuel flow rate at a nearly constant mixing condition exist in the literature. Tuttle et al. (1973)

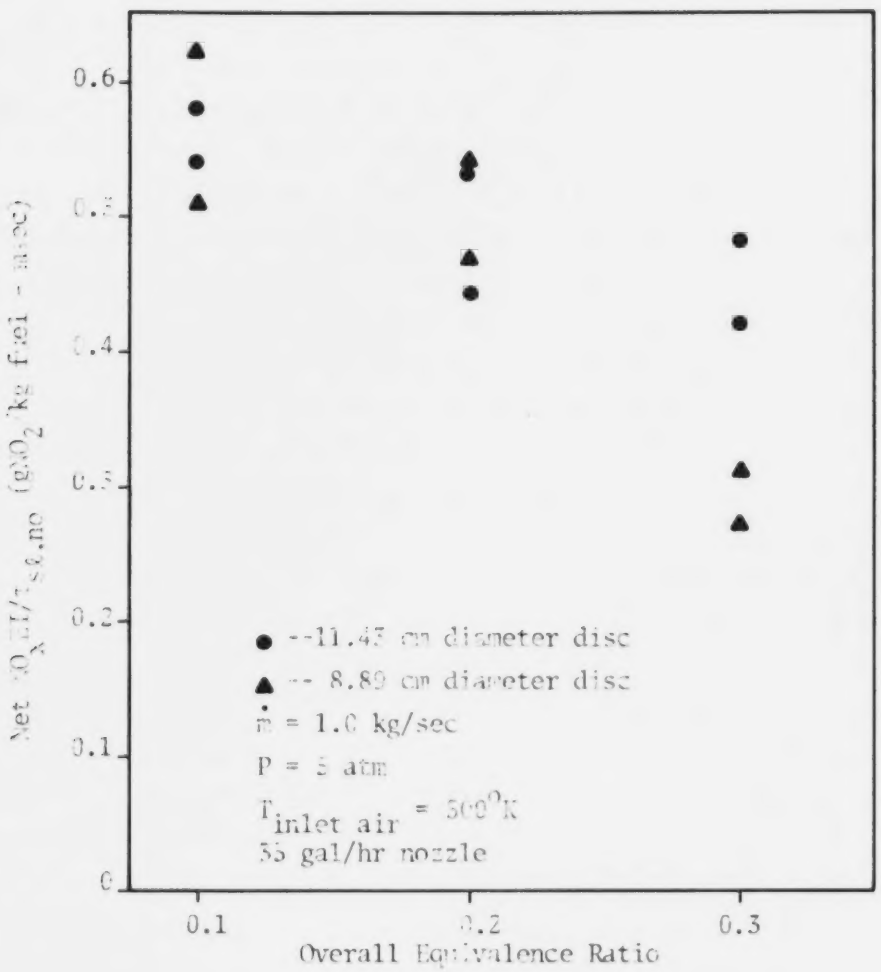

Figure 6-2. Overall Equivalence Ratio Variation

in studying the emissions characteristics of the Allison J-33 combustor, observed NOEI to decrease from 3.5 to 2.3 gNO_2/kg fuel as the overall equivalence ratio was increased from 0.15 to 0.25. Thus only a 34% decrease in NOEI was found for a 167% increase in the fuel flow rate. In addition for a conventional gas turbine liner, Friswell (1972) observed little change in NO_xEI over a four fold change in fuel flow rate. These two earlier studies together with the present investigation do indeed suggest that the combustion process in a liquid fueled gas turbine combustor occurs only over a narrow range of local equivalence ratios. Hence provided the droplet evaporation time is short, NO_xEI should correlate according to Equation 6-6.

All of the exhaust plane NO_x emissions data contained in Tables A-20 through A-24 are plotted in Figure 6-3 against the calculated values of $\tau_{s\ell,no}$ listed in Tables 6-2 and 6-3. Although some data scatter is expected since the effect of the inlet temperature variation upon chemical reaction rates has not been included, the results generally fall about a linear relationship for the various fuel nozzles and two disc diameters. The data points falling farthest from a linear relationship are for run conditions where the differential fuel injection pressure is lowest (below 6.5 atm) and are designated by flagged symbols. These low differential fuel injection points are presumably run conditions at which heterogeneous effects must be included in the NO_xEI correlating parameter.

The data scatter in Figure 6-3 would be somewhat reduced if straight lines were drawn through the points corresponding to a particular fuel nozzle. Hence a small influence of each particular nozzle performance is perhaps observed. In agreement with the calculations listed in Tables 6-1 and 6-2 which show the droplet lifetimes to be much less than the mixing times, the effect of a particular nozzle is small. In addition, a uniform trend between the measured emissions and the size of the nozzles is not observed. The 50 gal/hr nozzle generally resulted in the higher emissions while the lowest emissions were recorded for the 35 gal/hr nozzle rather than the 16 gal/hr nozzle. Thus the data scatter in Figure 6-2 about a linear relationship could result from other sources of measurement irreproducibility.

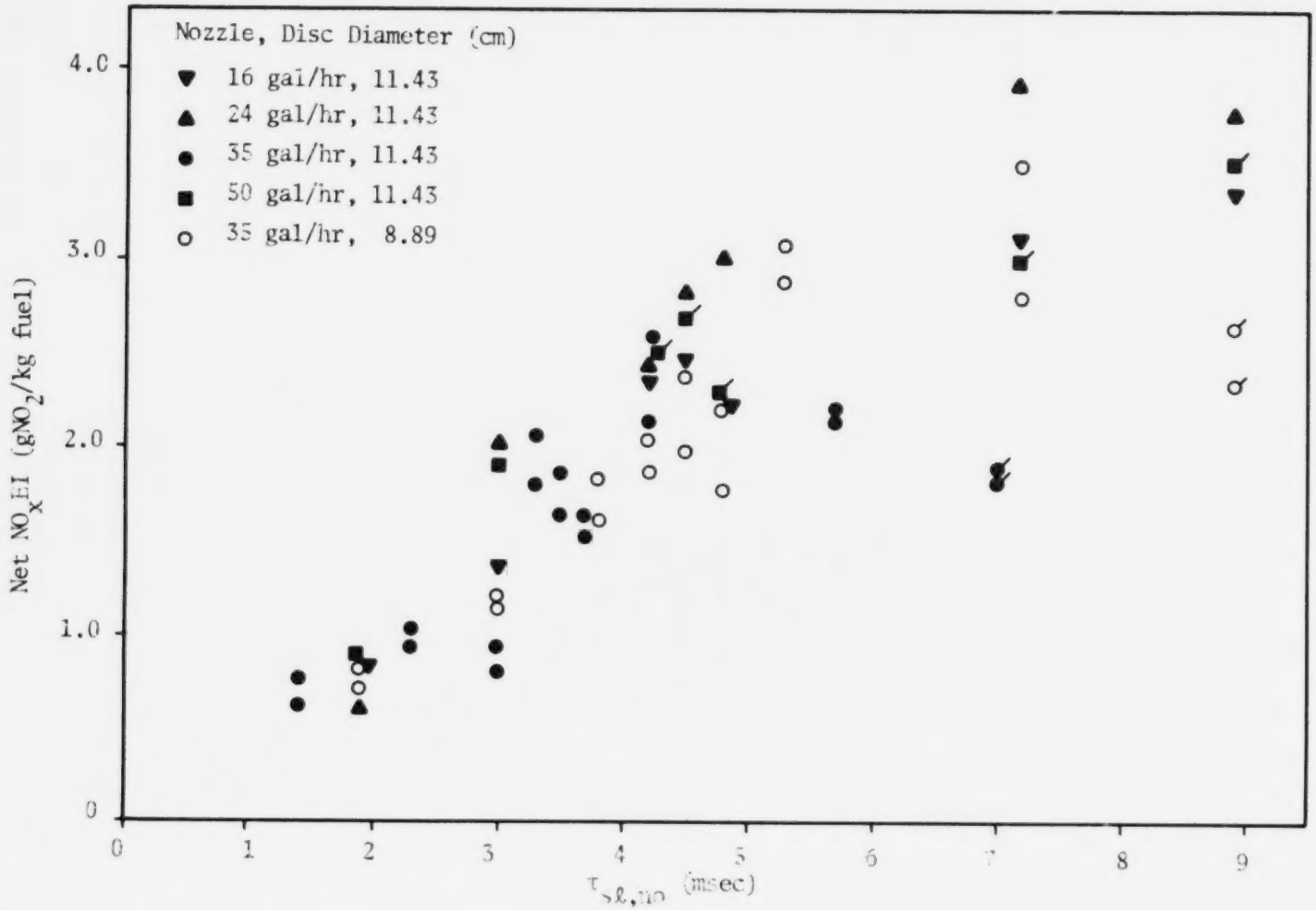

Figure 6-3. Net NO_xEI versus $\tau_{sl,no}$. Flagged symbols represent runs with low fuel differential injection pressure.

Figure 6-3 also shows the NO_xEI data for the smaller disc stabilizer to nearly fall in line with that of the larger disc. Thus credence is given to the selection of the disc diameter as the appropriate integral length scale of the turbulence in the NO producing region of the disc stabilized flame.

C. Correlation of CO and HC Emissions

Recall that in the discussion of the internal probing data, it was noted that a small percentage of the liquid fuel droplets penetrated through the shear layer into the colder main stream. Although these droplets are not sufficient in number to substantially affect NO emissions, they may represent a sizable contribution to both the CO and HC emissions. In particular if these fuel droplets evaporate far downstream in the combustor, the time allowed for complete oxidation to CO_2 is considerably reduced over the time allowed when the drops evaporate within the shear layer. The CO and HC emissions resulting from large droplet penetration should be closely related to the droplet lifetime. However the appropriate droplet lifetime is that of the largest droplets in the fuel spray rather than that of the SMD of the spray.

The second process producing CO and HC emissions in a gas turbine combustor, that of reaction quenching at the outer periphery of the shear layer, has been extensively discussed previously in Section IV B. These CO and HC emissions are derived from fuel droplets which have evaporated within the shear layer and should correlate with an appropriate mixing time since it is too rapid mixing which causes the oxidation reactions to be quenched. Decreasing $\tau_{s\ell,co}$ decreases the time a fluid element containing CO or HC remains at a sufficient temperature for either to undergo oxidation.

In the analysis of CO and HC combustor emissions data, it is generally observed that both species exhibit similar trends (Verkamp et al., 1974). From Figure 6-4 in which HCEI is plotted against COEI, it is seen that this is also true of the disc stabilized flame. For various fuel injectors and two disc sizes, a given level of HCEI corresponds to a unique level of COEI. This is not unexpected, as CO and HC emissions

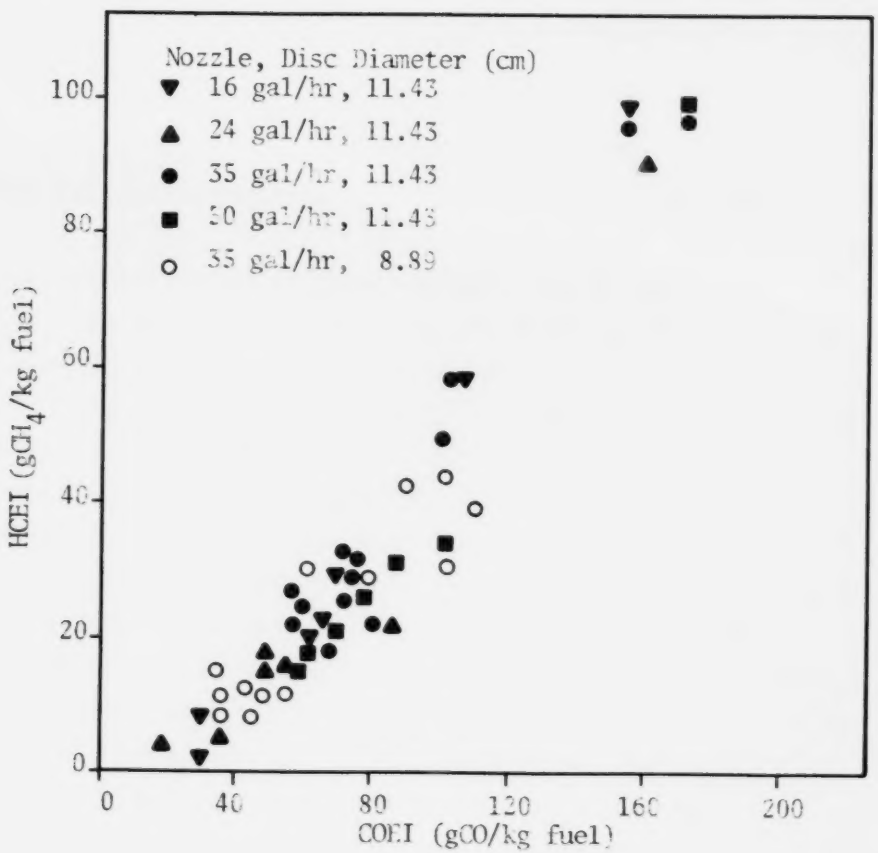

Figure 6-4. HCEI versus COEI

result from the same physical processes. Hence in the following, only CO data are correlated with $\tau_{s\ell,co}$.

For CO emissions resulting from quenching phenomena about the shear layer, CO burnup is proportional to the mixing time, $\tau_{s\ell,co}$. Stated differently, the level of CO emissions is inversely proportional to $\tau_{s\ell,co}$ if mixing is controlling (i.e. $\tau_{s\ell,co} >> \tau_{eb}$).

$$[CO] \sim \frac{1}{\tau_{s\ell,co}} \qquad 6\text{-}8$$

Hence for COEI plotted against $1/\tau_{s\ell,co}$, a mixing controlled combustion process will yield a straight line.

All of the CO measurements gathered in the present investigation are plotted versus the three different functional forms of $\tau_{s\ell,co}$ in Figures 6-5, 6-6, and 6-7. Net CO emissions have not been used since as can be seen in Tables A-20 through A-24, the CO emissions of the heating combustor are but a small fraction (typically less than 5%) of those measured at the exhaust of the test burner. Note that each of these three graphs does exhibit a nearly linear relationship. Although the shape of the curve in each figure suggests that the mixing time is controlling at most run conditions, the effect of large droplet penetration is evident at all run points. The two larger nozzles (35 and 50 gal/hr) which have the poorest atomization properties consistently yield the higher CO emissions. In addition, there are data points for the 35 and 50 gal/hr nozzles which fall far above a straight line in each figure, and these points correspond to run conditions in which the differential fuel injection pressure is low (poor atomization). The points off the curve are then at run conditions where the fuel spray contains a greater number of large fuel droplets and where droplet penetration is the primary physical process leading to CO emissions. This is particularly pronounced for the test point corresponding to the small disc and a low differential injection pressure. Here the length the fuel droplets must penetrate before reaching the colder main flow is reduced, and hence a greater dependence of CO emissions upon fuel atomization is exhibited.

Excluding the low fuel differential injection pressure data points, the three different functional forms for $\tau_{s\ell,co}$, Equation 4-7a,

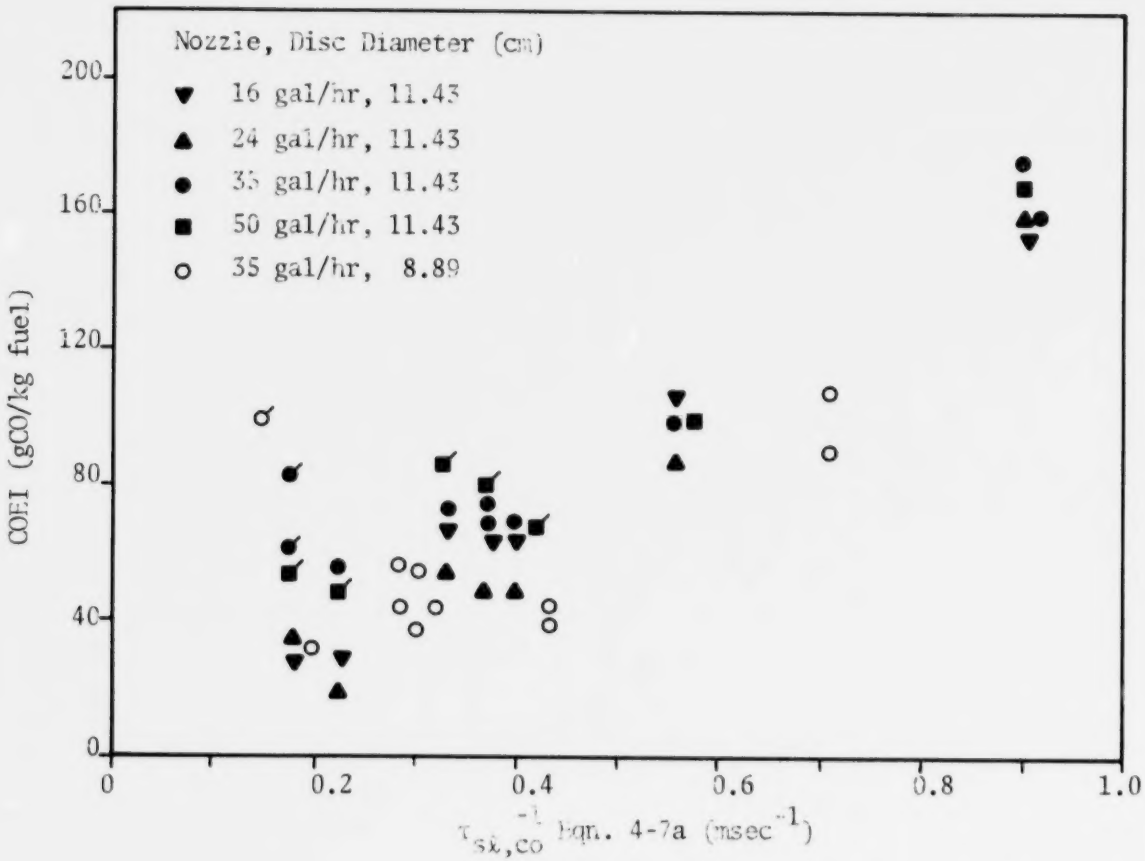

Figure 6-5. COEI versus $\tau_{s\ell,co}^{-1}$ (Eqn. 4-7a). Flagged symbols represent runs with low fuel differential injection pressure.

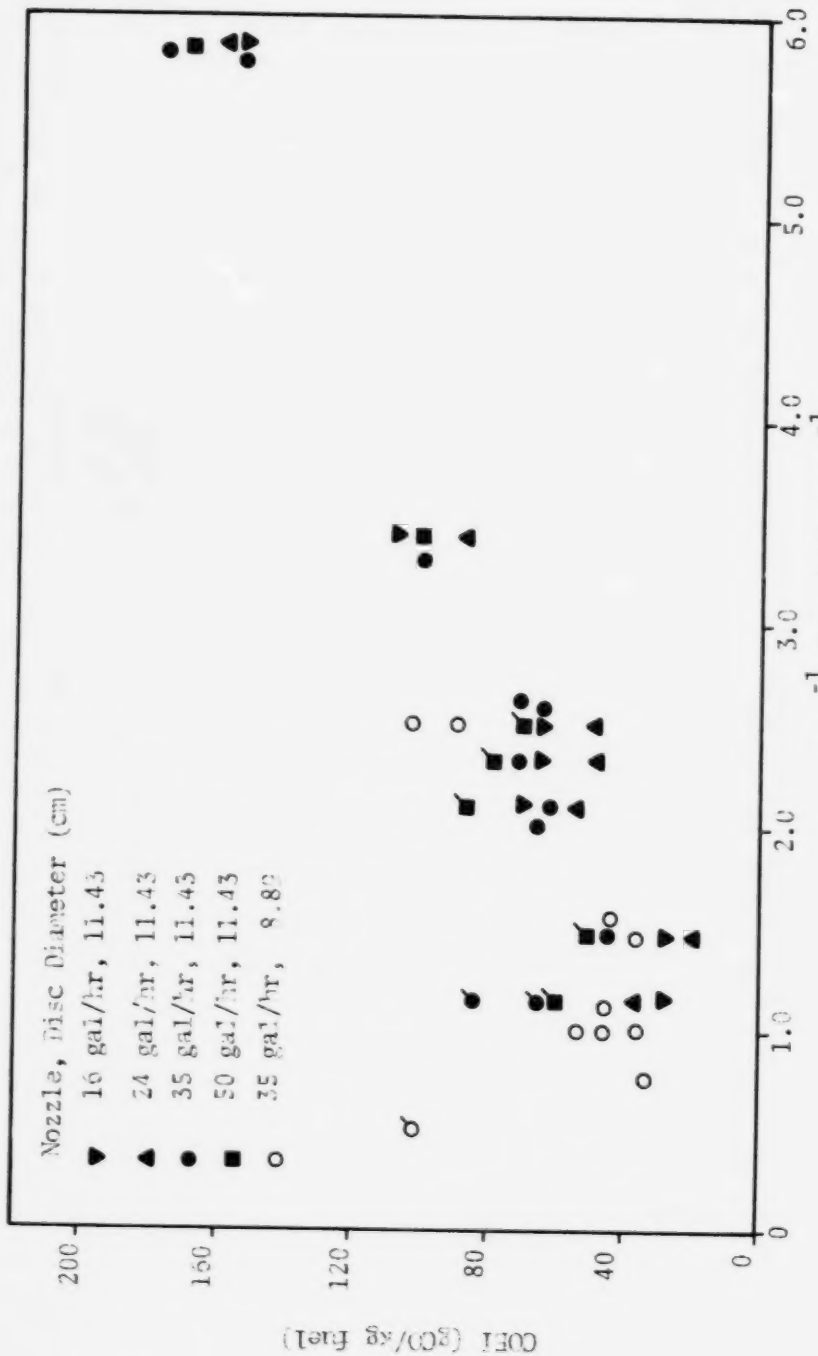

Figure 6-6. COEI versus $\tau_{sl,co}^{-1}$ (Eqn. 4-7b). Flagged symbols represent runs with low fuel differential injection pressure.

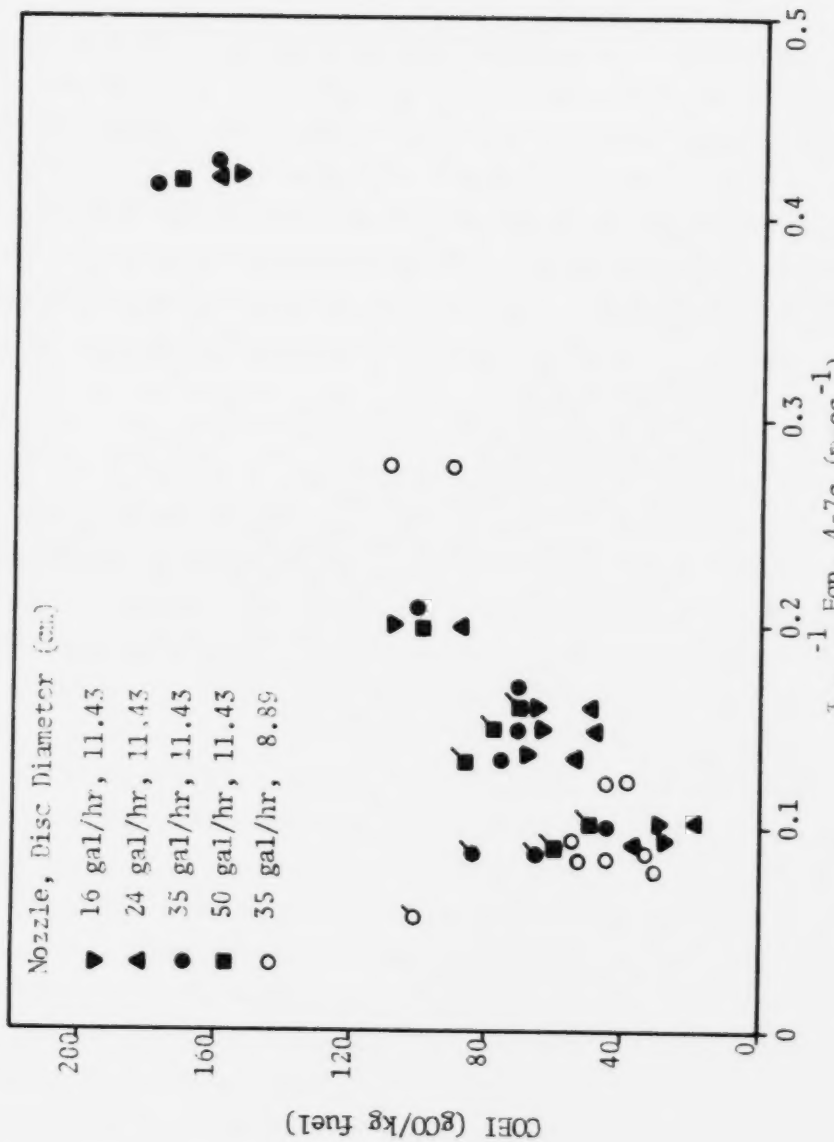

Figure 6-7. COEI versus $\tau_{\ell,co}^{-1}$ (Eqn. 4-7c). Flagged symbols represent runs with low fuel differential injection pressure.

4-7b, and 4-7c, each appear to successfully collapse the data for the two disc diameters onto a single curve, with no significant advantage of one over the other two. Thus based on the present experimental findings, no conclusion can be drawn as to which functional relationship for $\tau_{s\ell,co}$ is the more appropriate.

The CO emissions data do suggest that one additional time parameter may be necessary to totally correlate all the test points. This parameter would represent the time required for a droplet to traverse the distance from the fuel injector to the main flow. If this time is greater than the lifetime of the largest droplets in the fuel spray, then CO emissions result from quenching about the shear layer only. On the other hand, if this droplet traverse time is less than the lifetime of the largest droplets, then CO emissions resulting from droplet penetration may dominate.

D. Summary

The characteristic time parameters introduced in Section IV were used successfully to analyze and correlate both NO_x and CO exhaust plane emissions data. HC emissions were found to correlate well with CO emissions for various fuel nozzles and two disc diameters, indicating that similar physical processes are responsible for both of these pollutant species.

Results of the time parameter calculations suggest that for stable burner operating conditions, the fuel ignition delay and burning time is significantly shorter than either τ_{eb} or $\tau_{s\ell}$. Thus the flame structure and the resulting emissions are determined by the fuel evaporation rate and the subsequent mixing with oxidizer.

NO_x and CO exhaust plane emissions generally correlated well with $\tau_{s\ell,no}$ and $1/\tau_{s\ell,co}$ respectively, and thus are primarily mixing controlled. However for test points characterized by poor fuel atomization, these species could not be successfully correlated by mixing parameters. For the run conditions with poor fuel atomization (which are typical of Figure 4-2a), heterogeneous effects must also be considered in order to correlate the measurements.

The scaling relationships suggested in Section IV for correlating NO_x and CO emissions did collapse the experimental data obtained for the two disc diameters when the combustion process was mixing controlled. This demonstrates that indeed CO and NO_x exhaust emissions originate from two different regions within the flame and a different integral time scale is associated with each region. Since these two emissions producing regions are separate, the possibility exists of reducing both CO and NO_x emissions simultaneously by decreasing the mixing rate in the outer periphery of the shear layer where CO reactions are quenched and increasing the mixing rate in the inner shear layer where NO is formed.

According to the integral length scales for the turbulence suggested in Section IV, decreasing the disc diameter from 11.43 to 8.89 cm should decrease the mixing rate in the CO producing region and increase the mixing rate in the NO producing region. Thus both CO and NO_x emissions should decrease in going from the larger to the smaller disc.

COEI is plotted against NO_xEI in Figure 6-8 for the two disc diameters. As predicted by Equations 4-7 and 4-8 for a mixing controlled process, CO and NO_x emissions do decrease simultaneously in going from the larger to the smaller disc. However the atomization properties of the fuel nozzle cannot be neglected since the CO emissions at low differential fuel injection pressures are also dependent upon fuel droplet penetration. Thus the poor fuel atomization point for the small disc lies well above the curve for the mixing controlled emissions.

The exhaust plane measurements of CO and NO_x emissions for the two disc sizes and the 35 gal/hr fuel nozzle are compared with values of these species measured at the exhaust of existing gas turbine engines in Figure 6-9. The band of idle to maximum power emissions was obtained from exhaust measurements for a wide range of Detroit Diesel Allison, Pratt and Whitney, and General Electric engines (Verkamp et al., 1974). For reference, the figure also shows the dependence of the Environmental Protection Agency standards upon engine specific fuel consumption. Note that the emissions with the larger disc flame stabilizer overlap with those of gas turbine combustors but the emissions of the smaller disc show an improvement over existing combustors. Although this improvement

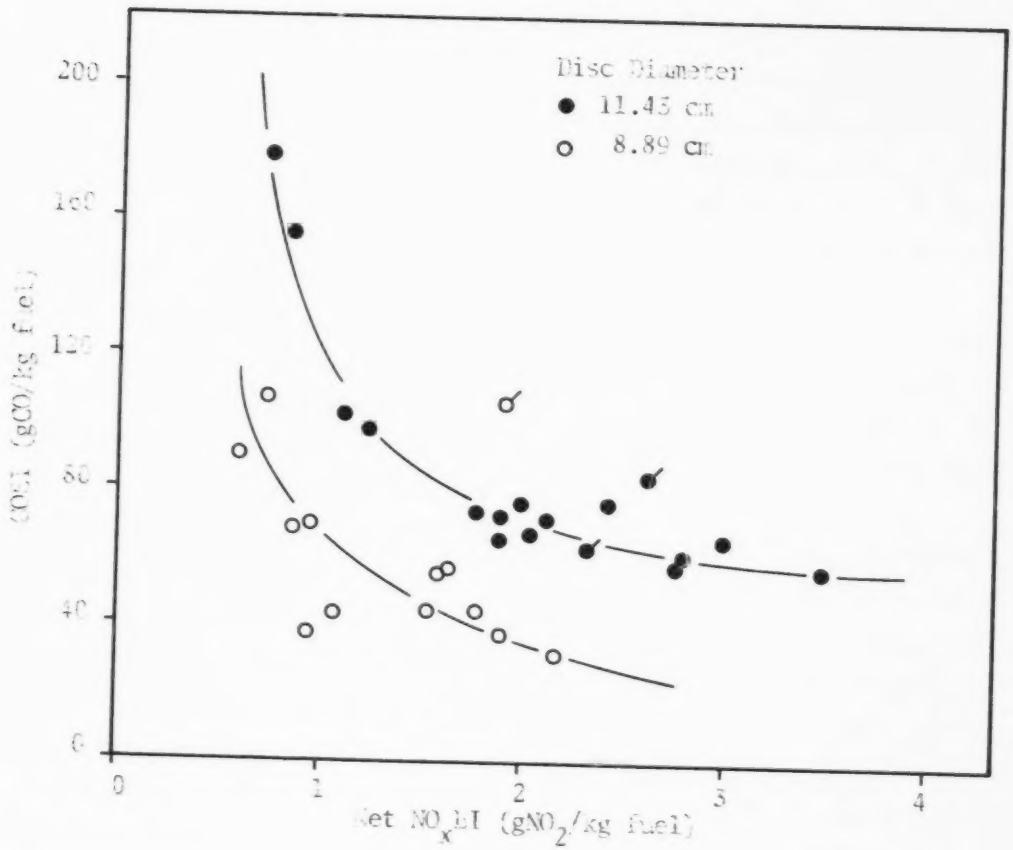

Figure 6-8. CO:I versus NO_xEI. Flagged symbols represent runs with low fuel differential injection pressure.

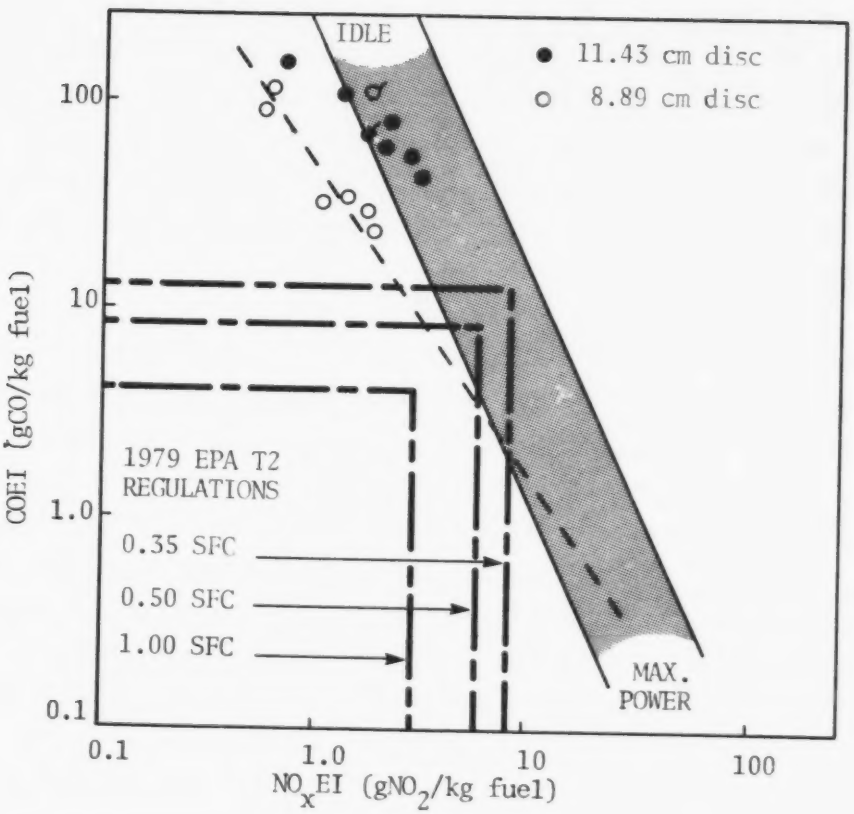

Figure 6-9. Emissions of Conventional Combustors (from Verkamp et al., 1974). Flagged symbols represent runs with low fuel differential injection pressure. The dashed line represents emissions characteristics for the disc diameter yielding the minimum CO emissions.

in exhaust characteristics may result in part from a reduced NO formation rate due to the use of vitiate inlet air, it is interesting to comment on the minimum levels of NO_x and CO emissions possible with a further reduction in the disc diameter. From Equation 4-8, it is seen that NO formation will continue to decrease with decreasing disc diameter. The same may not be true for CO emissions since Equations 4-7a and 4-7c contain maximum values of $\tau_{s\ell,co}$ for d/D values of 0.58 and 0.53 respectively. Thus for too small of a disc diameter, the size of the largest eddies may decrease at a more rapid rate than the reference velocity.

Using a d/D of 0.55, values of $\tau_{s\ell,co}$ and $\tau_{s\ell,no}$ were calculated for this lowest CO emissions disc diameter from Equations 4-7a and 4-8 for various burner operating parameters. Assuming a mixing controlled combustion process (i.e. $\tau_{s\ell} >> \tau_{eb}$), corresponding values of COEI and NO_xEI were obtained from Figures 6-5 and 6-3, respectively, and are shown as the dashed line on Figure 6-9. As is seen in Figure 6-9, the disc stabilized flame has improved emissions characteristics over conventional combustors for the portion of the graph corresponding to combustor idle operation but is poorer at the maximum power mode of combustors. Thus although the disc stabilized flame appears to show an improvement over combustors for the experimental operating points in this investigation, the geometry does suffer from poor combustion efficiency when extrapolated to high combustor loadings.

VII. FUTURE EXPERIMENTS--VARIATION OF τ_{eb} AND $\tau_{s\ell}$

Although the presence of the liquid fuel spray penetration is particularly noticable in the higher air flow rate flames discussed in Section V, generally the exhaust plane emissions of Section VI correlated well without including a function of τ_{eb} in the correlating parameter. Thus with the use of liquid propane fuel and the exception of the lowest air flow rate case, $\tau_{s\ell}$ appears to be the controlling characteristic time for all the operating points listed in Table 3-2. This experimental finding was anticipated since liquid propane is extremely volatile, and hence the effect of liquid droplets is minimal.

Additional experiments are planned in which $\tau_{s\ell}$ will remain relatively unchanged from the present experiments while τ_{eb} is greatly increased. In order to facilitate the comparison of the results of these future studies with those of Section VI, the burner will be operated over the same run points. Hence the fluid mechanic structure of the recirculation zone and shear layer regions will be generally maintained but the fuel spray penetration will be greatly augmented.

As discussed earlier in Section IV-A, the fuel droplet lifetime depends on the fuel properties, the fuel injector, and the environment into which the droplet is evaporating. However since both the run points and the fuel nozzles are to be unchanged, an increase in τ_{eb} requires a fuel alteration. The fuel selected for use in the test section for the future experiments is a kerosine base hydrocarbon fuel, Jet A, which has a viscosity of an order of magnitude greater than liquid propane at $40^{o}C$.

Similar τ_{eb} calculations to those of Section VI for propane have been repeated for Jet A and are listed in Table 7-1. Values of the initial spray SMD were taken from Figure 6-1 since the properties of Jet A are not too unlike those of JP-5. As a result of the wide variation

in components of Jet A and not wanting to bias the calculations by a small fraction of high boiling point compounds, the vaporization temperature of the fuel was taken to be the 90% vaporized point, with the necessary fuel property data taken from Moses (1975).

Table 7-1. Fuel Droplet Lifetimes, 35 gal/hr Nozzle

$\dot{m}$ kg/sec	P atm	$T_{inlet\ air}$ °K	ϕ_o	τ_{eb}, propane msec	τ_{eb}, Jet A msec
1.0	5	500	0.2	0.6	17.5
1.0	5	450	0.2	0.7	17.5
1.0	5	550	0.2	0.6	17.5
1.0	2	500	0.2	0.7	21.4
1.0	8	500	0.2	0.7	14.5
0.5	5	500	0.2	0.7	27.2
1.5	5	500	0.2	0.6	13.3
1.0	5	500	0.1	0.7	27.2
1.0	5	500	0.3	0.6	13.3

The values of τ_{eb} listed in Table 7-1 for Jet A are seen to be increased over those for propane by greater than an order of magnitude. These greatly increased evaporation times result primarily from the increased fuel viscosity of Jet A over propane and hence a correspondingly greater SMD of the fuel spray.

The heterogeneous effects within the combustion process are expected to be pronounced with Jet A fuel. The relatively high values of τ_{eb} correspond to an increased flame length and lower combustion efficiency.

Another study planned is to vary $\tau_{s\ell}$ while holding τ_{eb} constant. A nearly constant droplet lifetime results if the fuel type and nozzle are unchanged and a constant fuel flow rate is maintained. This, in turn, requires that in order to retain the same overall equivalence

ratio, the air flow rate must also be maintained. Hence for a constant τ_{eb}, $\tau_{s\ell}$ could in principle be varied through a combustor pressure change. In practice however (as noted in Section II), the ambient pressure into which the fuel is injected does affect the droplet size distribution. Thus it seems that any means of changing $\tau_{s\ell}$ through either pressure, temperature, or air flow rate variation will also alter τ_{eb}.

In order to hold τ_{eb} constant while $\tau_{s\ell}$ is varied then requires a change in the length scales. Again as in the present study, two different disc sizes will be employed in the future experiments. In addition, the length scales of a particular disc will also be varied by use of toothed discs (Figure 7-1). These discs will have the same duct blockage area as the untoothed disc and hence, V_{ref} is unchanged. The integral length scale of the turbulence for CO quenching, following Section IV-B, is now expected to be related to the spacing between adjacent teeth rather than the gap between the duct wall and the disc or the disc diameter. The integral length scale of the turbulence for NO formation (i.e., the disc diameter) should exhibit little change between toothed and untoothed discs.

The above investigation should aid in the clarification of an important concept of gas turbine emissions technology. If the CO emissions are substantially altered while the NO_x emissions are little affected, then the belief that any method of reducing CO emissions inherently increases NO_x emissions is refuted. That is to say CO and NO_x emissions originate in different regions of the flame and the possibility of reducing both of these pollutants through proper tailoring of the turbulent length scales does exist.

An additional study planned is to use the characteristic time parameters, introduced in Section IV, in the correlation of emissions data from gas turbine engines. This will require the determination of the length scales which determine the turbulent mixing rate. It is expected that the integral turbulent length scale in the outer periphery of the shear layer within a combustor would be related to the diameter of any air jets which penetrate into this region. The NO length scale is less

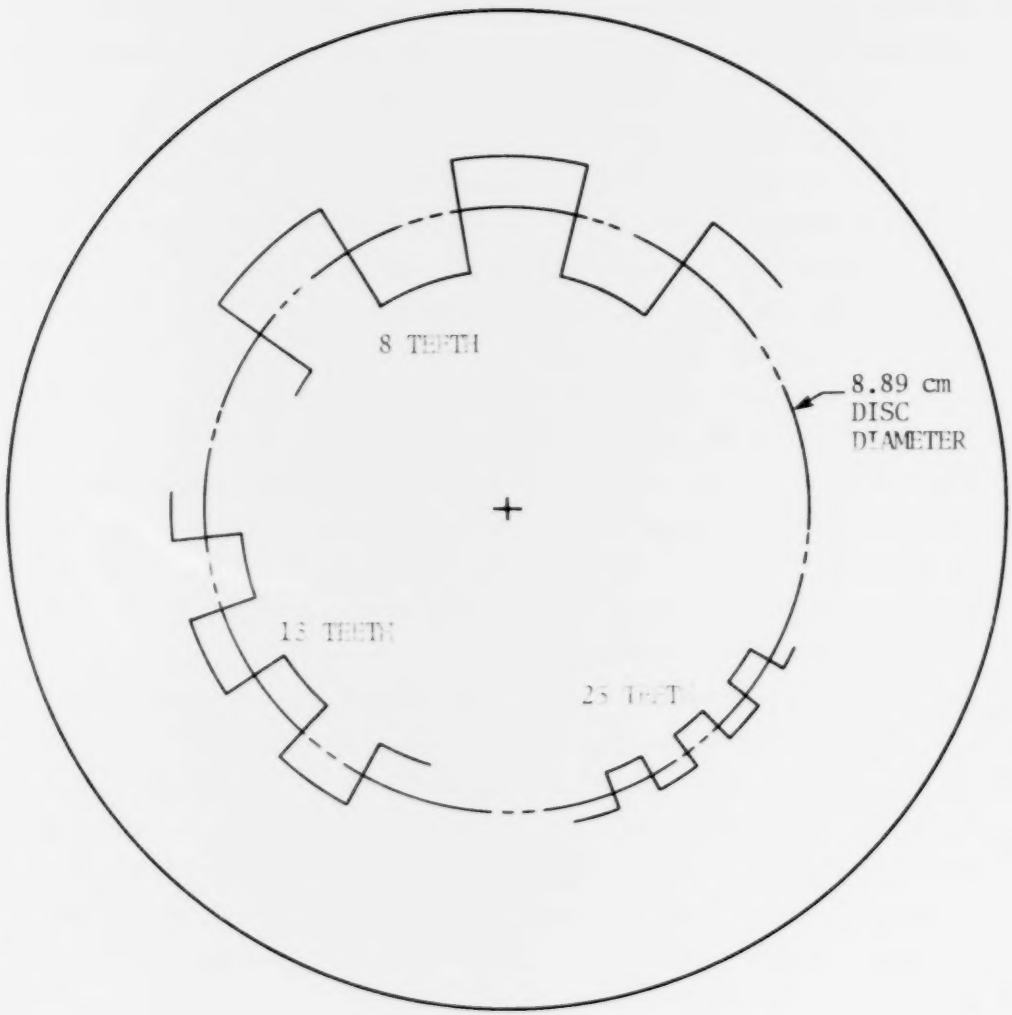

Figure 7-1. Toothed Disc Flame Stabilizers

obvious, but may be the combustor can diameter. If these characteristic times are successful in correlating pollutant emissions, then their utility as design aids in the development of new generation, low emissions combustors will have been strongly demonstrated.

LIST OF REFERENCES

Appleton, J. P. and Heywood, J. B. (1973). "The effects of imperfect fuel-air mixing in a burner on NO formation from nitrogen in the air and the fuel," 777-786, Fourteenth Symposium (International) on Combustion, The Combustion Institute, Pittsburgh.

Bilger, R. W. (1975). "Turbulent jet diffusion flames," Progress in Energy and Combustion Science 1, Pergamon Press, Oxford, in press.

Bryan, R., Godpole, P. S. and Norster, E. R. (1971). "Some observations of the atomizing characteristics of air-blast atomizers," 343-359, Combustion and Heat Transfer in Gas Turbine Systems, Pergamon Press, Oxford.

Chigier, N. A., Makepeace, R. W., and McCreath, C. G. (1973a). "Aerodynamic interaction between burning sprays and recirculation zones," 577-582, Combustion Institute European Symposium, Academic Press, London.

Corrsin, S. (1951). "The decay of isotropic temperature fluctuations in an isotropic turbulence," J. Aeronaut. Sci. 16, 417-423.

Corrsin, S. (1957). "Simple theory of an idealized turbulent mixer," A.I.Ch.E. J. 3, 329-330.

Decorso, S. M. and Kemeny, G. A. (1957). "Effect of ambient and fuel pressure on nozzle spray angle," Trans. ASME 79, 607-615.

Decorso, S. M. (1960). "Effect of ambient and fuel pressure on spray drop size," Trans. ASME 82, 10-18.

Evangelista, J. J., Katz, S., and Shinnar, R. (1969a). "Scale-up criteria for stirred tank reactors," A.I.Ch.E. J. 15, 843-853.

Evangelista, J. J., Shinnar, R., and Katz, S. (1969b). "The effect of imperfect mixing on stirred combustion reactors," 901-912, Twelth Symposium (International) on Combustion, The Combustion Institute, Pittsburgh.

Fraser, R. P. (1957). "Liquid fuel atomization," 687-701, Sixth Symposium (International) on Combustion, The Combustion Institute, Pittsburgh.

Friswell, N. J. (1972). "Emissions from gas-turbine-type combustors," 161-182, Emissions from Continuous Combustion Systems, Plenum Press, New York.

Giffen, E. and Muraszew, A. (1953). The Atomization of Liquid Fuels, Chapman and Hall, London.

Godsave, G. A. E. (1953). "Studies on the combustion of drops in a fuel spray--the burning of single drops of fuel," Fourth Symposium (International) on Combustion, The Williams and Wilkins Company, Baltimore.

Grobman, J. S. (1972). "Effect of operating variables on pollutant emissions from aircraft turbine engine combustors," 279-303, Emissions from Continuous Combustion Systems, Plenum Press, New York.

Hammond, D. C. and Mellor, A. M. (1973). "Analytical predictions of emissions from and within an Allison J-33 combustor," Comb. Sci. Tech. 6, 279-286.

Hawthorne, W. R., Weddell, D. S., and Hottel, H. C. (1949). "Mixing and combustion in turbulent gas jets," Third Symposium on Combustion and Flame and Explosion Phenomena, Williams and Wilkins, Baltimore.

Heywood, J. B., Fay, J. A., and Linden, L. H., AIAA Paper No. 70-115.

Hunter, S. C., Johnson, K. M., Mongia, H. C. and Wood, M. P. (1974). "Advanced, small high-temperature-rise combustor program. Volume I: Analytical model derivation and combustor-element rig tests (phases I and II)," UCAAMROL Tech. Rep. 74-3A.

Jones, R. E. and Grobman, J. (1973). "Design and evaluation of combustors for reducing aircraft engine pollution," Atmospheric Pollution by Aircraft Engines, AGARD CP No. 125.

Longwell, J. P. (1943). Fuel Oil Atomization, Ph.D. Thesis, Massachusetts Institute of Technology.

MacFarlane, J. J. (1971). "Liquid fuel atomizers for use in a gas turbine combustion model experiments," 327-339, Combustion and Heat Transfer in Gas Turbine Systems, Pergamon Press, Oxford.

Maxwell, J. B. (1957). Data Book on Hydrocarbons, D. Van Nostrand Company, Princeton.

McCreath, C. G. and Chigier, N. A. (1973b). "Liquid spray burning in the wake of a stabilizer disc," 1355-1363, Fourteenth Symposium (International) on Combustion, The Combustion Institute, Pittsburgh.

Mellor, A. M. (1972). "Current kinetic modeling techniques for continuous flow combustors," 23-53, Emissions from Continuous Combustion Systems, Plenum Press, New York.

Mellor, A. M., Anderson, R. D., Altenkirch, R. A. and Tuttle, J. H. (1972). "Emissions from and within an Allison J-33 combustor," Comb. Sci. Tech. 6, 169-176.

Mellor, A. M. (1973). "Simplified physical model of spray combustion in a gas turbine engine," Comb. Sci. Tech. 8, 101-109.

Mellor, A. M. (1974). "Spray combustion from an air-assist nozzle," Comb. Sci. Tech. 9, 165-169.

Mellor, A. M. (1975). "Gas turbine engine pollution," Progress in Energy and Combustion Science 1, Pergamon Press, Oxford, in press.

Mellor, R., Chigier, N. A. and Beer, J. M. (1971). "Hollow-cone liquid spray in uniform air stream," 291-305, Combustion and Heat Transfer in Gas Turbine Systems, Pergamon Press, Oxford.

Moses, C. A. (1975). "Studies of fuel volatility effects on turbine combustor performance," presented at Joint Spring Meeting of Western and Central States Sections of the Combustion Institute.

Mugele, R. A. and Evans, H. D. (1951). "Droplet size distribution in sprays," J. Ind. Eng. Chem. 43, 1317-1324.

Norster, E. R. and Lefebvre, A. H. (1972). "Effects of fuel injection method on gas turbine emissions," 255-278, Emissions from Continuous Combustion Systems, Plenum Press, New York.

Nukiyama, S. and Tanasawa, Y. (1939). "Experiments on the atomization of liquids in an air stream," Trans. Soc. Mech. Eng. (Japan). 5, 68-75.

Radcliffe, A. (1960). "Fuel injection, Section D," High Speed Aerodynamics and Jet Propulsion: Design and Performance of Gas Turbine Power Plants, Oxford Press, London.

Ranz, W. E. and Marshall, W. R. (1952). "Evaporation from drops," Chem. Eng. Prog. 48, 173-180.

Rizkalla, A. A. and Lefebvre, A. H. (1974). "Influence of liquid properties on air-blast atomizer characteristics," ASME Paper No. 74-GT-1.

Shisler, R. A., Tuttle, J. H. and Mellor, A. M. (1974). "Emissions from and within a film-cooled combustor," Report CL-74-01, School of Mech. Eng., Purdue Univ.

Simmons, H. (1975). Parker-Hannifin Corporation, personal communication to J. H. Tuttle.

Taylor, G. I. (1950). "The boundary layer in the converging nozzle of a swirl atomizer," Quart. J. Mech. Appl. Math 3, 129-139.

Tuttle, J. H., Altenkirch, R. A. and Mellor, A. M. (1973). "Emissions from and within an Allison J-33 combustor. II. The effect of inlet air temperature," Comb. Sci. Tech. 7, 125.

Tuttle, J. H., Shisler, R. A. and Mellor, A. M. (1974). "Nitrogen dioxide formation in gas turbine engines: measurements and measurement methods," Comb. Sci. Tech. 9, 261-271.

Van de Vusse, J. G. (1955). "Mixing by agitation of miscible liquids," Chem. Eng. Sci. 4, 178-200.

Vaught, J. M., Johnsen, S. E. J., Parks, W. M., and Johnson, R. L. (1971). "Collection and assessment of aircraft emission baseline data turboprop engines (Allison T56-A-15)," Detroit Diesel Allison EDR-7200.

Verkamp, F. J., Verdouw, A. J., and Tomlinson, J. G. (1974). "Impact of emission regulations on future gas turbine engine combustors," J. Aircraft 11, 340-344.

Vranos, A. (1974). "Turbulent mixing and NO_x formation in gas turbine combustors," Comb. Flame 22, 253-258.

Watson, E. A. and Clark, J. S. (1947). "Combustion and combustion equipment for aero gas turbines," J. Inst. Fuel 21, October.

Winterfeld, G. (1965). "On processes of turbulent exchange behind flame holders," 1265-1275, Tenth Symposium (International) on Combustion, The Combustion Institute, Pittsburgh.

APPENDIX I. DATA LISTING

All of the experimental data obtained in the present investigation and analyzed in Section V and VI are included in the tables of this Appendix. The first nineteen tables contain the individual measurements for the three internally probed flames discussed in Section V. Although these data did not appear directly, they were used to construct the contour maps which were presented.

Tables A-1 through A-7 contain the single point probe measurements from within the $\dot{m}$ = 1 kg/sec, ϕ_o = 0.1, P = 5 atm, and $T_{\text{inlet air}}$ = 500°K flame; Tables A-8 through A-13 contain the measurements from within the $\dot{m}$ = 1.5 kg/sec, ϕ_o = 0.2, P = 5 atm, and $T_{\text{inlet air}}$ = 500°K flame; and Tables A-14 through A-19 contain the measurements from within the $\dot{m}$ = 3.0 kg/sec, ϕ_o = 0.2, P = 5 atm, and $T_{\text{inlet air}}$ = 500°K flame. Each of these tables is for a fixed radial distance from the burner centerline with CO, HC, NO, NO_2, NO_x, and gas temperature listed versus the axial distance from the fuel injector.

Measurement of NO_x, as discussed in Section III, was via a thermal NO_2 to NO converter. In agreement with earlier work from this laboratory and others (Tuttle et al., 1974), the converter did not operate properly when the equivalence ratio of the sample gas neared or exceeded unity. Hence NO_x measurements with this instrument were not possible in the fuel rich regions close to the fuel injector and no entry in the tables is given at these locations. In the construction of the contour maps, the sum of the NO and NO_2 measurements was used at the grid points where the NO_2 to NO converter did not operate.

Care has been taken to list the level of the incoming pollutant emissions to the test section in each of the first nineteen tables. These values are given as the first entries in each table and are listed at an axial location of -16.0 cm which is the distance from the fuel injector

to the upstream gas sampling rake. It should be remembered that the magnitude of the incoming pollutant emissions have not been subtracted out of the internal flame data given in these tables.

Tables A-20 through A-24 contain only burner exhaust plane emissions data which were obtained for the test section operating conditions listed in Table 3-2. Tables A-20, A-21, A-22, and A-23 list the CO, HC, NO, NO_x, and NO_2 measurements obtained for a disc diameter of 11.43 cm and utilizing the 16, 24, 35, and 50 gal/hr fuel nozzles respectively. Table A-24 contains similar data but gathered for a disc diameter of 8.89 cm and for the 35 gal/hr nozzle.

In each of the exhaust plane tables, the levels of the incoming pollutants to the test section (measured via the upstream gas sampling rake) are listed in parentheses immediately following the recorded levels for the same species in the sample gas from the downstream rake. Again, the magnitudes of the incoming pollutant emissions have not been subtracted out of the exhaust plane data given in these tables.

Table A-1. Radial Distance From Centerline = 0.0cm
$\dot{m}_{air}$ = 1.0 Kg/sec, ϕ_o = 0.1, P = 5 atm, T_{in} = 500°K

Axial Distance From Injector(cm)	CO(ppm)	HC(ppm)	NO(ppm)	NO_2(ppm) (NDUV)	NO_x(ppm) (Chem)	Temp(°K)
-16.0	31.3	10.4	8.3	4.4	12.4	500
1.27	24500	>50000	0.2	4.5	----	928
	25700	>50000	1.2	6.5	----	1008
3.81	52250	>50000	6.4	11.5	----	947
	48200	>50000	3.7		----	947
6.35	54700	50000	15.5	11.5	----	1178
	49800	50000	10.0		----	1133
8.89	45800	32500	26.9	8.5	----	1360
	35000	31000	28.1		----	1373
11.43	24000	15000	39.6	4.0	----	1511
	18700	15000	49.9	34.0	74.2	1436
13.97	7300	5000	52.2	2.0	62.4	1444
	8800	2000	64.5	12.0	69.3	1330
16.51	2300	600	47.2	1.5	54.8	1343
	4700	400	49.9	7.5	57.3	1191
19.05	1400	200	37.0	2.0	49.7	1231
	2750	170	40.2	6.5	43.9	1087
21.59	480	180	26.9	3.5	47.2	1169
	331	140	35.4	8.5	37.8	1036
24.13	395	170	23.4	8.5	42.1	1096
	350	140	28.1	10.5	35.4	994
26.67	395	170	19.8	12.0	34.5	1051
	368	140	23.3	13.0	34.2	947
29.22	395	190	16.3	15.0	29.4	1022
	377	150	19.4	14.0	30.6	894

Table A-2. Radial Distance From Centerline = 1.27cm
$\dot{m}_{air}$ = 1.0 Kg/sec, ϕ_o = 0.1, P = 5 atm, T_{in} = 500°K

Axial Distance From Injector(cm)	CO(ppm)	HC(ppm)	NO(ppm)	NO_2(ppm) (NDUV)	NO_x(ppm) (Chem)	Temp(°K)
-16.0	31.3	10.4	8.3	4.4	12.4	500
1.27	56500	>50000	7.2	31.5	----	966
	56300	>50000	11.0		----	800
	62000	>50000	11.7		----	1155
3.81	55000	>50000	4.6	23.5	----	830
	58000	>50000	8.3		----	825
	58000	>50000	7.8		----	947
6.35	62000	36000	8.7	21.5	----	1060
	48200	47500	15.5		----	947
	54700	47500	13.1		----	1155
8.89	56300	21000	24.5	21.5	----	1369
	31800	27000	31.5		----	1169
	37000	27000	33.2		----	1415
11.43	31250	11000	32.2	----	44.9	1561
	13000	13000	51.4	29.0	68.9	1222
	15900	12000	57.6		74.8	1477
13.97	9700	2000	27.1	----	37.3	1494
	4000	2500	53.9	14.0	63.9	1142
	4600	2000	60.1		67.4	1406
16.51	3900	280	27.1	----	37.3	1309
	851	350	51.4	10.0	56.4	1050
	960	300	52.7		57.6	1257
19.05	770	200	19.7	----	29.6	1169
	404	200	43.9	4.5	46.4	985
	597	200	43.0		49.1	1169
21.59	550	180	20.2	----	24.5	1078
	350	170	33.9	4.0	38.9	913
	395	180	38.1		40.5	1083
24.13	506	180	13.6	----	22.5	1004
	358	160	31.5	4.5	35.2	879
	376	170	30.7		35.6	1027
26.67	484	160	11.3	----	20.2	966
	368	160	25.2	6.0	31.5	850
	395	170	27.1		30.7	990
29.21	463	160	13.3	----	18.9	947
	377	160	21.5	8.0	27.7	810
	405	180	23.4		29.5	899

Table A-3. Radial Distance From Centerline = 2.54cm
$\dot{m}_{air}$ = 1.0 Kg/sec, ϕ_o = 0.1, P = 5 atm, T_{in} = 500°K

Axial Distance From Injector(cm)	CO(ppm)	HC(ppm)	NO(ppm)	NO_2(ppm) (NDIR)	NO_x(ppm) (Chem)	Temp(°K)
-16.0	31.3	10.4	8.3	4.4	12.4	500
1.27	72500	40000	14.0		----	908
	71000	35000	22.4	16.0	----	999
	57000	27500	31.8	11.5	----	1530
3.81	62500	>50000	7.5		----	770
	63000	>50000	14.2	16.0	----	1222
	51500	35000	23.9	11.5	----	1394
6.35	63000	50000	15.5	15.0	----	889
	53000	35000	20.0	10.5	----	1287
	37500	28000	35.8	7.5	69.6	1426
8.89	47000	24000	29.8	7.0	----	1411
	40000	21000	37.4	6.0	73.7	1478
	20000	17000	53.7	3.5	75.5	1488
11.43	17000	10000	40.1	7.0	45.2	1528
	14750	9000	56.8	4.0	73.7	1519
	6200	3000	63.6	2.0	69.6	1415
13.97	4800	2000	42.7	8.0	45.2	1394
	4000	1400	51.9	2.5	66.4	1415
	820	250	55.7	1.5	57.7	1283
16.51	1560	750	40.1	8.0	42.7	1240
	900	600	48.3	1.7	54.3	1257
	445	100	41.8	2.0	49.7	1155
19.05	1150	400	32.4	9.0	37.5	1169
	573	300	44.7	2.0	44.7	1184
	385	125	37.8	4.0	43.7	1074
21.59	820	320	29.8	9.5	29.8	1088
	443	250	37.4	1.0	39.8	1101
	385	130	29.8	7.5	39.8	1016
24.13	720	300	27.3	10.7	32.4	1050
	423	220	35.0	1.3	37.4	1042
	395	150	25.8	9.5	35.8	956
26.67	670	290	27.3	11.3	32.4	985
	405	220	32.6	1.7	35.0	1018
	415	175	21.9	9.5	31.8	918
29.21	625	290	24.5	12.0	32.4	966
	414	200	30.1	2.0	32.6	990
	415	200	20.0	9.5	31.8	887

Table A-4. Radial Distance From Centerline = 3.81cm
$\dot{m}_{air}$ = 1.0 Kg/sec, ϕ_o = 0.1, P = 5 atm, T_{in} = 500°K

Axial Distance From Injector(cm)	CO(ppm)	HC(ppm)	NO(ppm)	NO_2(ppm) (NDUV)	NO_x(ppm) (Chem)	Temp(°K)
-16.0	31.3	10.4	8.3	4.4	12.4	500
1.27	74000	31000	23.2		----	850
	70000	30000	30.5	17.5	----	1436
	62500	30000	37.2	14.0	----	1540
3.81	71000	40000	16.0		----	956
	60000	32000	25.6	16.5	----	1266
	52000	30000	29.8	10.5	----	1461
6.35	62000	29000	21.5		----	993
	58000	29000	24.5	10.5	----	1436
	39000	24000	39.7	5.5	74.5	1498
8.89	42000	17000	33.6		----	1511
	35700	16000	42.7	6.5	----	1581
	13500	7500	52.1	3.0	67.0	1436
11.43	10400	3300	41.0		50.9	1461
	11500	3800	55.0	4.0	72.1	1581
	3500	1400	49.7	1.5	54.6	1287
13.97	1470	600	41.0		48.4	1292
	1920	750	55.0	1.5	64.8	1415
	700	200	44.7	1.0	47.2	1213
16.51	1040	620	24.9		33.6	1133
	900	400	45.2	1.3	50.1	1266
	385	180	37.2	1.5	42.2	1069
19.05	700	450	26.2		33.6	1086
	670	350	40.3	1.5	42.7	1187
	350	160	34.8	2.0	39.7	972
21.59	700	400	21.7		31.1	1022
	574	300	35.4	1.5	39.0	1124
	370	180	32.3	4.5	34.8	956
24.13	642	360	19.3		33.6	975
	562	250	30.5	3.0	35.4	1046
	400	200	27.3	8.0	32.3	918
26.67	596	350	18.8		31.1	956
	395	200	24.8	9.0	29.8	884
29.21	596	320	19.3		33.6	956
	410	220	23.6	10.5	27.3	874

Table A-5. Radial Distance From Centerline = 5.09cm
$\dot{m}_{air}$ = 1.0 Kg/sec, ϕ_o = 0.1, P = 5 atm, T_{in} = 500°K

Axial Distance From Injector(cm)	CO(ppm)	HC(ppm)	NO(ppm)	NO_2(ppm) (NDUV)	NO_x(ppm) (Chem)	Temp(°K)
-16.0	31.3	10.4	8.3	4.4	12.4	500
1.27	76500	32500	21.7		----	928
	72500	34000	23.2	18.0	----	708
3.81	55000	27500	11.5		----	810
	67000	37500	20.7	15.0	----	698
6.35	32500	17500	15.6		39.0	1494
	49800	22250	27.5	6.5	----	1577
8.89	8000	4200	24.8		35.1	1509
	28100	13500	26.9	4.0	47.8	1676
11.43	1920	1500	27.4		35.1	1343
	6300	2500	30.6	3.5	42.9	1618
13.97	1080	950	26.1		30.0	1204
	1470	650	38.0	2.5	47.8	1469
16.51	940	900	24.3		30.0	1096
	955	650	25.6	3.0	35.5	1287
19.05	807	800	22.5		27.4	1004
	793	600	21.9	5.0	30.6	1124
21.59	727	700	24.3		30.0	985
	727	550	19.5	7.0	28.1	1041
24.13	690	550	23.8		32.5	966
26.67	642	500	25.9		31.2	947
29.21	625	450	22.8		27.4	928

Table A-6. Radial Distance From Centerline = 5.72 cm
$\dot{m}_{air}$ = 1.0 Kg/sec, ϕ_o = 0.1, P = 5 atm, T_{in} = 500°K

Axial Distance From Injector(cm)	CO(ppm)	HC(ppm)	NO(ppm)	NO_2(ppm) (NDUV)	NO_x(ppm) (Chem)	Temp(°K)
-16.0	31.3	10.4	8.3	4.4	12.4	500
1.27	o3000	27000	27.4		----	1494
	67000	33000	28.3	12.5	----	1519
3.81	34300	16500	26.2		54.6	1494
	53000	25000	23.4	6.0	----	1560
6.35	10600	6000	36.1		50.9	1544
	17500	8000	28.3	2.0	48.0	1671
8.89	1970	2000	28.6		36.1	1494
	7000	2800	28.3	2.0	40.6	1655
11.43	1260	900	26.2		33.6	1343
	1510	1050	25.8	3.0	38.1	1519
13.97	807	750	26.2	8.0	31.1	1187
	960	700	28.3	4.0	38.1	1360
16.51	678	650	23.5	9.0	28.6	1060
	752	550	24.6	5.5	33.2	1200
19.05	585	550	23.2	10.0	27.4	985
	665	550	22.6	6.5	30.8	1101
21.59	540	500	22.5	10.5	28.6	947
	596	480	21.4	8.0	30.8	1036
24.13	518	450	22.0	11.0	28.6	928
26.67	540	420	20.2	12.0	28.6	928
29.21	495	350	21.2	12.5	26.2	908

Table A-7. Radial Distance From Centerline = 6.35cm
$\dot{m}_{air}$ = 1.0 Kg/sec, ϕ_o = 0.1, P = 5 atm, T_{in} = 500°K

Axial Distance From Injector(cm)	CO(ppm)	HC(ppm)	NO(ppm)	NO_2(ppm) (NDIR)	NO_x(ppm) (Chem)	Temp(°K)
-16.0	31.3	10.4	8.3	4.4	12.4	500
1.27	37000	19000	17.2	5.5	43.8	1486
	270	500	8.8	4.0	11.8	1326
	2500	2000	9.4	4.5	15.1	1436
3.81	35000	6500	33.9	10.0	38.8	1552
	960	2000	4.5	5.4	11.3	1369
	1560	1750	12.6	5.5	26.2	1373
6.35	2960	3000	18.7	6.5	28.9	1502
	1380	2500	4.5	7.8	12.8	1427
	1150	800	15.8	8.0	28.7	1330
8.89	1750	2400	16.5	6.0	20.4	1377
	1260	1600	5.8	9.3	16.3	1373
	850	500	16.3	9.0	26.2	1178
11.43	1040	1100	18.0	5.5	22.7	1169
	1030	1000	7.5	10.5	18.7	1253
	600	250	15.8	10.0	27.5	1042
13.97	845	600	21.4	5.0	23.9	1106
	900	750	10.8	11.5	22.5	1191
	520	350	16.1	9.5	27.5	928
16.51	790	600	24.4	5.5	25.2	1060
	845	650	11.8	11.5	23.7	1087
	485	200	17.3	10.5	28.7	889
19.05	753	550	24.9	5.5	26.4	1004
	794	550	12.5	13.0	26.2	1055
	460	240	16.1	10.0	30.0	850
21.59	678	500	22.7	6.3	26.4	947
	740	550	15.0	14.0	27.5	----
	485	280	13.9	11.0	27.5	815
24.13	630	480	22.7	7.0	26.4	928
	485	260	13.1	11.0	27.5	795
26.67	596	450	21.9	8.0	26.4	899
	485	280	12.6	11.5	27.5	780
29.21	550	300	25.2	7.5	28.8	908
	485	240	12.6	11.5	27.5	790

Table A-8. Radial Distance From Centerline = 0.0cm
$\dot{m}_{air}$ = 1.5 Kg/sec, ϕ_o = 0.2, P = 5 atm, T_{in} = 500°K

Axial Distance From Injector(cm)	CO(ppm)	HC(ppm)	NO(ppm)	NO_2(ppm) (NDUV)	NO_x(ppm) (Chem)	Temp(°K)
-16.0	67	16.0	7.0	6.9	12.7	500
1.27	12000	>50000	1.5	9.5	----	1023
	63000	>50000	14.9	25.0	----	----
3.81	31800	>50000	4.4	12.0	----	719
	41200	>50000	7.2	17.0	----	----
6.35	41400	>50000	6.2	13.3	----	719
	46500	>50000	9.8	16.0	----	----
8.89	39000	50000	34.7	8.0	----	923
	47900	>50000	26.0	12.5	----	1115
11.43	12700	10000	72.0	5.4	84.5	1821
	20500	24000	63.5	6.0	----	1655
13.97	4500	1100	57.5	7.5	76.2	1742
	5000	2800	74.5	3.5	----	1676
16.51	1145	420	51.3	14.0	61.7	1634
	1120	460	63.5	3.5	----	1548
19.05	960	400	36.7	16.8	55.4	1511
	900	350	37.0	8.0	----	1106
21.59	1000	450	26.4	20.5	47.1	1411
24.13	1100	550	20.1	23.0	43.0	1339
	1080	480	22.6	12.5	----	1266
29.21	1340	700	11.2	26.0	36.7	1222
	1180	600	12.1	19.0	----	1169

Table A-9. Radial Distance From Centerline = 1.27cm
$\dot{m}_{air}$ = 1.5 Kg/sec, ϕ_o = 0.2, P = 5 atm, T_{in} = 500°K

Axial Distance From Injector(cm)	CO(ppm)	HC(ppm)	NO(ppm)	NO_2(ppm) (NDUV)	NO_x(ppm) (Chem)	Temp(°K)
-16.0	67	16.0	7.0	6.9	12.7	500
1.27	66700	>50000	14.9	23.4	----	1027
	65000	>50000	16.9	25.5	17.3	869
3.81	56500	>50000	12.7	16.8	----	879
	57500	>50000	15.5	19.5	16.1	560
6.35	48500	>50000	14.1	12.4	----	889
	48000	>50000	18.1	13.5	18.1	889
8.89	28500	31000	47.1	5.0	----	1601
	27250	30000	48.8	4.5	57.0	1676
11.43	8500	6000	63.7	2.0	66.6	1684
	8600	5800	59.0	3.0	67.1	1742
13.97	3300	800	53.3	4.2	63.7	1560
	4000	700	48.8	5.5	52.9	----
16.51	1300	550	34.7	13.4	53.3	1469
19.05	1300	720	24.3	20.4	43.0	1394
	1380	700	26.5	16.0	32.6	----
24.13	1425	920	11.6	24.2	34.7	1244
	1400	900	14.0	19.0	18.9	----
29.21	1465	1000	7.26	25.0	32.6	1160
	1480	1000	8.55	22.5	14.0	----

Table A-10. Radial Distance From Centerline = 2.54cm
$\dot{m}_{air}$ = 1.5 Kg/sec, ϕ_o = 0.2, P = 5 atm, T_{in} = 500°K

Axial Distance From Injector(cm)	CO(ppm)	HC(ppm)	NO(ppm)	NO_2(ppm) (NDUV)	NO_x(ppm) (Chem)	Temp(°K)
-16.0	67	16.0	7.0	6.9	12.7	500
1.27	63000	>50000	18.1	24.0	----	961
	64000	>50000	17.7	26.5	17.7	603
3.81	61000	>50000	26.1	18.0	----	1204
	60000	>50000	21.4	20.0	21.4	630
6.35	46500	38000	45.9	7.5	----	1423
	45000	43000	34.6	10.0	34.6	640
8.89	19300	19000	62.6	3.5	----	1725
	18000	21000	57.0	3.5	75.3	1630
11.43	6000	2200	61.5	2.0	79.2	1688
	5500	3400	54.9	5.5	75.3	1601
13.97	1700	640	50.0	7.5	62.6	1544
	1640	700	44.8	9.0	65.1	1477
16.51	1430	520	33.4	12.5	50.0	1415
19.05	1430	600	22.9	17.0	41.7	1305
	1180	680	24.4	14.0	42.7	1266
24.13	1560	920	9.8	22.0	33.4	1169
	1260	900	13.0	19.0	32.6	1119
29.21	1700	960	10.4	23.0	34.4	1142
	1340	940	8.6	21.5	28.5	1041

Table A-11. Radial Distance From Centerline = 3.81cm
$\dot{m}_{air}$ = 1.5 Kg/sec, ϕ_o = 0.2, P = 5 atm, T_{in} = 500°K

Axial Distance From Injector(cm)	CO(ppm)	HC(ppm)	NO(ppm)	NO_2(ppm) (NDUV)	NO_x(ppm) (Chem)	Temp(°K)
-16.0	67	16.0	7.0	6.9	12.7	500
1.27	69000	46000	22.9	21.0	----	----
	65000	45000	21.2	24.0	21.2	1032
3.81	60000	27000	36.5	8.0	----	1585
	60000	27000	42.4	11.0	42.4	869
6.35	17500	6200	45.9	3.0	66.7	1783
	31250	15000	50.8	5.0	50.8	----
8.89	6600	2400	36.5	12.0	58.4	1659
	11500	7000	50.8	3.0	50.8	----
11.43	4200	1100	30.2	18.0	49.0	1519
	5500	1600	44.5	8.0	46.6	----
13.97	1460	800	26.1	20.0	44.8	1415
	1260	560	33.9	14.0	33.9	1891
16.51	1260	780	21.9	22.5	41.7	1343
19.05	1150	720	19.8	23.0	40.7	1274
	1120	600	23.3	19.0	23.3	1585
24.13	1150	740	12.1	26.0	36.5	1133
	1120	640	14.4	21.5	----	1444
29.21	1150	780	9.4	26.0	33.4	1060
	1220	-----	8.47	24.5	----	1309

Table A-12. Radial Distance From Centerline = 5.08cm
$\dot{m}_{air}$ = 1.5 Kg/sec, ϕ_o = 0.2, P = 5 atm, T_{in} = 500°K

Axial Distance From Injector(cm)	CO(ppm)	HC(ppm)	NO(ppm)	NO_2(ppm) (NDIR)	NO_x(ppm) (Chem)	Temp(°K)
-16.0	67	16.0	7.0	6.9	12.7	500
1.27	17500	18000	2.9	7.0	14.6	1343
	49000	35000	12.6	9.0	33.7	1452
3.81	14200	15000	3.2	12.6	18.6	1535
	20500	14000	15.8	17.5	37.9	1626
6.35	7000	4400	3.3	16.0	19.8	1535
	8500	4400	11.4	22.0	33.7	1469
8.89	5200	2700	4.1	19.0	23.0	1419
	6300	3400	7.4	23.5	28.5	1330
11.43	2180	2100	5.2	23.2	27.1	1335
	2250	1900	7.4	26.0	28.5	1231
13.97	1760	1600	5.4	24.0	28.2	1244
	1450	1300	10.1	26.0	31.6	1155
16.51	1520	1500	5.4	25.0	29.2	1187
	-----	-----	----	----	----	1151
19.05	1380	1100	6.7	26.5	30.5	1169
	1050	680	11.0	26.0	32.7	1069
24.13	1300	950	7.3	28.0	32.5	1115
	960	620	10.1	27.0	31.6	1060
29.21	1190	920	7.7	30.0	34.4	1076
	1000	620	8.9	28.5	32.7	1032

Table A-13. Radial Distance From Centerline = 6.35cm
$\dot{m}_{air}$ = 1.5 Kg/sec, ϕ_o = 0.2, P = 5 atm, T_{in} = 500°K

Axial Distance From Injector(cm)	CO(ppm)	HC(ppm)	NO(ppm)	NO_2(ppm) (NDIR)	NO_x(ppm) (Chem)	Temp(°K)
-16.0	67	16.0	7.0	6.9	12.7	500
1.27	95	110	8.2	5.5	13.0	619
	110	140	6.9	7.0	11.9	548
3.81	508	1500	5.9	7.5	13.0	805
	385	1000	5.4	7.5	11.7	698
6.35	1150	3400	2.9	9.5	12.3	1041
	1040	2800	2.9	11.0	12.1	719
8.89	1460	3400	1.9	12.5	13.0	1101
	1840	2700	2.3	12.5	12.7	688
11.43	1520	3000	1.8	14.0	14.6	1110
	1160	1800	2.5	15.0	14.4	749
13.97	1420	2400	1.9	16.0	16.8	1115
	1260	2100	2.7	16.0	15.6	820
19.05	1380	2000	2.4	20.0	21.3	1092
	1300	1700	2.9	20.0	19.8	899
24.13	1340	1500	2.9	23.5	24.4	1064
	1300	1500	3.3	24.0	25.0	1069
29.21	1150	660	10.7	30.0	36.9	1155
	1120	660	1.0	31.0	35.5	1477

Table A-14 Radial Distance From Centerline = 0.0cm
$\dot{m}_{air}$ = 3 kg/sec, ϕ_o = 0.2, P = 5 atm, T_{in} = 500°K

Axial Distance From Injector(cm)	CO(ppm)	HC(ppm)	NO(ppm)	NO_2(ppm) (NDUV)	NO_x(ppm) (Chem)	Temp(°K)
-16.0	104	28.7	5.0	9.1	12.9	500
1.27	31250	>50000	2.7	5.5	----	----
	47400	>50000	10.1	8.0	----	----
3.81	61500	>50000	18.8	6.5	----	----
	60500	>50000	9.5	17.0	----	----
6.35	57000	30000	32.3	12.0	----	----
	60500	36000	15.4	21.5	----	----
8.89	52200	24000	25.0	19.0	50.0	----
	58000	25000	15.4	33.0	----	----
11.43	47500	22000	17.5	25.5	54.2	----
	50200	21000	12.2	40.0	56.7	----
13.97	32500	14000	16.7	31.0	54.2	----
	37000	16000	9.3	47.0	60.9	----
16.51	20500	6800	16.3	35.0	53.1	----
	22200	8500	8.0	53.0	54.6	----
19.05	13500	4000	12.5	34.5	47.9	----
	12700	4200	5.2	48.0	48.2	----
24.13	7000	2200	9.8	32.5	39.6	----
	6300	3100	1.6	40.5	35.5	----
29.21	6000	2200	6.5	30.0	36.5	----
	4600	2400	1.0	34.0	30.2	----

Table A-15. Radial Distance From Centerline = 1.27cm
$\dot{m}_{air}$ = 3 Kg/sec, ϕ_o = 0.2, P = 5 atm, T_{in} = 500°K

Axial Distance From Injector(cm)	CO(ppm)	HC(ppm)	NO(ppm)	NO_2(ppm) (NDUV)	NO_x(ppm) (Chem)	Temp(°K)
-16.0	104	28.7	5.0	9.1	12.9	500
1.27	62500	>50000	18.1	12.0	----	----
	60000	>50000	12.7	14.0	----	----
3.81	50000	>50000	4.2	11.0	----	----
	49000	>50000	2.4	19.0	----	----
6.35	62500	>50000	6.3	20.5	----	----
	62500	>50000	5.6	23.5	----	----
8.89	62500	39000	7.3	27.0	----	----
	62500	35000	5.4	32.0	----	----
11.43	47500	31000	6.9	37.0	54.2	----
	49000	27500	4.3	42.0	51.5	----
13.97	33500	21000	7.1	43.5	56.3	----
	36000	18000	2.8	46.0	51.5	----
16.51	21000	11000	6.3	47.0	46.9	----
	17500	10000	1.9	43.0	45.1	----
19.05	13250	6800	3.5	42.0	45.8	----
	11700	7600	1.0	36.5	36.5	----
24.13	8500	5600	1.6	35.0	36.5	----
	7800	6400	0.8	31.0	32.2	----
29.21	6000	4400	1.3	31.0	31.3	----
	6500	5000	0.5	28.0	25.8	----

Table A-16. Radial Distance From Centerline = 2.54cm
$\dot{m}_{air}$ = 3 Kg/sec, ϕ_o = 0.2, P = 5 atm, T_{in} = 500°K

Axial Distance From Injector(cm)	CO(ppm)	HC(ppm)	NO(ppm)	NO_2(ppm) (NDUV)	NO_x(ppm) (Chem)	Temp(°K)
-16.0	104	28.7	5.0	9.1	12.9	500
1.27	67500	41000	27.2	10.0	----	----
	67500	50000	23.4	11.5	----	----
3.81	56500	>50000	10.3	15.0	----	----
	57000	>50000	11.7	19.0	----	----
6.35	56300	35000	15.5	24.5	----	----
	45000	38000	8.1	33.0	----	----
8.89	45000	22000	20.8	37.5	65.2	----
	23500	21000	7.4	40.4	51.0	----
11.43	28100	15000	12.0	49.5	61.0	----
	11400	10500	3.6	38.5	40.4	----
13.97	14500	6000	8.1	47.0	52.6	----
	4500	4000	2.1	28.0	27.6	----
16.51	9200	3000	4.8	43.0	44.1	----
	2020	3000	1.2	26.0	23.4	----
19.05	6700	3200	1.8	36.5	37.8	----
	1860	3200	0.9	25.0	22.3	----
24.13	6300	4200	0.6	34.5	31.4	----
	2440	4500	0.8	27.0	23.4	----
29.21	6000	5500	0.3	25.0	25.1	----
	2860	5600	0.5	25.0	21.3	----

Table A-17. Radial Distance From Centerline = 3.81cm
$\dot{m}_{air}$ = 3 Kg/sec, ϕ_o = 0.2, P = 5 atm, T_{in} = 500°K

Axial Distance From Injector(cm)	CO(ppm)	HC(ppm)	NO(ppm)	NO_2(ppm) (NDUV)	NO_x(ppm) (Chem)	Temp(°K)
-16.0	104	28.7	5.0	9.1	12.9	500
1.27	67000	40000	23.4	12.0	----	----
	14250	17000	6.4	15.0	18.2	----
3.81	46600	41000	12.4	27.0	----	----
	1700	8000	1.6	15.5	13.9	----
6.35	28700	27000	5.2	36.5	49.8	----
	700	2600	1.3	13.0	10.7	----
8.89	5600	6600	1.9	21.5	31.1	----
	880	2800	0.9	14.0	11.3	----
11.43	4700	4000	2.1	25.0	24.5	----
	1000	2800	0.9	14.0	12.0	----
13.97	2430	3000	1.9	24.0	22.9	----
	1080	2600	0.8	15.5	12.0	----
16.51	1910	2100	1.0	23.0	20.8	----
	1120	2000	1.0	16.5	13.5	----
19.05	1850	1800	0.8	23.0	20.8	----
	1040	1600	1.0	17.5	14.5	----
24.13	1850	1500	1.4	27.0	25.1	----
	1300	2750	0.8	19.5	15.8	----
29.21	1970	1600	1.9	31.5	28.3	----
	2360	2850	0.4	21.0	10.9	----

Table A-18. Radial Distance From Centerline = 5.09cm
$\dot{m}_{air}$ = 3 Kg/sec, ϕ_o = 0.2, P = 5 atm, T_{in} = 500°K

Axial Distance From Injector(cm)	CO(ppm)	HC(ppm)	NO(ppm)	NO_2(ppm) (NDUV)	NO_x(ppm) (Chem)	Temp(°K)
-16.0	104	28.7	5.0	9.1	12.9	500
1.27	1150	1200	4.0	9.0	13.0	----
	170	5000	3.2	9.0	10.8	----
3.81	596	1800	3.1	10.0	11.7	----
	280	500	2.8	11.0	11.4	----
6.35	680	2200	2.1	10.5	11.5	----
	530	1250	2.1	11.5	11.4	----
8.89	900	3000	2.3	13.5	11.9	----
	840	2500	1.5	13.0	11.4	----
11.43	1180	3800	1.5	14.5	12.6	----
	920	2000	1.1	14.0	12.7	----
13.97	1560	4000	1.3	15.5	15.3	----
	1000	2000	1.2	14.0	12.7	----
16.51	1860	5000	1.7	14.5	14.4	----
	960	1600	1.4	16.0	14.5	----
19.05	2030	4400	0.9	18.0	16.3	----
	1040	1500	1.3	17.5	15.3	----
24.13	2340	3400	1.7	25.0	22.8	----
	1310	1900	1.2	19.0	17.1	----
29.21	2510	4250	0.9	24.5	22.8	----
	2440	4000	0.4	20.5	18.1	----

Table A-19. Radial Distance From Centerline = 6.35cm
$\dot{m}_{air}$ = 3 Kg/sec, ϕ_o = 0.2, P = 5 atm, T_{in} = 500°K

Axial Distance From Injector(cm)	CO(ppm)	HC(ppm)	NO(ppm)	NO_2(ppm) (NDUV)	NO_x(ppm) (Chem)	Temp(°K)
-16.0	104	28.7	5.0	9.1	12.9	500
1.27	108	43	4.0	12.5	12.3	----
	20	42	4.6	9.5	12.1	----
3.81	191	200	3.3	15.0	12.0	----
	250	340	3.8	11.5	12.1	----
6.35	380	750	2.3	17.0	12.3	----
	440	1000	2.7	12.0	12.6	----
8.89	586	1100	1.4	18.5	12.5	----
	695	1500	2.3	13.5	13.2	----
11.43	667	1100	1.3	17.5	13.1	----
	850	1650	2.1	15.0	14.0	----
13.97	713	1000	1.5	19.0	14.6	----
	917	1400	2.0	17.0	15.1	----
19.05	740	750	2.1	20.5	17.1	----
	910	1000	2.7	18.0	16.3	----
24.13	935	850	2.1	25.0	18.8	----
	1080	1250	2.3	20.0	18.4	----
29.21	1350	1300	1.2	29.0	23.1	----
	3240	720	0.8	24.0	20.1	----

Table A-20. Exit Plane Data, 11.43 cm Diameter Disc, 16 gal/hr Nozzle

Variable Parameter	CO(ppm)	HC(ppm)	NO(ppm)	NO_x(ppm) (Chem)	NO_2(ppm) (NDUV)
At P = 5 atm, ϕ_o = 0.2, $T_{inlet\ air}$ = 500°K					
$\dot{m}_{air}$ = 0.5 kg/sec	386 (13)	60 (7)	26.1 (10.3)	41.0 (14.0)	18.8 (5.0)
1.0	850 (29)	550 (10)	1.4 (8.1)	31.1 (11.5)	36.5 (5.0)
1.5	1430 (40)	1350 (12)	0.2 (7.6)	23.7 (12.8)	27.0 (7.2)
At $\dot{m}_{air}$ = 1.0 kg/sec, ϕ_o = 0.2, $T_{inlet\ air}$ = 500°K					
P = 2 atm	2030 (94)	2300 (29)	0.2 (3.8)	18.7 (11.8)	17.4 (7.2)
8	386 (6)	200 (9)	10.1 (9.3)	37.3 (12.3)	33.0 (4.0)
At P = 5 atm, $\dot{m}_{air}$ = 1.0 kg/sec, ϕ_o = 0.2					
$T_{inlet\ air}$ = 450°K	918 (18)	680 (11)	0.9 (6.1)	28.6 (10.8)	32.0 (5.2)
550	838 (28)	500 (10)	1.7 (10.6)	33.6 (14.8)	38.0 (6.0)

Table A-21. Exit Plane Data, 11.43 cm Diameter Disc, 24 gal/hr Nozzle

Variable Parameter	CO(ppm)	HC(ppm)	NO(ppm)	NO_x(ppm) (Chem)	NO_2(ppm) (NDUV)
At P = 5 atm, ϕ_o = 0.2, $T_{inlet\ air}$ = 500°K					
$\dot{m}_{air}$ = 0.5 kg/sec	485 (16)	100 (9)	24.0 (9.2)	41.5 (11.0)	22.5 (3.5)
1.0	650 (28)	400 (12)	6.0 (8.5)	36.5 (13.5)	42.0 (5.0)
1.5	1150 (45)	500 (12)	0.7 (7.5)	29.0 (12.5)	37.0 (5.5)
At $\dot{m}_{air}$ = 1.0 kg/sec, ϕ_o = 0.2, $T_{inlet\ air}$ = 500°K					
P = 2 atm	2100 (115)	2100 (26)	0.3 (4.2)	18.0 (13.0)	21.0 (8.0)
8	260 (14)	100 (10)	18.7 (10.5)	44.0 (12.5)	33.0 (5.5)
At P = 5 atm, $\dot{m}_{air}$ = 1.0 kg/sec, ϕ_o = 0.2					
$T_{inlet\ air}$ = 450°K	720 (24)	350 (10)	8.5 (7.2)	35.5 (11.0)	39.0 (4.5)
550	650 (32)	380 (12)	9.5 (11.0)	36.5 (17.0)	50.0 (5.5)

Table A-22. Exit Plane Data, 11.43 cm Diameter Disc, 35 gal/hr Nozzle

Variable Parameter	CO(ppm)	HC(ppm)	NO(ppm)	NO_x(ppm) (Chem)	NO_2(ppm) (NDUV)
At P = 5 atm, ϕ_o = 0.2, $T_{inlet\ air}$ = 500°K					
$\dot{m}_{air}$ = 0.5 kg/sec	1110 (21)	500 (1)	6.4 (10.5)	37.5 (16.2)	36.5 (8.0)
	820 (16)	500 (4)	5.2 (8.9)	31.4 (12.7)	----
1.0	1000 (33)	720 (5)	1.0 (8.3)	28.0 (12.1)	33.5 (5.3)
	992 (28)	680 (19)	0.9 (8.1)	32.7 (13.5)	34.5 (5.3)
1.5	1300 (51)	1150 (6)	7.8 (7.0)	22.0 (12.4)	24.3 (10.7)
	1340 (47)	1400 (7)	.1 (6.3)	20.7 (11.6)	30.8 (5.3)
At P = 5 atm, $\dot{m}_{air}$ = 1.0 kg/sec, $T_{inlet\ air}$ = 500°K					
ϕ_o = 0.1	434 (31)	225 (7)	5.6 (7.8)	25.0 (12.7)	20.5 (5.3)
	404 (24)	220 (6)	5.7 (6.8)	26.3 (14.8)	31.7 (4.5)
0.3	1340 (31)	950 (7)	0.6 (7.8)	34.8 (12.7)	37.3 (5.3)
	1340 (24)	750 (6)	0.8 (6.8)	34.1 (14.8)	41.2 (4.5)
At $\dot{m}_{air}$ = 1.0 kg/sec, ϕ_o = 0.2, $T_{inlet\ air}$ = 500°K					
P = 2 atm	2340 (85)	2300 (23)	0.2 (2.9)	17.6 (11.9)	17.8 (7.0)
	2030 (138)	2200 (29)	0.1 (3.6)	17.0 (10.5)	17.8 (6.0)
8	765 (18)	540 (2)	1.8 (9.1)	43.0 (14.9)	38.3 (3.5)
	753 (13)	650 (2)	0.8 (8.4)	34.1 (11.6)	----
At P = 5 atm, $\dot{m}_{air}$ = 1.0 kg/sec, ϕ_o = 0.2					
$T_{inlet\ air}$ = 450°K	960 (19)	740 (10)	0.8 (6.1)	25.5 (11.3)	29.8 (5.0)
	955 (18)	720 (2)	0.7 (6.5)	28.7 (11.1)	32.0 (4.5)
550	955 (33)	620 (30)	1.3 (11.1)	32.1 (15.1)	36.5 (6.0)
	883 (31)	600 (6)	0.7 (10.3)	34.1 (17.8)	37.3 (11.0)

Table A-23. Exit Plane Data, 11.43 cm Diameter Disc, 50 gal/hr Nozzle

Variable Parameter	CO(ppm)	HC(ppm)	NO(ppm)	NO_x(ppm) (Chem)	NO_2(ppm) (NDUV)
At P = 5 atm, ϕ_o = 0.2, $T_{inlet\ air}$ = 500°K					
$\dot{m}_{air}$ = 0.5 kg/sec	790 (21)	400 (8)	5.2 (8.1)	40.4 (11.8)	46.0 (3.6)
1.0	1040 (33)	600 (10)	1.8 (7.4)	33.1 (11.6)	38.0 (5.0)
1.5	1340 (47)	800 (12)	0.5 (7.2)	28.2 (12.8)	33.0 (6.0)
At $\dot{m}_{air}$ = 1.0 kg/sec, ϕ_o = 0.2, $T_{inlet\ air}$ = 500°K					
P = 2 atm	2260 (130)	2300 (33)	0.6 (3.2)	18.2 (10.8)	17.0 (6.5)
8	660 (23)	380 (7)	3.5 (9.9)	38.0 (13.8)	41.5 (3.6)
At P = 5 atm, $\dot{m}_{air}$ = 1.0 kg/sec, ϕ_o = 0.2					
$T_{inlet\ air}$ = 450°K	1150 (29)	750 (10)	1.5 (5.2)	28.2 (10.3)	32.5 (4.0)
550	910 (43)	500 (10)	3.2 (10.1)	35.5 (15.0)	37.5 (5.0)

Table A-24. Exit Plane Data, 8.89 cm Diameter Disc, 35 gal/hr Nozzle

Variable Parameter	CO(ppm)	HC(ppm)	NO(ppm)	NO_x(ppm) (Chem)	NO_2(ppm) (NDUV)
At P = 5 atm, ϕ_o = 0.2, $T_{inlet\ air}$ = 500°K					
$\dot{m}_{air}$ = 0.5 kg/sec	1380 (16)	700 (2)	11.9 (13.0)	31.9 (16.9)	45.5 (4.0)
	1380 (19)	1000 (1)	5.0 (12.0)	28.9 (14.1)	26.5 (9.5)
1.0	496 (36)	180 (3)	11.4 (11.4)	29.1 (13.9)	18.8 (3.0)
	727 (36)	300 (3)	7.4 (8.5)	26.0 (12.8)	24.0 (5.0)
1.5	506 (40)	260 (6)	3.0 (9.1)	21.6 (14.1)	22.5 (5.6)
	573 (47)	300 (6)	1.7 (6.9)	21.1 (12.8)	24.0 (10)
At P = 5 atm, $\dot{m}_{air}$ = 1.0 kg/sec, $T_{inlet\ air}$ = 500°K					
ϕ_o = 0.1	377 (33)	310 (4)	4.7 (9.1)	24.1 (15.5)	20.5 (4.0)
	444 (29)	380 (4)	2.3 (9.0)	25.7 (15.2)	24.0 (6.5)
0.3	1320 (33)	1000 (4)	3.3 (9.1)	25.2 (15.5)	26.0 (4.0)
	1380 (29)	850 (4)	2.6 (9.0)	26.3 (15.2)	30.7 (6.5)
At $\dot{m}_{air}$ = 1.0 kg/sec, ϕ_o = 0.2, $T_{inlet\ air}$ = 500°K					
P = 2 atm	1184 (128)	1000 (20)	1.9 (5.8)	18.3 (13.3)	13.3 (6.0)
	1420 (147)	900 (21)	0.5 (4.2)	18.2 (12.0)	18.7 (8.6)
8	424 (18)	340 (1)	5.5 (9.7)	31.9 (14.7)	27.0 (4.0)
	444 (16)	330 (1)	7.1 (9.6)	34.3 (16.6)	35.5 (4.0)
At P = 5 atm, $\dot{m}_{air}$ = 1.0 kg/sec, ϕ_o = 0.2					
$T_{inlet\ air}$ 450°K	585 (28)	280 (4)	6.9 (7.5)	24.1 (11.9)	19.5 (3.5)
	765 (23)	360 (4)	5.5 (6.6)	25.2 (12.0)	25.0 (5.3)
550	----	---	14.7 (12.5)	31.9 (17.7)	15.0 (4.0)
	573 (40)	180 (3)	13.9 (12.0)	34.3 (17.6)	24.0 (5.0)

APPENDIX II. DERIVATION OF THE CORRSIN TIME SCALE

With stationary, isotropic turbulence postulated, the mixing process within an idealized turbulent mixer was analyzed by Corrsin (1951, 1957). The results give a means of estimating the rate of decrease in concentration fluctuations of a scalar component in terms of the turbulence scales and the power input to the system.

In the analysis, the mixing process is examined on a microscale basis, and the mean square fluctuation in concentration, $\overline{\gamma^2}$ (analogous to $\overline{\xi'^2}$ in Table 4-2), is taken to be a measure of the non-uniformity in the fluid mixer. Following Corrsin (1951, 1957), an expression for $\overline{\gamma^2}$ can be derived from the species material conservation equation written at a point P in the flow.

$$\frac{\partial \gamma}{\partial t} + u_k \frac{\partial \gamma}{\partial x_k} = D \nabla^2 \gamma \qquad \text{A-1}$$

where u_k is the turbulent velocity, D is the molecular diffusivity of species γ, and the concentration fluctuation, γ, is defined below.

$$\gamma(x,y,z,t) \equiv \Gamma(x,y,z,t) - \overline{\Gamma} \qquad \text{A-2}$$

where Γ is the concentration and $\overline{\Gamma}$ is the mean concentration. Similarly, a material conservation equation can be written at another point P' in the flow (concentration fluctuation of γ').

$$\frac{\partial \gamma'}{\partial t} + u_k' \frac{\partial \gamma'}{\partial x_k} = D \frac{\partial^2 \gamma'}{\partial x_k^2} \qquad \text{A-3}$$

On multiplying Equation A-1 by γ' and Equation A-3 by γ, time averaging each, adding the two results together and assuming homogeneity, a differential equation for $\overline{\gamma^2}$ results.

$$\frac{\overline{\partial \gamma^2}}{\partial t} = -2D \frac{\partial \gamma}{\partial x_k} \frac{\partial \gamma}{\partial x_k} \qquad \text{A-4}$$

If a further restriction to isotropic turbulence is assumed, the mean square concentration fluctuation derivatives can be characterized by a single length, λ_c, analogous to Taylor's microscale, λ, for the velocity field (see Table 4-2).

$$\frac{\partial \gamma}{\partial x_k} \frac{\partial \gamma}{\partial x_k} = 6 \frac{\gamma^2}{\lambda_c^2} \qquad \text{A-5}$$

Upon substituting Equation A-5 into Equation A-4, an ordinary differential equation for $\overline{\gamma^2}$ results, which can be integrated directly.

$$\overline{\gamma^2} = \overline{\gamma_o^2} \exp \left(-12D \int_o^t \frac{dt}{\lambda_c^2} \right) \qquad \text{A-6}$$

where γ_o^2 represents the unmixedness at time zero.

For a high turbulent Reynolds number, Re_λ (based on u' and λ), experimental evidence suggests (Corrsin, 1957)

$$\frac{\lambda_c^2}{\lambda^2} = \frac{2D}{\nu} \qquad \text{A-7}$$

Both the diffusivity, D, and the kinematic viscosity, ν, are assumed constant. In addition, for stationary turbulence (i.e., statistically steady) λ is also constant. Hence λ_c is also constant and the integration of Equation A-6 is trivial. The time constant for the exponential decay to uniformity in the mixer, T_c, is then

$$T_c = \frac{\lambda^2}{6\nu} \qquad \text{A-8}$$

It should be noted that T_c is the reciprocal of the "β" parameter commonly used in stirred reactor theory to characterize the mixing (see for example, Evangelista et al., 1969b).

In order to maintain a steady state, the dissipation of turbulent kinetic energy per unit mass, ε, must be balanced by the energy per unit mass supplied by the main flow. For locally isotropic turbulent flow, a proportionality can thus be written

$$\varepsilon \sim \frac{\nu \overline{u^2}}{\lambda^2} \sim \frac{\dot{W}}{M} \qquad \text{A-9}$$

where $\dot{W}$ is the power input and M is the mass of the fluid to be mixed. For large Re_λ, a relationship exists between λ and the integral scale, L (Corrsin, 1957)

$$\frac{\lambda}{L} \sim \frac{1}{Re_\lambda} \qquad \text{A-10}$$

After combining Equations A-9 and A-10, the time constant can be expressed as

$$T_c \sim \left[\frac{M L^2}{\dot{W}}\right]^{1/3} \qquad \text{A-11}$$

which is the expression given by Corrsin (1957) for an idealized turbulent mixer.